

Rochester Institute of Technology

RIT Digital Institutional Repository

Theses

5-1-2007

Exploration of a hybrid locomotion robot

Jeffrey Webb

Follow this and additional works at: <https://repository.rit.edu/theses>

Recommended Citation

Webb, Jeffrey, "Exploration of a hybrid locomotion robot" (2007). Thesis. Rochester Institute of Technology. Accessed from

This Thesis is brought to you for free and open access by the RIT Libraries. For more information, please contact repository@rit.edu.

Exploration of a Hybrid Locomotion Robot

By

Jeffrey B. Webb

A Thesis submitted in Partial Fulfillment
of the Requirement for the

**MASTER OF SCIENCE
IN
MECHANICAL ENGINEERING**

Approved By:

Dr. Wayne W. Walter
Department of Mechanical Engineering

Dr. Agamemnon L. Crassidis
Department of Mechanical Engineering

Dr. Daniel B. Phillips
Department of Electrical Engineering

Dr. Edward C. Hensel
Department Head of Mechanical Engineering

**DEPARTMENT OF MECHANICAL ENGINEERING
ROCHESTER INSTITUTE OF TECHNOLOGY**

May, 2007

REPRODUCTION PERMISSION STATEMENT

Permission Granted:

Exploration of a Hybrid Locomotion Robot

I, Jeffrey B. Webb, hereby grant permission to the Wallace Library of the Rochester Institute of Technology to reproduce my thesis in whole or in part. Any reproduction will not be for commercial use or profit.

Date: _____

Signature of Author: _____

Abstract

In this work, a hybrid locomotion robotic platform is evaluated. This system combines the benefits of both rolling and walking, with the intent on having the ability to traverse variable terrain. A quadruped leg-wheeled robot was designed, built, and tested. Experimental trials were conducted to demonstrate the overall feasibility of the design. Finally, important conclusions about the effectiveness and value of hybrid locomotion were reached. Posture control is specifically identified as an effective area with great potential.

Acknowledgements

First and foremost, I wish to thank my parents. Their unwavering support made everything possible. They were always there throughout my scholastic endeavors.

I sincerely thank Dr. Walter for his support, dedication, and knowledge. His advising pushed me to achieve goals I previously thought were not possible. Likewise, Dr. Hensel, Dr. Phillips, and Dr. Crassidis were always willing and able to answer questions along the way.

I would also like to thank the Department of Mechanical Engineering at the Rochester Institute of Technology. The faculty provided me with the skills necessary to achieve many personal and professional goals. A special thank you to the staff in the Mechanical Engineering Office. Sheila Garwood, Connie LaBarre, and Diane Selleck were instrumental in my positive experience and outcome. Thanks to Rob Kraynik, Steve Kosciol, and Dave Hathaway in the Mechanical Engineering Machine Shop, whose knowledge and patients made this project physically possible.

I am also grateful to everyone I have met and talked to in the Robotics Lab throughout my years. Their support, laughs, suggestions, and ideas were a tremendous help.

A final thank you to my friends, family, and Sarah. You all helped make the process not only bearable, but immensely enjoyable.

Table of Contents

Abstract	i
Acknowledgements	ii
List of Figures	vii
List of Tables	ix
Nomenclature	x
1 Introduction	1
1.1 <i>Assessment of Need</i>	2
1.2 <i>History</i>	2
1.3 <i>Scope</i>	10
2 Overview	11
3 Legs	15
3.1 <i>Needs</i>	15
3.2 <i>Concepts</i>	15
3.3 <i>Design</i>	17
3.4 <i>Construction</i>	20
3.5 <i>Analysis</i>	21
3.6 <i>Tests</i>	24
3.7 <i>Conclusion</i>	25
4 Motor Selection	26
4.1 <i>Needs</i>	26
4.2 <i>Design</i>	27
4.3 <i>Analysis</i>	31
4.3.1 <i>Stress</i>	31
4.3.2 <i>Kinematics</i>	36
4.3.3 <i>Scrubbing</i>	37
4.4 <i>Testing</i>	39
4.4.1 <i>Dynamometer</i>	39
4.4.2 <i>Efficiency</i>	42

4.5	<i>Conclusion</i>	44
5	Position Feedback	45
5.1	<i>Needs</i>	45
5.2	<i>Concepts</i>	45
5.3	<i>Design</i>	47
5.4	<i>Theory</i>	48
5.5	<i>Testing</i>	50
5.5.1	Output	50
5.5.2	Steering	51
5.5.3	Dead Reckoning.....	54
5.6	<i>Conclusion</i>	62
6	Power Electronics	64
6.1	<i>Needs</i>	64
6.1.1	Battery.....	64
6.1.2	Motor Control	65
6.2	<i>Concepts</i>	66
6.2.1	Battery.....	66
6.2.2	Motor Control	71
6.3	<i>Theory</i>	73
6.4	<i>Design</i>	76
6.4.1	Battery.....	76
6.4.2	H-Bridge	77
6.5	<i>Test</i>	78
6.6	<i>Redesign</i>	79
6.7	<i>Conclusion</i>	82
7	Sensors	83
7.1	<i>Needs</i>	83
7.1.1	Motion Control.....	83
7.1.2	Environmental Information.....	83
7.1.3	Locomotion Characterization.....	84
7.2	<i>Concepts</i>	84
7.2.1	Tilt Sensor	84
7.2.2	Ground Contact.....	85
7.2.3	Obstacle Detection	85
7.3	<i>Design</i>	86
7.3.1	Tilt Sensor.....	86

7.3.2	Ground Contact.....	87
7.3.3	Object Detection	88
7.3.4	Current Sensor	90
7.4	<i>Test</i>	91
7.4.1	Inclinometer	91
7.4.2	Current Transducer	93
7.5	<i>Conclusion</i>	93
8	Microcontroller	94
8.1	<i>Needs</i>	94
8.2	<i>Concepts</i>	97
8.3	<i>Design</i>	97
8.4	<i>Test</i>	103
8.5	<i>Redesign</i>	111
8.6	<i>Conclusion</i>	113
9	Chassis.....	114
9.1	<i>Needs</i>	114
9.1.1	Mechanical.....	114
9.1.2	Electrical	114
9.2	<i>Design</i>	115
9.2.1	Mechanical.....	117
9.2.2	Electrical	117
9.3	<i>Conclusion</i>	119
10	Hybrid Locomotion.....	121
10.1	<i>Posture Control</i>	121
10.2	<i>Obstacle Traversing</i>	125
11	Conclusions.....	128
11.1	<i>Efficiency</i>	128
11.2	<i>Effectiveness</i>	131
11.2.1	Rolling.....	131
11.2.2	Walking.....	131
11.2.3	Hybrid Locomotion.....	131
12	Recommendations.....	133
13	References.....	136

14	Appendices.....	142
14.1	<i>Appendix A – Bill of Materials.....</i>	<i>142</i>
14.2	<i>Appendix B – Test Code.....</i>	<i>143</i>
14.2.1	Steering Encoder Test.....	143
14.2.2	Steering Encoder Test.....	146
14.2.3	Posture Control Test.....	150
14.2.4	Walking Gait Test.....	154
14.3	<i>Appendix D – Select Manufacturer Specifications.....</i>	<i>156</i>

List of Figures

Figure 1: Wheel Types [3]	4
Figure 2: a) Biped Robot [13]; b) Quadruped Robot [14]; c) Hexapod Robot [15].....	6
Figure 3: Shrimp III [18].....	8
Figure 4: Wheeleg [19].....	8
Figure 5: a) Walk'n Roll [22] and b) WorkPartner [23].....	9
Figure 6: HAL – a) Front View with Legs Down; b) Side View with Legs Up; c) Isometric View.....	11
Figure 7: Functional Decomposition of HAL	12
Figure 8: Leg Examples – a) Kydonas [24]; b) Whieg [25]; c) Typical Retail Leg [27]; d) Robot III Leg [25]	16
Figure 9: Working Model Proof of Concept.....	18
Figure 10: Leg Prototype.....	19
Figure 11: Leg – Mechanical Only	20
Figure 12: Leg Stress Analysis.....	21
Figure 13: Total Leg Stroke	24
Figure 14: Preliminary Leg Sketch Showing Motor Positions	28
Figure 15: Shoulder Abduction Worm and Worm-gear	29
Figure 16: Selected Gear-motor [30].....	30
Figure 17: Gear-motor Dimensions and Mounting Pattern (mm) [30]	31
Figure 18: Worm and Worm-Gear Mesh [31]	32
Figure 19: Ramp Free Body Diagram.....	36
Figure 20: Wheel Scrubbing Diagram	38
Figure 21: Dynamometer Test Setup	39
Figure 22: Dynamometer Experimental Results Superimposed with Manufacturer's Data [30].....	41
Figure 23: Motor Torque Constant Trend Line	43
Figure 24: Encoder on Gear-motor	47
Figure 25: Quadrature Encoder Fundamentals [41].....	48
Figure 26: Encoder Components.....	49
Figure 27: Encoder Output	50
Figure 28: Steering Encoder Test Video Screen Shot.....	52
Figure 29: Steering Encoder Test Run 1 Data	52
Figure 30: Steering Encoder Test Run 2 Data	53
Figure 31: Steering Encoder Test Run 3 Data	53
Figure 32: Tile Dimensions	54
Figure 33: Dead Reckoning Test Video Screen Shot	55
Figure 34: Robot Model.....	56
Figure 35: Incremental Turn	57
Figure 36: Wheel Model	57
Figure 37: Run 1 Dead Reckoning Test	61
Figure 38: Run 2 Dead Reckoning Test	61

Figure 39: Battery Data.....	70
Figure 40: a) H-bridge Theory; b) Typical H-bridge Schematic [50].....	72
Figure 41: PWM Duty Cycles [51]	74
Figure 42: PWM Characterization [52].....	75
Figure 43: Battery	76
Figure 44: H-Bridge/ Surfboard Assembly.....	78
Figure 45: Good H-Bridge versus Bad H-Bridge.....	79
Figure 46: Motor Control Redesign Wiring Diagram.....	81
Figure 47: Shoulder Abduction Motor Controller	82
Figure 48: Ground Contact Sensor Design.....	87
Figure 49: Ground Contact Sensor a) Off Ground; b) On Ground.....	88
Figure 50: Limit Switch [57]	88
Figure 51: Limit Switch Assembly	89
Figure 52: Switch Wiring Diagram.....	90
Figure 53: Inclinometer Test Setup.....	91
Figure 54: Inclinometer Test Results	92
Figure 55: Current Transducer Test Results	93
Figure 56: OOPic S-Board Layout [59]	99
Figure 57: OOPic S-Board Wiring Diagram [59]	99
Figure 58: PWM High at 50% Duty	103
Figure 59: PWM Low at 50% Duty	104
Figure 60: PWM High and PWM Low Output at 50% Duty.....	105
Figure 61: PWM High and PWM Low at 100% Duty	106
Figure 62: If Statement Test	107
Figure 63: Encoder Test Virtual Circuit	108
Figure 64: Virtual Circuit Test.....	109
Figure 65: Quadrature Encoder Virtual Circuit	110
Figure 66: Encoder Wheel Comparison	112
Figure 67: Modified Encoder Output	113
Figure 68: Chassis: a) Top View; b) Front View; c) Side View; d) Orthogonal View..	115
Figure 69: Chassis Diagram: a) Level 1; b) Level 2; c) Level 3.....	116
Figure 70: HAL Wiring Diagram.....	119
Figure 71: Posture Control Simulation [21]	121
Figure 72: Posture Control Logic Flow Chart	123
Figure 73: No Posture Control vs. Posture Control.....	124
Figure 74: Step Traversing	125
Figure 75: Instantaneous Power Usage.....	129
Figure 76: Total Work Done.....	130

List of Tables

Table 1: Rechargeable Batter Comparison [46-48]	68
Table 2: 7.2V Battery Values	70
Table 3: H-Bridge Function Table [53]	78
Table 4: Needed Inputs and Outputs	94
Table 5: OOPic Connections	102

Nomenclature

<u>Symbol</u>	<u>Definition</u>	<u>Units</u>
a	Addendum, Left Most Value	in, s
A	Area	in ²
AC	Alternating Current	n/a
ADC	Analog to Digital Converter	n/a
b	Width, Right Most Value	in, s
β	Correction Factor, Turning Radius	n/a, degrees
c	Clearance	in
CCW	Counter-Clockwise	n/a
CG	Center of Gravity	n/a
CORDIC	Coordinate Rotation Digital Computer	n/a
COTS	Commercial Off-the-Shelf	n/a
C_t	Center of Turning	n/a
CW	Clockwise	n/a
d	Height, Diameter, Pitch Diameter	in
D	Total Distance Traveled, Duty Cycle	in, %
DARPA	Defense Advanced Research Projects Agency	n/a
DC	Direct Current	n/a
DIP	Dual In-Line Package	n/a
DOF	Degree of Freedom	n/a
DPDT	Double-Pole Double-Throw	n/a
e	Efficiency	%
EEPROM	Electrically Erasable Programmable Read-Only Memory	n/a
eff	Efficiency	%
f	Coefficient of Friction, Frequency, Function	n/a, Hz, n/a
F	Force	lbs
h	Data Point Difference	s
HAL	Hybrid Autonomous Locomotion	n/a
H_o	Output Horsepower	hp
HS	High State	n/a
I	Current	A
I/O	Input/Output	n/a
K_a	Application Factor	n/a
l	Length, Distance to Left Wheel	in, in
L	Lead Length	in

λ	Lead Angle	degrees
Li-Ion	Lithium-Ion	n/a
LS	Low State	n/a
m	Mass	g
μ	Coefficient of Static Friction	n/a
N	Number of Teeth	n/a
n	Angular Velocity	RPM
N	Counts per Revolution	n/a
NASA	National Aeronautics and Space Agency	n/a
n_d	Design Factor	n/a
NiCd	Nickel-Cadmium	n/a
NiMH	Nickel-Metal Hydride	n/a
ω	Angular Velocity	rad/s
OOPic	Object Oriented PIC	n/a
P	Pressure, Power	psi, W
PCB	Printed Circuit Board	n/a
Φ_n	Pressure Angle	degrees
PIC	Peripheral Interface Controllers	n/a
P_n	Normal Circular Pitch	in
Ψ	Heading Change	degrees
P_t	Tangential Diametrical Pitch	in
PWM	Pulse Width Modulation	n/a
PWMH	High Frequency PWM	n/a
PWML	Low Frequency PWM	n/a
P_x	Axial Pitch	in
R	Wheel Radius	in
r	Distance to Right Wheel, Turning Radius	in, in
RAM	Rechargeable Alkaline-Manganese	n/a
RPM	Revolution per Minute	n/a
ρ	Density, Instantaneous Turning Radius	lbs/in ³ , in
s	Arc Length, Path Distance	in
σ	Stress	psi
SLA	Sealed Lead-Acid	n/a
SOIC	Small Outline Integrated Circuit	n/a
SPST	Single-Pole Single-Throw	n/a
T	Torque, Period	ft-lb or kg-cm, s
θ	Ramp Angle, Travel Angle	degrees, degrees
τ	Torque Constant	A/kg-cm

V	Voltage, Tangential Speed, Velocity	V, in/s, in/s
v	Volume	in ³
V _s	Sliding Velocity	in/s
W	Load	lbs
w	Wheel Width, Wheel Radius	in, in
W ^t	Transmitted Force	lbs
x	X Coordinate	in
X	Global X Coordinate	in
y	Y Coordinate, Voltage	in, V
Y	Global Y Coordinate	in
Z	Section Modulus	in ³

1 Introduction

Within the vast field collectively known as robotics, there is a large subset of vehicles that require some form of locomotion. Self-propelled motion from place to place is an essential part of robotic technology and research. The ability to traverse various terrain and obstacles is paramount in mobile platforms.

Many forms of locomotion have been developed. Some are meant to perform very specific tasks, while others are designed to be extremely robust. Depending on the application the robot is meant to be used for, there may not be a need for an overly complex locomotion scheme. However, there are a seemingly infinite number of applications for a truly robust form of locomotion.

Traditional robotic locomotion focused on exclusively wheeled or legged solutions. Designers often opt for the ease of implementing wheels, especially on flat surfaces. Legs are sometimes used to negotiate tougher terrain. Many mobile robots are made to imitate the types of legged locomotion that can be found in nature.

Another approach to the problem of traversing variable terrain is to combine the benefits of multiple individual forms of locomotion. This thesis discusses such an approach. Many advantages will be shown in the combination of both rolling and walking.

1.1 Assessment of Need

Research in the area of robotics is becoming more and more prevalent. Most mobile robots are restricted to the confines of a laboratory environment. New and exciting results can be obtained if a truly robust variable terrain platform can be developed. While the first generation of system intended to achieve this goal will not necessarily be developed for hostile environments, the feasibility for future use can be evaluated.

A new robotic platform is needed, and must be designed, built, and tested. This platform must demonstrate the ability to carry modest payloads over various types of terrain conditions. It should also be small, with a footprint minimized as much as feasibly effective. The cost and intricacy should be kept to a minimum, meaning commercial off-the-shelf (COTS) parts will most likely be used. Since this new platform is meant for research purposes, an emphasis will be placed on the analysis and characterization.

1.2 History

Since their inception, robotic devices have had a vast number of uses. Traditionally, their uses were limited by computing power and cost. Early industrial robotic applications included “pick and place” tasks. Machines like the PUMA and SCARA robotic arms performed repetitive tasks that were undesirable to humans [1]. Other arms that were meant for following a more complicated pattern were programmed or “taught” by following the movements of an operator [2]. Yet, for all of their successes, these commercial robots suffer from a fundamental disadvantage – lack of mobility. A fixed manipulator has a limited range

of motion that depends on where it is bolted down. In contrast, a mobile robot is able to travel throughout its environment [3].

Mobile and autonomous robots also began with relatively primitive platforms. Most were designed to perform tasks within a very narrow scope. A famous example of this is the Stanford Cart. Developed at Stanford University in the 1970's, this robot was capable of following a painted white line. A prototype vision analysis system was also developed, allowing the robot to navigate a 30-meter obstacle course autonomously. However, the time required to complete this task was over five hours [4].

Much advancement in mobile robotics was spearheaded by the National Aeronautics and Space Agency (NASA). One important application was the Mars Viking Landers.

Developed by Jet Propulsion Laboratories, they had a 6000 word memory [5]. Recently, the Mars Exploration Rovers have successfully used autonomous navigation to much more effectively conduct remote research on Mars [6].

Some of the most sophisticated autonomous mobile robots compete in the Defense Advanced Research Projects Agency (DARPA) Challenge [7]. This challenge features autonomous ground vehicles that conduct simulated military supply missions in a mock urban area. They not only aim to be able to navigate and drive across open and difficult terrain from city to city, but also to navigate and operate in traffic.

The field of robotics has, and is, advancing at an extremely rapid pace. Every successive generation sees great improvements. This sophistication in robotic platforms occurs in tandem with the advancement of microcontrollers, sensors, and motion devices.

Inspiration for locomotion can come from any number of sources. Existing machines and vehicles could be used or copied. Most of these result in wheeled platforms. There are four basic wheel types: standard, castor, Swedish, and spherical [3] (shown in Figure 1). Each has its own advantage and can often be used in combination, depending on the application.

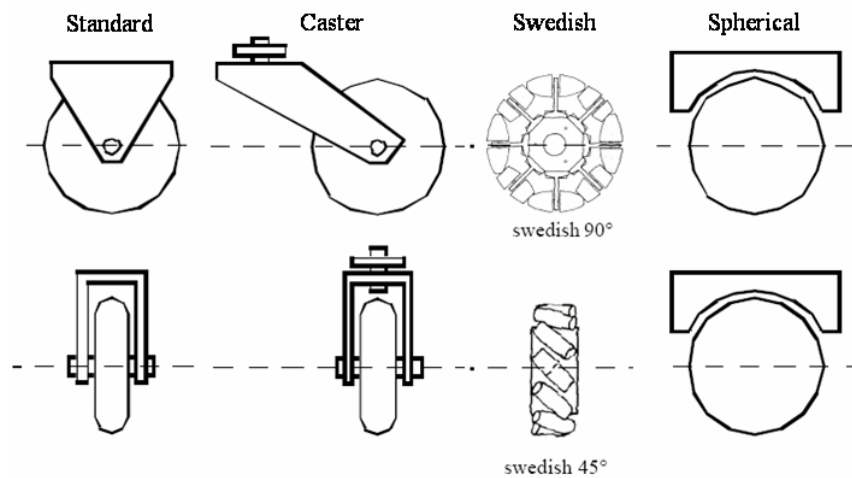


Figure 1: Wheel Types [3]

Wheeled vehicles have been shown to have many advantages. They are extremely fast and efficient on flat surfaces, and are easy to design and build. A large amount of wheel vehicle analysis is available. Motion control is of specific importance when developing a wheeled robotic platform. There are two major types of controlled vehicle motion using wheels – skid

steering and explicit steering. Skid steering is accomplished by creating a differential velocity between the inner and outer wheels. Explicit steering is accomplished by changing the heading of the wheels to cause a change in the heading of the vehicle [8]. While skid steering uses one less degree of freedom (DOF) for each wheel, it also must use a tremendous amount of energy to overcome the force created by scrubbing. Explicit steering can also be much more complex, especially when performing trajectory analysis [9].

Another subset of wheeled vehicles that is much better for “off-road” conditions are tracked vehicles. Tracked type locomotion has good terrain adaptability. Like a tank, tracked robots have superior mobility over uneven terrain and harsh natural conditions [10]. The drive systems are also relatively simple to implement because they usually contain only one DOF. However, in the “robot world” skidding has a severe disadvantage because of the negative effect it has on odometry. When the tracks skid, they are not tracking the robot’s exact movements. Since odometry is significant for position determination, skid-steer is not commonly used on robots with sparse sensing that require accurate position determination [11]. Other negative aspects of tracked vehicles include low efficiency and high track wear.

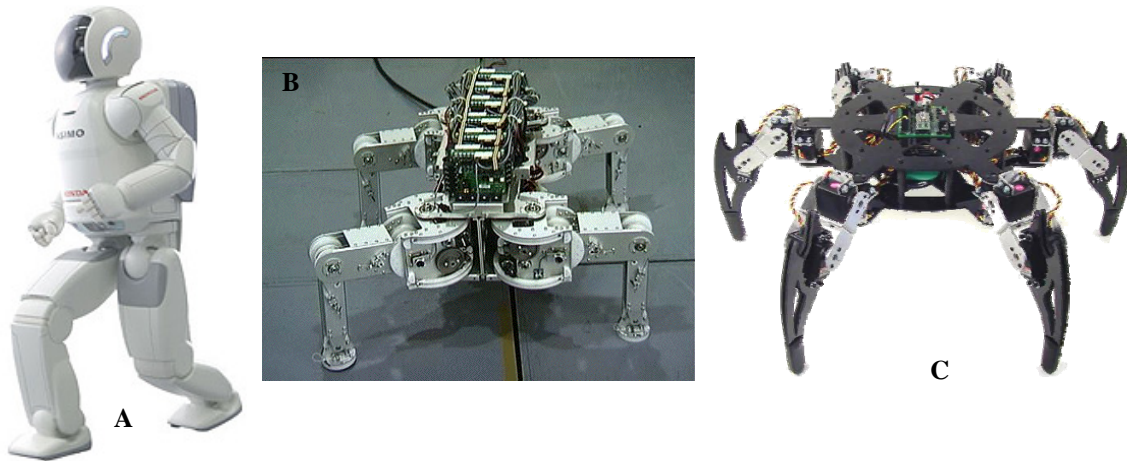


Figure 2: a) Biped Robot [13]; b) Quadruped Robot [14]; c) Hexapod Robot [15]

A common form of locomotion for robotic projects is walking. This form of locomotion is usually created to mimic nature. Two legged mammals, four legged reptiles, or six legged insects are the most common forms. Generally speaking, the fewer the legs, the more complicated the locomotion. Figure 2 shows examples of previously developed walking robots. For static walking, six legs are required, since fewer legs would require some form of balance [3].

If implemented properly, walking robots can be good at maneuvering over irregular terrain. However, these robots are extremely hard to control and can be very complex. Most require a continuous feedback loop to maintain balance. Autonomous dynamic adaptation capable of coping with an infinite variety of terrain irregularities still remains largely unsolved. Unlike modern robots, animals show marvelous abilities in autonomous adaptation. A great deal of research has been done in an attempt to mimic this autonomously adaptable dynamic walking using a neural system modeled after living creatures [12]. Navigation can also become an

extremely difficult because of the large number of individual movements needed to take each step.

Although the majority of robots use some form of rolling or walking for locomotion, there are many other ways to get from place to place. Hopping can be used to overcome obstacles much larger than the robot itself, but has problems with energy storage and absorption that must be overcome [16]. Crawling, sliding, and slithering have also been examined in detail. The snake's "serpenoid curve" motion is usually modeled and mimicked in an attempt to be able to climb a hill, wind up a tree, or move through other ill-conditioned environments [17]. Other robots designed for use in underwater environments employ different forms of swimming. When designing robotic platforms, environmentally specific locomotion can be used for unique environments.

Combining multiple individual forms of locomotion into one hybrid platform can be very appealing for many reasons. Each type has its own advantages and disadvantages. When combined, the collective locomotion outcome can minimize the disadvantages, while simultaneously maximizing the advantages. Although there are any number of different combinations, for the purposes of this thesis, the focus will be on wheel-legged locomotion.



Figure 3: Shrimp III [18]

Many of the hybrid wheel-legged robots that already exist use a passive (not actively controlled) form of suspension to help overcome large obstacles. Sophisticated chassis kinematics can optimize the contact between the ground and all wheels. The ability to passively adapt to various terrains allows hybrid platforms to roll over obstacles much larger than they would with wheeled locomotion alone [18]. Figure 3 shows a robot named Shrimp III traversing obstacles that would be impossible without its passive leg form of hybrid locomotion.

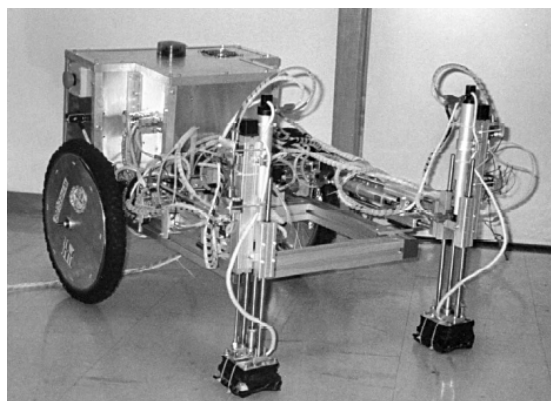


Figure 4: Wheelleg [19]

Another form of wheel-legged hybrid locomotion is to separate the wheels and legs. This category has been designed to investigate possible applications that are for humanitarian purposes or for the exploration of unstructured environments. The Wheeleg robot (shown in Figure 4) was designed with two rear wheels and two front legs. The main idea was to use rear wheels to carry most of the weight of the robot, and front legs to improve the grip on the surface and to climb over obstacles [19].

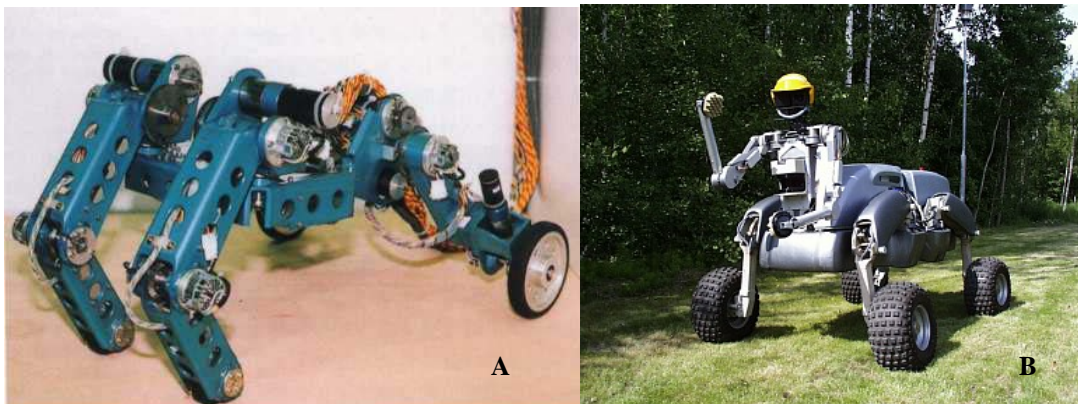


Figure 5: a) Walk'n Roll [22] and b) WorkPartner [23]

A very robust way to enhance the locomotion performance of mobile robots is to use actively articulated locomotion systems. Many of these systems use actively actuated legs with wheels on the end of each. This combines legged locomotion's high adaptability for rough terrain with wheeled locomotion's speed and efficiency. One such robot, called Roller-Walker, uses passive wheels on legs, giving the option to either use pure walking or to "skate" on flat surfaces [20]. Other robots that drive their wheels can use their legs as a way

to enhance stability. When traveling on an irregular slope or uneven terrain, the legs can be actuated to prevent the platform from tipping [21]. Two other robots that effectively used the combination of wheels and legs are Walk'n Roll [22] and WorkPartner [23] (shown in Figure 5). The former is a small machine built for testing purposes in the lab, while the latter is a large machine designed for urban outdoor environments.

1.3 Scope

This thesis consists of an investigation of a hybrid locomotion, variable-terrain robotic platform that combines the benefits of both walking and rolling. A fully functional system will be designed, built, and tested. All aspect of the platform will be characterized, and the benefits of hybrid locomotion will be shown. The robotic platform will be referred to as HAL, short for Hybrid Autonomous Locomotion.

In an effort to keep the scope manageable, it was decided to clarify the focus. Little emphasis will be given to true autonomous navigation. However, HAL will have the ability to function without human interaction (no tether or remote control). The robot will not have an overly complicated motion algorithm or set of sensors to make decisions. HAL will also be designed to function in a controlled environment. It will not be intended for use outside of the lab environment.

2 Overview

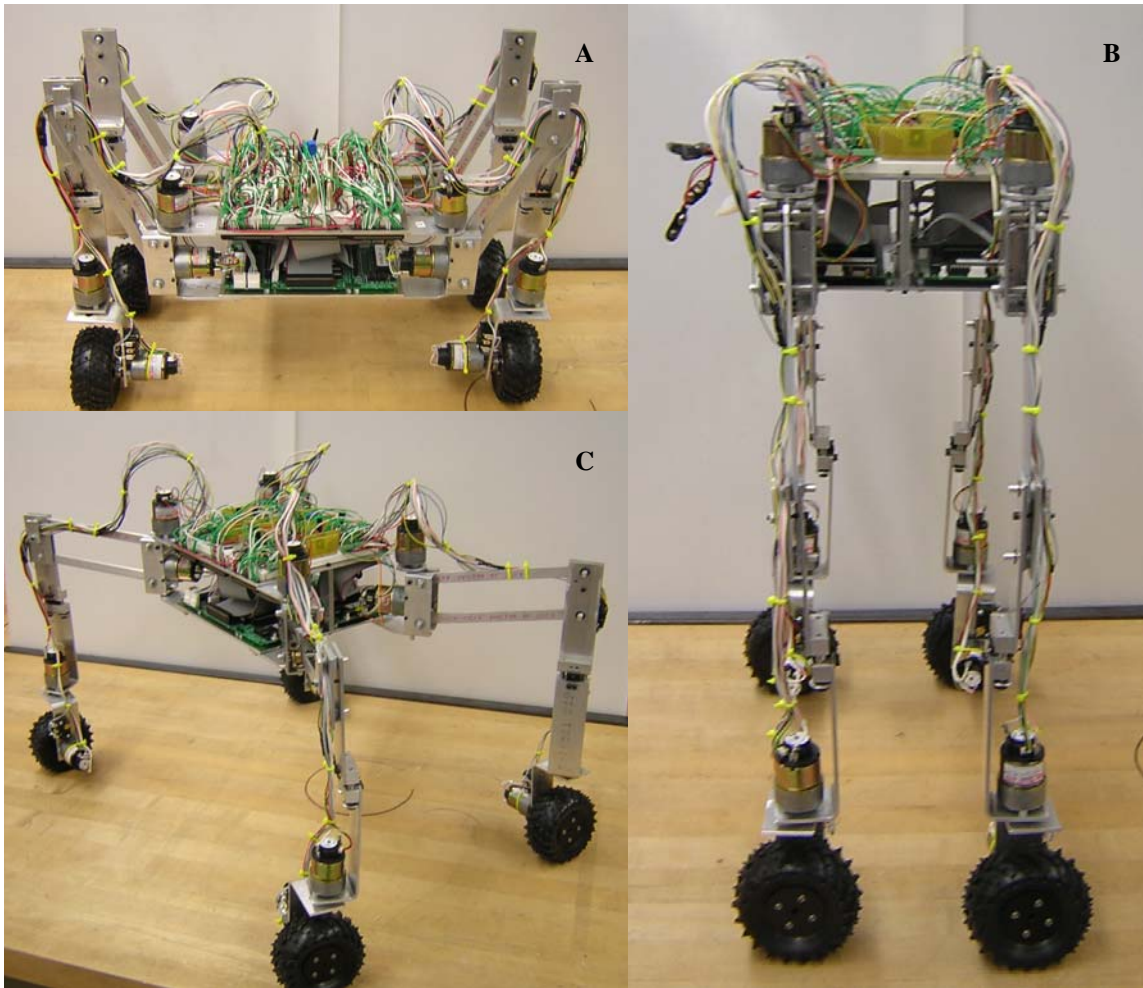


Figure 6: HAL – a) Front View with Legs Down; b) Side View with Legs Up; c) Isometric View

HAL is designed as a hybrid locomotion quadruped. It has four legs, each with four DOFs, giving 16 for the robot as a whole. Each leg has a wheel located on the end, giving it the ability to perform pure rolling. The legs are designed in such a way as to be able to actuate

individually for pure walking. When combined, the benefits of hybrid locomotion can be demonstrated and evaluated.

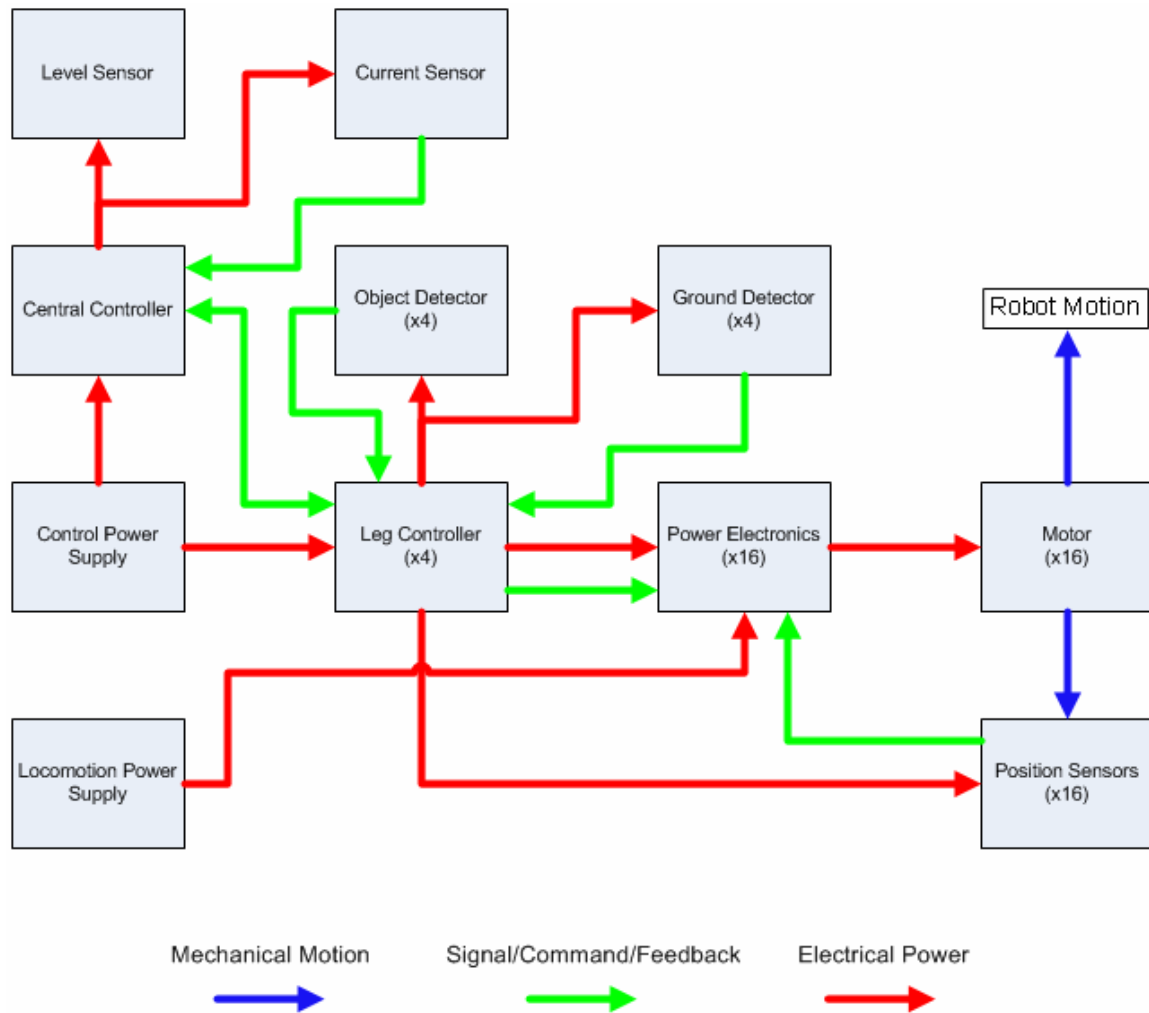


Figure 7: Functional Decomposition of HAL

Figure 7 shows the function decomposition for HAL. Although each subsystem will be examined in much more detail later in this thesis, a brief overview is appropriate here. Since HAL is designed to be semi-autonomous (no tether), it is independent of any external sources of power or control. Everything is self-contained, meaning no tethers are necessary. There

are no inputs (excluding sensor data) to the system. The only output present is HAL's mechanical motion.

The control system consists of five microcontrollers. There are four used to control the legs – one for each. One central microcontroller is responsible for coordinating the entire platform. A variety of sensors and feedback loops are used to give HAL the ability to keep stable, verify motion, and interact with its surroundings. These sensors are located throughout and have different purposes.

HAL is designed to go over a multitude of different terrain scenarios. It takes little imagination to envision a scenario in which one side of the robot would be so much higher than the other would result in tipping. Therefore, a sensor was needed to make certain HAL's chassis is level at all times. If the central microcontroller realizes the platform was not stable in either of the two axes, it will send a signal to the appropriate legs to move in such a way as to make it level.

To fully characterize the system as a whole, some form of power usage measurement is essential. Since the voltage being supplied remains virtually constant, a method for measuring the current draw will quantify the power. This is easily shown using the electrical power equation, where P is power in Watts, V is voltage in Volts, and I is current in Amperes:

$$P = VI \tag{1.3.1}$$

Another important factor when keeping the platform stable is ground contact. Keeping the base level is not enough if all four wheels are not on the ground. It would also be helpful, when creating motion algorithms, to have a method for determining if a leg had completed its motion and returned to the ground plane. To accomplish this, an input was added to each leg that confirms ground contact.

Although advanced object detection and avoidance is beyond the scope of this project, it is necessary to determine when something gets in HAL's path. Simple sensors (discussed later) are attached to not only determine when an obstacle is present, but also to tell if it has been cleared. Ideally, HAL will only raise his legs as high as they would need to go when going over obstacles such as steps.

Position sensors are also needed on each joint for multiple reasons. Feedback is very important to be able to move each limb with precision. Ideally, these sensors will also help move the wheels at a specific desired constant speed. Synchronization is impossible without some sort of feedback.

3 Legs

3.1 Needs

After it was decided HAL would be a quadruped with wheels, the next step was to determine the specifics about how the legs will function. One of the goals of this project is to create a robot that can not only perform hybrid locomotion, but also do pure walking and pure rolling. The legs also need to be strong and robust to be able to hold the entire weight of the robot and other future payloads. As with all of HAL's components, cost and ease of manufacturing are high on the list of needs.

3.2 Concepts

Since legged robot locomotion is not a novel idea in and of itself, performing benchmarking is necessary. The most basic function of a robot legs is to raise and lower the feet off the ground. After researching the subject, it was determined that there are currently three categories of leg design.

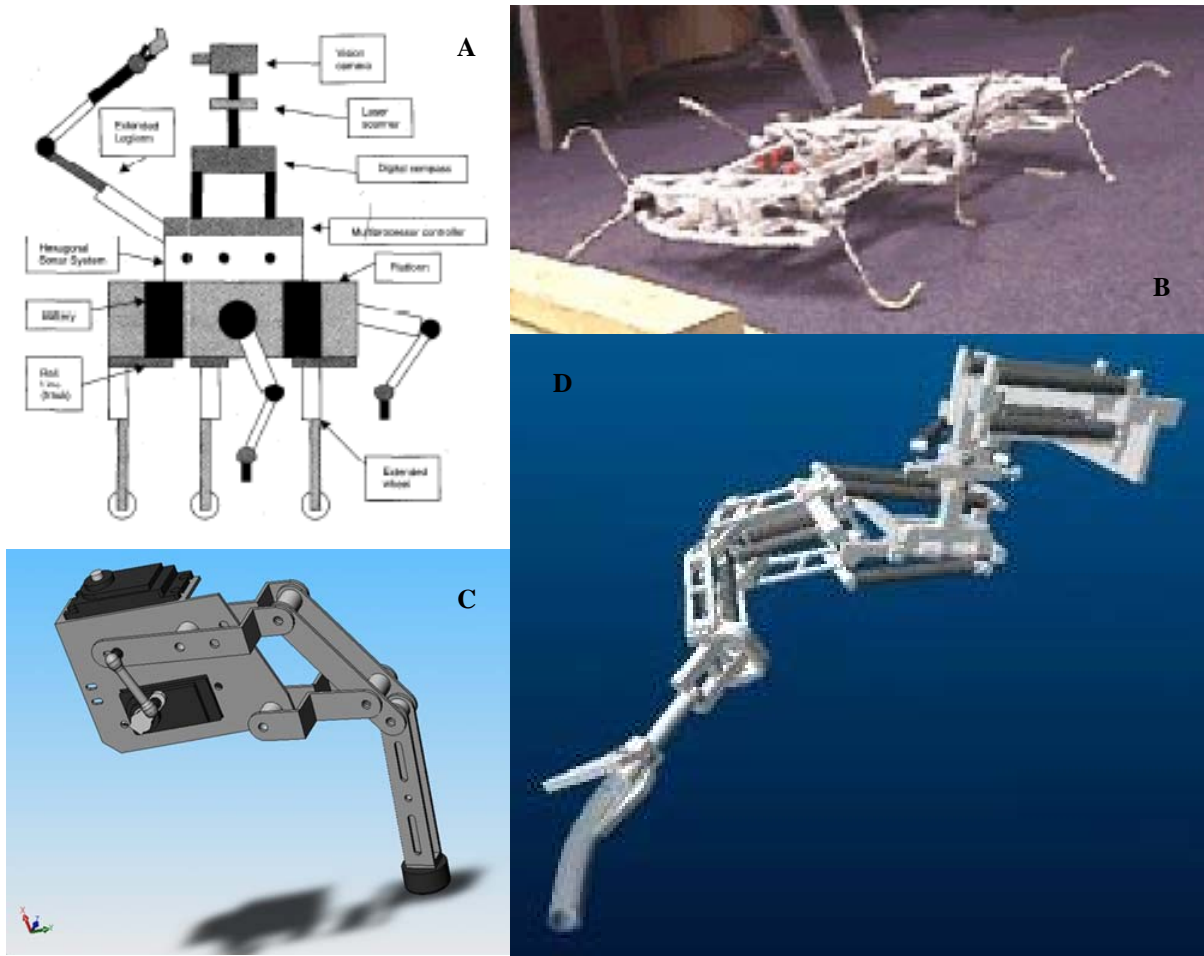


Figure 8: Leg Examples – a) Kydonas [24]; b) Wheg [25]; c) Typical Retail Leg [27]; d) Robot III Leg [25]

The first, most simple category consists of a single vertical linear actuation. An autonomous robot named Kydonas (shown in Figure 8) successfully used this leg design and was able to travel over small height obstacles [24]. Kydonas used wheels on each leg to move, and did not have the ability to walk without rolling. If a second “hip” joint was used on each leg, pure walking could be achieved.

Another, more unorthodox type of legged motion is “spoked appendages.” Researchers at the Case Western Reserve University Biorobotics Laboratory developed a robot they named Whegs (shown in Figure 8). Whegs has six tri-spoked motors and nominally walks in a tripod gait. This one drive motor per leg design is beneficial because the maximum onboard torque can be delivered to any leg. Whegs was shown to have the ability to climb over a large number of different obstacles [25].

The final, most typical form of legged locomotion is the classic jointed approach. There are a vast number of robots that use this type of walking. Some are extremely simple, while others are very complex mechanisms. To have the ability to walk, these legs can have as low as one DOF. Although they most typically have two DOF, some have much more. A cricket inspired robot named Robot III (shown in Figure 8) has five DOF in each of its six legs [25].

There are a vast number of methods for actuating individual portions of a robot’s legs. The most common seems to be DC motors. Simple hobby servos are used for a large number of prototypes and retail robots. Other methods for moving joints include pulleys, cables, pneumatic or hydraulic actuators, linear actuators, synthetic muscles, or even electroactive polymers – usually on microrobots [26].

3.3 Design

HAL’s legs are designed using the classic jointed approach. A motor attached to a wheel at the end of each leg provides four wheel drive. In order to make the locomotion as robust as possible, it was decided to have individual steering for each wheel. This four wheel steering

gives HAL the ability to turn with a zero turning radius, and also to drive in any two dimensional vector from any instantaneous location. Traditional two wheeled differential steering is also an option, which utilizes much simpler trajectory planning, generation, and analysis.

The two previously mentioned joints give HAL traditional rolling locomotion. To achieve a traditional form of walking locomotion, another three joints are needed on each leg. These three joints split the tasks of raising and lowering the leg and rotating the shoulder.

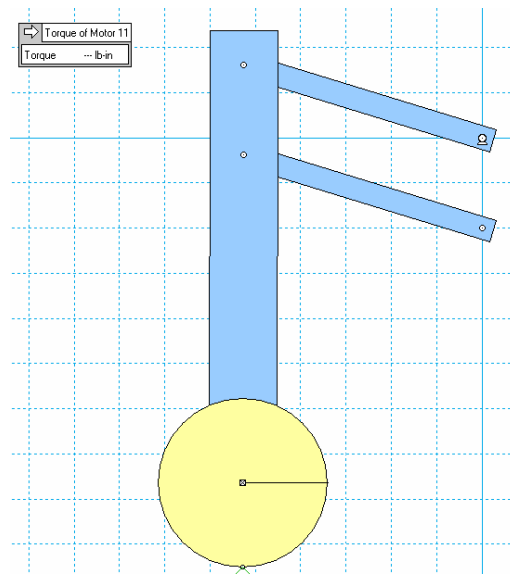


Figure 9: Working Model Proof of Concept

With the style of hybrid locomotion being used, it is necessary to keep the wheel orthogonal to level ground. One solution to this problem is to incorporate a fifth, powered elbow joint. However, a more simple and elegant solution was developed that called for a four bar

mechanism. This is designed into the leg to eliminate the need for the elbow motor, which in turn greatly simplifies the system as a whole. A two dimensional analysis tool named Working Model was used to perform a proof of concept on the four bar mechanism, shown in Figure 9. After modeling the basic structure, a virtual motor was added to show the motion of the leg, and later used to ensure the motor is powerful enough to actuate the leg.

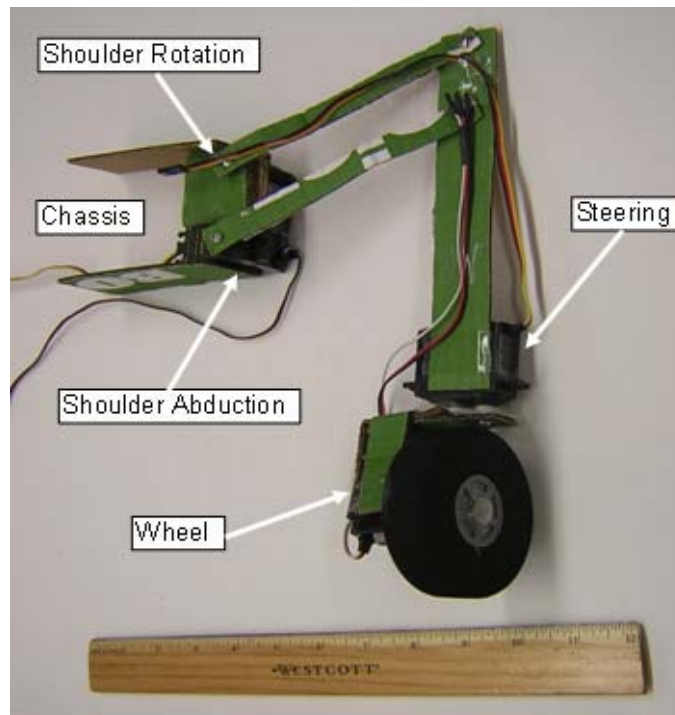


Figure 10: Leg Prototype

After a basic design was determined, a prototype was needed to prove it would provide all necessary functionality. Figure 10 shows a prototype that was built using hobby continuous servo motors and cardboard. The servo motors could be actuated to show the movements of all four joints.

3.4 Construction

Ease of manufacturing and low cost were imperative to successfully creating working legs. All machining needed to be done in the Rochester Institute of Technology Department of Mechanical Engineering Machine Tool Laboratory. The laboratory had a wide range of tools and machines. The ones specifically used to create the legs were the end mills, speed lathes, band saw, drill press, belt sander, and various hand tools.

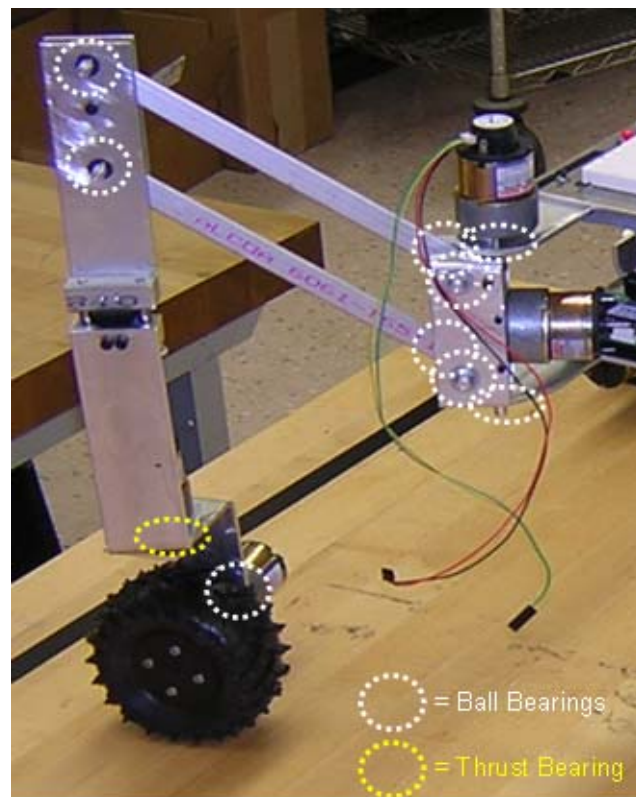


Figure 11: Leg – Mechanical Only

Aluminum was chosen as the material to build the leg components, due to its low weight, high specific strength, low cost, and ease of machining. To keep the legs as efficient as

possible, small flanged ball bearings were specified and used at each joint, as well as small thrust ball bearings on the steering joints. The purpose of these bearings is two fold: 1) they greatly reduced the friction of each joint; and 2) they prevented large transverse and/or axial loads on the motor output shafts.

The design incorporates many ideas to simplify the assembly and disassembly of the robot. E-clips are used throughout to hold all shafts axially. They are easy to implement, but more importantly, easy to remove and replace. Machine screws, set screws, and pins make up the remaining connections.

3.5 Analysis

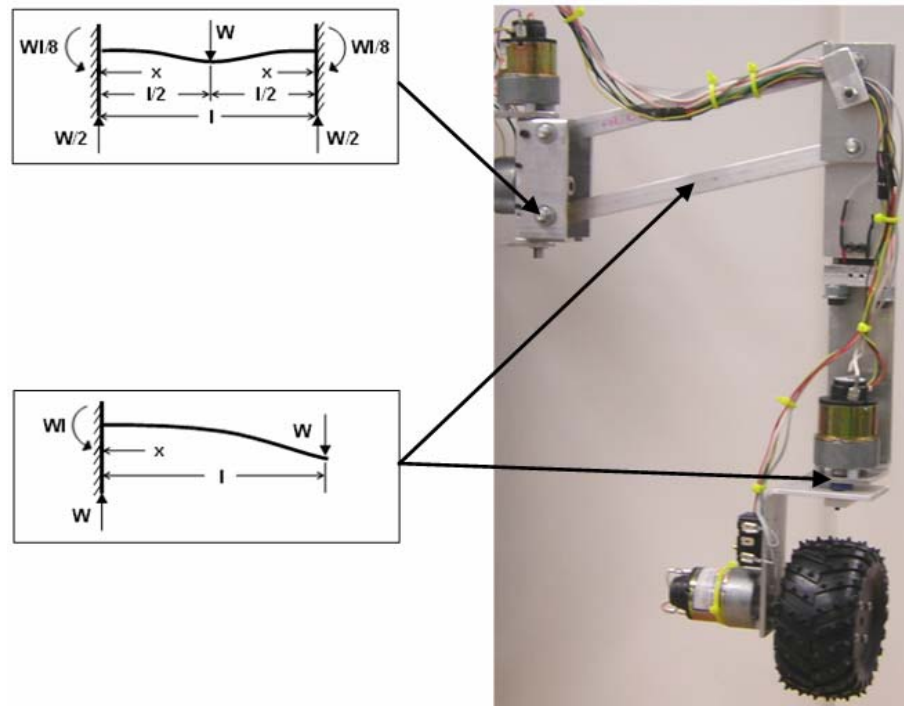


Figure 12: Leg Stress Analysis

The areas of greatest concern for possible mechanical failure are shown in Figure 12. The equations in this section are taken from a machinery handbook [28]. Each segment was intentionally investigated using slightly unrealistic worst case assumptions. These assumptions will be discussed for each area individually.

The right angle formed where the turning motor connects to the “foot” is the first area to be analyzed. There is some elastic deformation that occurs at the angle, effectively reducing the stress on the segment in question. However, to simplify the analysis, it is modeled as a simple cantilever beam that is rigidly fixed at the angle. The resulting calculated stress will be higher than that actually experienced by the member – giving a good worst case scenario. For this type of loading, the maximum stress occurs at the support. This is calculated by using:

$$\sigma_{\max} = \frac{Wl}{2Z} \quad (3.5.1)$$

Where σ_{\max} is the maximum stress, W is the load, l is the length, and Z is the section modulus of the cross-section of the beam. Z is determined by taking the quotient of the moment of inertia of the cross-section from the distance between the neutral axis and extreme fiber. For a rectangular beam with a given width (b) and height (d), Z is:

$$Z = \frac{bd^2}{6} \quad (3.5.2)$$

Since the approximate weight of HAL is calculated as 15 lbs and the worst case scenario would have three legs contacting the ground, W can be assumed to be 5lbs. Inputting the appropriate values into Equation 3.5.1 results in a maximum stress of 0.80 ksi. Knowing that

the yield strength of the aluminum (6061) is 21 ksi [27], a factor of safety of 26 can be shown.

The next area of possible concern is the stresses exerted on the aluminum bar (6061) that transmits motion from the shoulder to the elbow joint. The same worst case assumption is made about the type of loading, as in the previous calculations. It is further assumed that all of the weight is held by the single bar attached to the worm-gear, and that the elbow forms a right angle. Therefore, Equation 3.5.1 is also used to determine the maximum stress. This value comes out to 3.50 ksi, a factor of safety of 6.

The final possibly problematic area is the shoulder joint. The circular rods holding the bars that transmit motion from the shoulder to the elbow make up the weakest part of the entire subsystem. The design has the aforementioned bars bolted directly to the worm-gear. Because of this, and the fact the rods are free to rotate because of bearings on each attachment, there is no torsion experienced by the rods. The only force present is the normal force from HAL's weight. Figure 12 shows the loading conditions. For this type of loading, the maximum stress is:

$$\sigma_{\max} = \frac{Wl}{8Z} \quad (3.5.3)$$

The section modulus of the cross-section of a cylindrical beam is:

$$Z = \frac{\pi d^3}{32} \quad (3.5.4)$$

Where d is the diameter of the rod.

The resulting maximum stress is 0.61 ksi. The rods are made with the same type of aluminum as the rest of the leg, giving a factor of safety of 35.

The calculations presented in this section show the safety of HAL's legs. Even under harsh worst case conditions, safety can be assured. The worm and worm-gear combination is another possible area of concern. A safety analysis of this subsystem is presented in a later section.

3.6 Tests

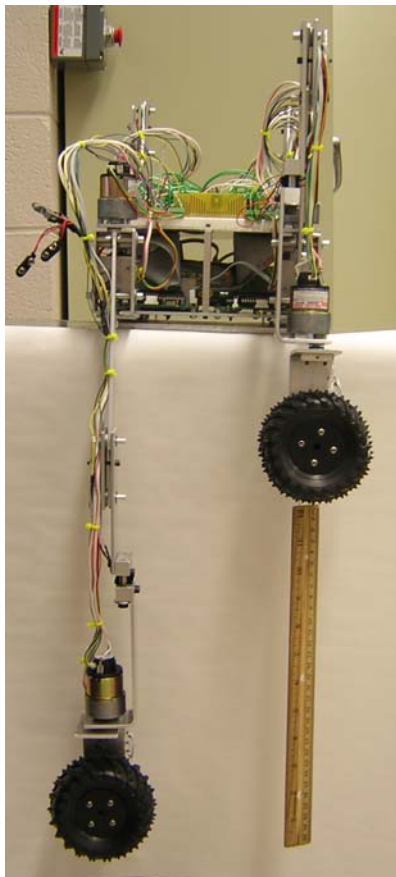


Figure 13: Total Leg Stroke

The leg is able to move freely about all four DOF. Figure 13 shows the total stroke of each leg, which is approximately twelve inches – the total length of the ruler shown. That means, when operating with hybrid locomotion, HAL should be able to get over objects under 1 ft tall. More analysis involving HAL's legs will be given later on in this document.

3.7 Conclusion

The legs are successfully designed and built to be able to perform wheeled rolling locomotion, limited legged walking locomotion, and hybrid rolling/walking locomotion. They are able to efficiently and effectively move about all necessary DOFs. No problems were encountered when trying to carry loads on flat surfaces.

The biggest issue with the current leg design is stability. The elbow joint was originally too loose, causing problems with HAL's steadiness. A slight modification, which included the addition of another piece of aluminum plate to the elbow, significantly reduced the instability. Even after that fix, there is still too much slack in the entire leg system, creating problems with pure walking.

4 Motor Selection

4.1 Needs

After doing a feasibility analysis of all the different joint actuation options, it was decided to use a motor. Since alternating current (AC) is not common place in robotics and is much harder to implement, direct current (DC) was chosen. AC motors are also very hard to use where speed control is needed. It was decidedly beneficial to have identical motors. This is helpful for ease of design, construction, and also for controlling the robot. If all motors perform the same, the time associated with coding and testing will be reduced. The motors reaction to power electronic signals remains constant throughout all of HAL's systems.

There are many factors that must be taken into consideration when trying to choose the most optimal motors for HAL. An exhaustive search was performed to find the best choice. All types of DC motors were researched, including brushed, brushless, stepper, spur gear-head, planetary gear-head, and servo. The criteria used to choose a motor is listed below:

1. *Cost:* With four motors per leg, and four legs total, the price associated with buying and shipping sixteen motors can easily become significant.
2. *Torque and Weight:* The ratio of weight and torque is the overriding factor. The motor responsible for shoulder abduction needs to have a large enough stall torque to be able to lift an entire leg. Since the largest percentage of leg weight belongs to the other three motors, the weight had to be as small as possible. The manufacturer's

- values given for torque and weight were inputted into the leg Working Model simulation (Figure 9) previously discussed to ensure successful operation.
3. *Voltage and Current*: The voltage and current ratings have to be within a range feasible for commercially available batteries. Robotics retail and hobby web sights are the best for finding motor and battery combinations for relatively low cost.
 4. *Strength*: The strength of the motor shaft and the ability to withstand axial and transverse loads is important. Some smaller plastic servos were immediately eliminated because of their low strength ratings.
 5. *Position Control*: Being able to actively track the position of each motor is imperative to coordinating the operation of HAL's systems. While stepper motors are very appealing in this sense, they are lacking in many other areas. For other types of motors, providing an encoder output shaft is a huge advantage, and is outlined later in this document.
 6. *Speed*: The angular speed, usually rated as revolutions per minute (RPM), is not a deciding factor. Most of HAL's joints require small precise movements where the typical DC motor would never get close to full speed, or even 50% duty cycle.

4.2 Design

Simultaneous to searching for the ideal motor to meet all necessary criteria, it became necessary to design a way to give the shoulder abduction motor a further mechanical advantage. It became obvious early on in the motor search that no motor combination can give the torque required to effectively raise and lower the leg. A secondary problem is the ability to manually drive the motors with the output shaft when they are not active. This

means the legs would sag due to the weight of the chassis, if not actively held in place. Actively holding the shoulder joint would use a significant amount of energy, as well as a complicated control system.

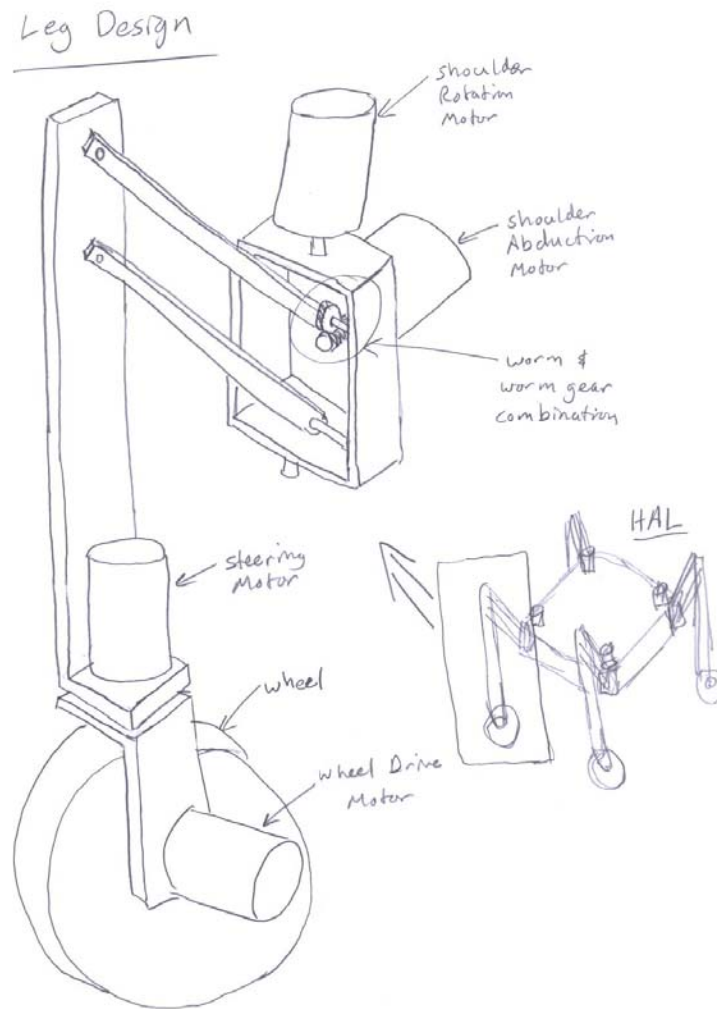


Figure 14: Preliminary Leg Sketch Showing Motor Positions

After looking at several different methods for gaining a mechanical advantage (i.e. gear, belt, pulley, and lever combinations), a worm and worm-gear combination was chosen. The most

cost effective combination gave a gear ratio of 30:1. Unlike ordinary gear trains, the direction of transmission is not reversible on the worm-gear. This eliminates the possibility of the output driving the input, and is said to be “self-locking” [29]. The shoulder abduction joint will only move when desired and driven by the control system. Figure 14 shows the preliminary sketch created during the design process. This sketch was important in determining the layout of the motors, and also shows the placement of the worm and worm-gear. A photograph of the final shoulder abduction system is shown in Figure 15. Alignment of the gears was tricky during the building process, as well as determining the best way to attach the components to the shafts. Pins were chosen over set screws because of their ability to hold larger loads, and because they eliminate the problem of slipping.

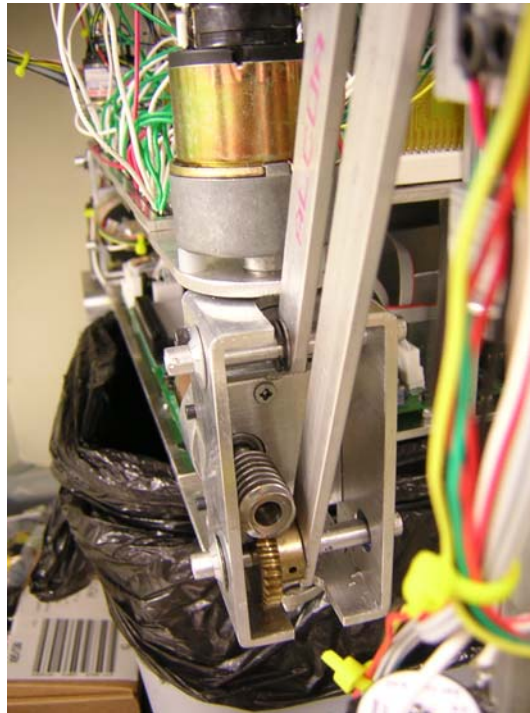


Figure 15: Shoulder Abduction Worm and Worm-gear

The motor that was finally chosen for all sixteen joints was a spur gear-head motor. It is a 7.2V motor, with 50:1 gear-head ratio, no load RPM of 175, and stall torque of 99.04 oz-in [30]. With a weight of only 119g, the ratio of torque to weight is comparatively higher than the vast majority of other motors. More specifications are given in the appendix. One of the most desirable aspects of this motor is the existence of a second output shaft, specifically designed for use with an encoder. This shaft is connected directly to the motor armature, giving a very fine resolution for the highly geared-down output shaft.



Figure 16: Selected Gear-motor [30]

Mounting the motors on the robot is not a trivial task, due to the complicated mounting pattern and the off-center output shaft (Figure 17). All of the holes drilled for the screws and bearings must be within tight tolerances to ensure proper alignment. A hub had to be specially modified to attach the wheels to the driving motors.

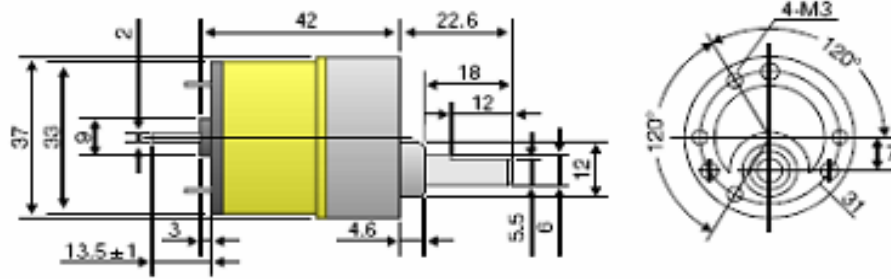


Figure 17: Gear-motor Dimensions and Mounting Pattern (mm) [30]

4.3 Analysis

4.3.1 Stress

An analysis was performed to ensure the worm and worm-gears will be able to handle the forces that will be exerted on them. Because worm teeth are inherently much stronger than worm-gear teeth, they will not be considered in the stress analysis.

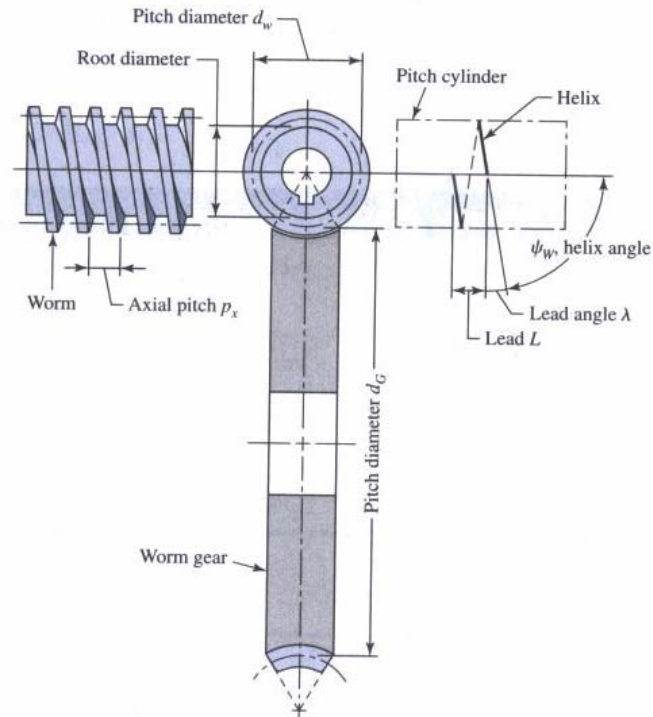


Figure 18: Worm and Worm-Gear Mesh [31]

The following equations are based on information given in a mechanical engineering design text book [31]. Variables with a subscript of “W” are those related to the worm, and those with a subscript of “G” are related to the worm-gear.

First, the tangential diametrical pitch (P_t) must be determined. This can be found knowing the total number of worm teeth (N_w), given as 7 teeth, and the total lead length (L_w), given to be 11/16 in.

$$P_t = \frac{N_w}{L_w} \tag{4.3.1}$$

This yields a tangential diametrical pitch of 10.18 teeth/in. The axial pitch (P_x) can then be calculated by the following:

$$P_x = \frac{\pi}{P_t} \quad (4.3.2)$$

The normal circular pitch (P_n) is related to the axial pitch and lead angle (λ), using:

$$P_n = P_x \cos(\lambda) \quad (4.3.3)$$

The normal circular pitch is calculated to be 0.308 in.

The next step is to solve for the magnitude of the gear transmitted force (W_G^t), which is related to the output horsepower (H_o), the application factor (K_a), the tangential speed (V_G), the efficiency (e), and the design factor (n_d) by:

$$W_g^t = \frac{33000n_d H_o K_a}{V_G e} \quad (4.3.4)$$

To calculate the tangential speed, the angular speed must first be determined. The motor characteristic curves, provided by the manufacturer in Figure 22, can be used to find the worst case speed for raising the leg. The angular speed of the worm-gear is related to the torque needed to actuate the leg, in order to raise the robot. Since the approximate weight of HAL is calculated as 15 lbs and the length of the first leg segment is 7.25 in, the torque needed to raise a worst case load (3 legs contacting ground) is 36.25 in-lbs. Dividing by the mechanical advantage of 30 and converting to the units given on the curve, the torque at the gear-motor is 1.40 kg-cm. Finding this value on the RPM curve gives an angular speed (n)

of about 140 RPM for the worm and 4.67 RPM for the worm-gear (using the 30:1 gear reduction).

The tangential speed of the worm-gear can simply be found, knowing the angular speed and the pitch diameter (d).

$$V_G = n_G d_G \quad (4.3.5)$$

The efficiency of the meshed gears is:

$$e = \frac{\cos \phi_n - f \tan \lambda}{\cos \phi_n + f \cot \lambda} \quad (4.3.6)$$

Where f is the coefficient of friction and Φ_n is the pressure angle. While the pressure angle is given as 14.5° , the coefficient of friction must be determined. The American Gear Manufacturers Association (AGMA) reports the coefficient of friction as:

$$f = \begin{cases} 0.15 & V_s = 0 \\ 0.124 \exp(-0.074V_s^{0.645}) & 0 < V_s \leq 10 \text{ ft/min} \\ 0.103 \exp(-0.110V_s^{0.450}) + 0.012 & V_s > 10 \text{ ft/min} \end{cases} \quad (4.3.7)$$

The sliding velocity (V_s) must now be calculated to determine the proper equation for the coefficient of friction. This is solved using the equation:

$$V_s = \frac{\pi \cdot d_w n_w}{12 \cos \lambda} \quad (4.3.8)$$

This equation results in a sliding velocity of 16.1 ft/min. Looking at Equation 4.3.7, the coefficient of friction is given by the third equation, and is 0.0821. Inserting the values from Equation 4.3.7 and Equation 4.3.8 into Equation 4.3.6, results in an efficiency of 45.5%.

The output horse power is defined using torque (T) and angular velocity [32]. For the worm-gear, this equation is:

$$H_o = \frac{T_G(ft-lb) \cdot n_G(RPM)}{5252} \quad (4.3.9)$$

Since the character of the prime mover is uniform and the character of the load on the driven machine has light shock, a design factor of 1 and an application factor of 1.25 are used. Inserting this and the values found in Equation 4.3.5 - 4.3.9 into Equation 4.3.4, the gear transmitted force is 212.5 lbs.

The next step is to determine the worm-gear face width (F_G) which is determined by:

$$F_G = \begin{cases} 2d_m/3 & p_x > 0.16in \\ 1.125\sqrt{(d_0 + 2c)^2 - (d_0 - 4a)^2} & p_x \leq 0.16in \end{cases} \quad (4.3.10)$$

Where d_0 is the worm outside diameter, a is the addendum, and c is the clearance. Since the axial pitch is greater than 0.16 in, the face width is 0.625 in.

The stress experienced by the worm-gear teeth (σ_G) can now be solved. Buckingham adapted the Lewis equation for this case [33].

$$\sigma_G = \frac{W^t_G}{P_n F_G y} \quad (4.3.11)$$

The value of y is a function of the pressure angle, and is given as 0.100. The stress is found to be 11.0 ksi for the worst case scenario. With a yield strength of 40 ksi for the worm-gear

brass composite, the factor of safety is 3.6. This means the worm and worm-gear combination should be able to easily handle all stresses acted on them during testing.

4.3.2 Kinematics

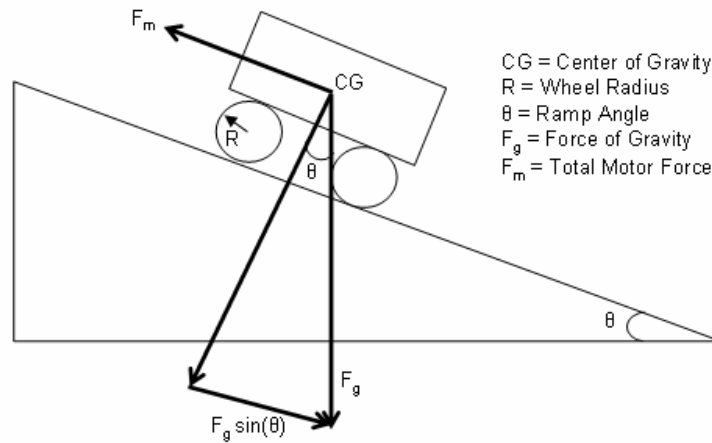


Figure 19: Ramp Free Body Diagram

To determine if the motors are powerful enough to drive HAL up a ramp, a kinematic analysis was performed. Figure 19 physically illustrates the properties used. Assuming there is no wheel slip, no vehicle acceleration, and T is the stall torque of the motor:

$$F_m = \frac{T}{R} \quad (4.3.12)$$

$$F_m = F_g \sin(\theta) \quad (4.3.13)$$

Combining equations 4.3.12 and 4.3.13 and solving for θ will give the maximum ramp angle HAL will be able to drive up using rolling locomotion.

$$\theta = \sin^{-1}\left(\frac{T}{R \cdot F_g}\right) \quad (4.3.14)$$

The stall torque (T) is given by the manufacturer to be 99.04 oz-in, the radius of the wheels (R) is 1.875 in, and the total weight of HAL (F_g) is measured to be 15.4 lbs. Substituting these values and multiplying the stall torque by four (four wheel drive) results in a maximum ramp angle (θ) of 59.0°. This shows the motor selected has more than enough torque to go up any reasonable ramp. The wheels would likely slip well before a drive motor would stall.

4.3.3 Scrubbing

Next, the steering motor needed to be analyzed to ensure it has enough torque to overcome the friction due to wheel scrubbing. Scrubbing resistance is the torque required to twist a wheel around its vertical axis. During steering, a wheel is scrubbing against the surface it is rolling over. Scrubbing torque can be calculated by integrating the frictional force elements over the entire contact patch between the wheel and the ground. This calculation is difficult because of the shape of the contact patch and the pressure distribution that can be determined using the Hertzian contact model that is a function of the load, the compliance, and the profile of the wheel. Nevertheless, this torque will be estimated based on assumptions made about the contacting patch and pressure distribution. The following model is based on work done at Massachusetts Institute of Technology [34].

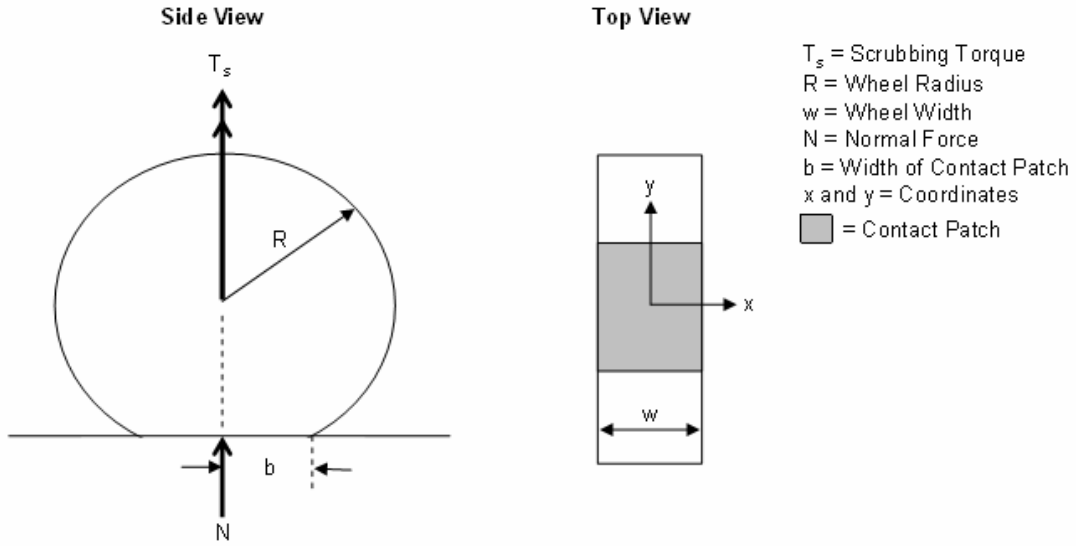


Figure 20: Wheel Scrubbing Diagram

Assuming a simple rectangular pressure distribution for the wheel, as shown in Figure 20, the scrubbing torque is estimated as:

$$T_s = \frac{2\beta\mu N}{wb} \int_0^b \int_0^{w/2} \sqrt{x^2 + y^2} dx dy \quad (4.3.15)$$

Where β is the correction factor, which is 0.3 assuming the pressure is evenly distributed.

The coefficient of static friction (μ) is estimated to be approximately 0.8, after reviewing the ASTM D-2047 standard used for the Federal Standard for Floor Friction [35]. The wheel radius and weight used to calculate the normal force (assuming even distribution over all four wheels) are the same as those used in equation 4.3.14. Since the deformation of the wheel is 5%, b is assumed to be $0.3R$ [34].

Inputting the variable values into equation 4.3.15 yields a scrubbing torque of 0.58 in-lbs.

The motor stall torque, which is 6.19 lb-in, is over ten times the value needed to overcome the estimated static friction. Therefore, there are no foreseeable problems with the steering motor with regard to torque output.

4.4 Testing

4.4.1 Dynamometer

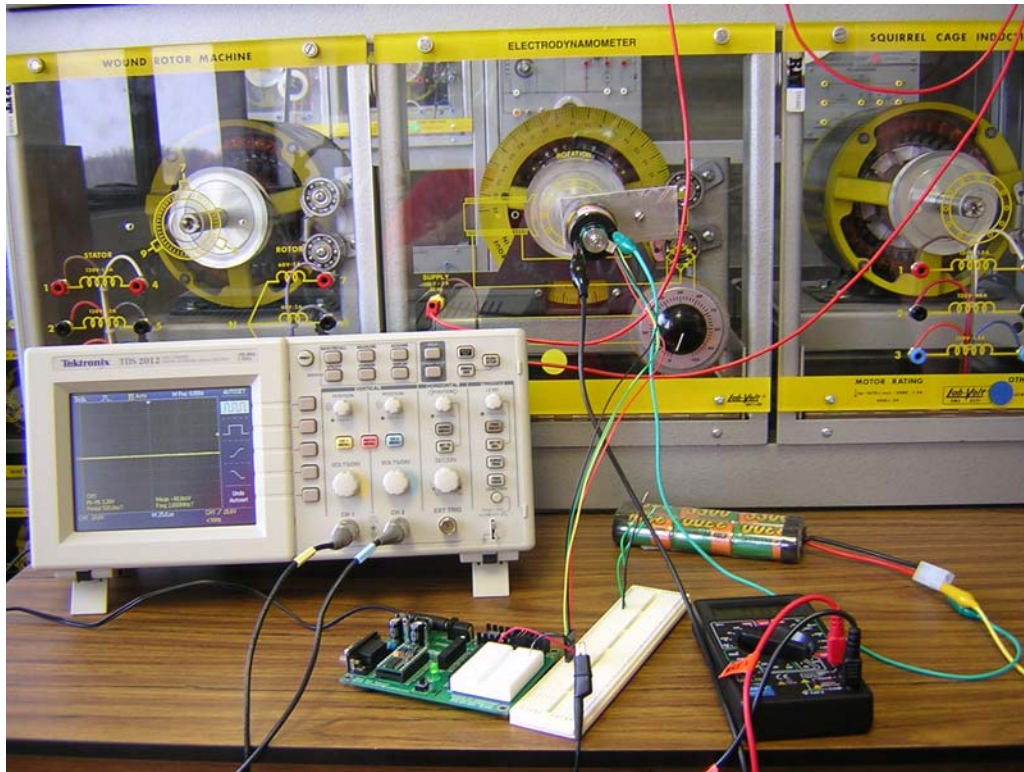


Figure 21: Dynamometer Test Setup

Although the manufacturer provided motor characteristic curves, it was deemed prudent to confirm the data. A test was run with an electric motor dynamometer that is calibrated up to

27 in-lbs. The setup used is shown in Figure 21. The dynamometer (manufactured by Lab-Volt) was used to measure the gear-motor output torque, the motor was powered by a NiMH battery pack (GP TC204; 7.2 V and 3300 mAh), the current was measured using a multimeter (Jameco BP-1562), and the speed was derived using an oscilloscope (Tektronix TDS2012; 100 MHz) that read incremental encoder output frequencies.

Once the data was collected, a few mathematical operations were needed to calculate the variables used in the equations depicted in Figure 22. The motor RPM was determined using the encoder frequency (f) and dividing by the known number of counts per revolution (N) of the output shaft.

$$RPM = \frac{f}{N} \quad (4.4.1)$$

The motor mechanical power (P_m) was calculated by multiplying the torque (T) by the angular velocity (ω).

$$P_m = T \cdot \omega \quad (4.4.2)$$

The efficiency (eff) was then determined by dividing the electrical power (given in Equation 1.3.1) by the mechanical power (P_m).

$$eff = \frac{V \cdot I}{P_m} \quad (4.4.3)$$

The results are shown in Figure 22.

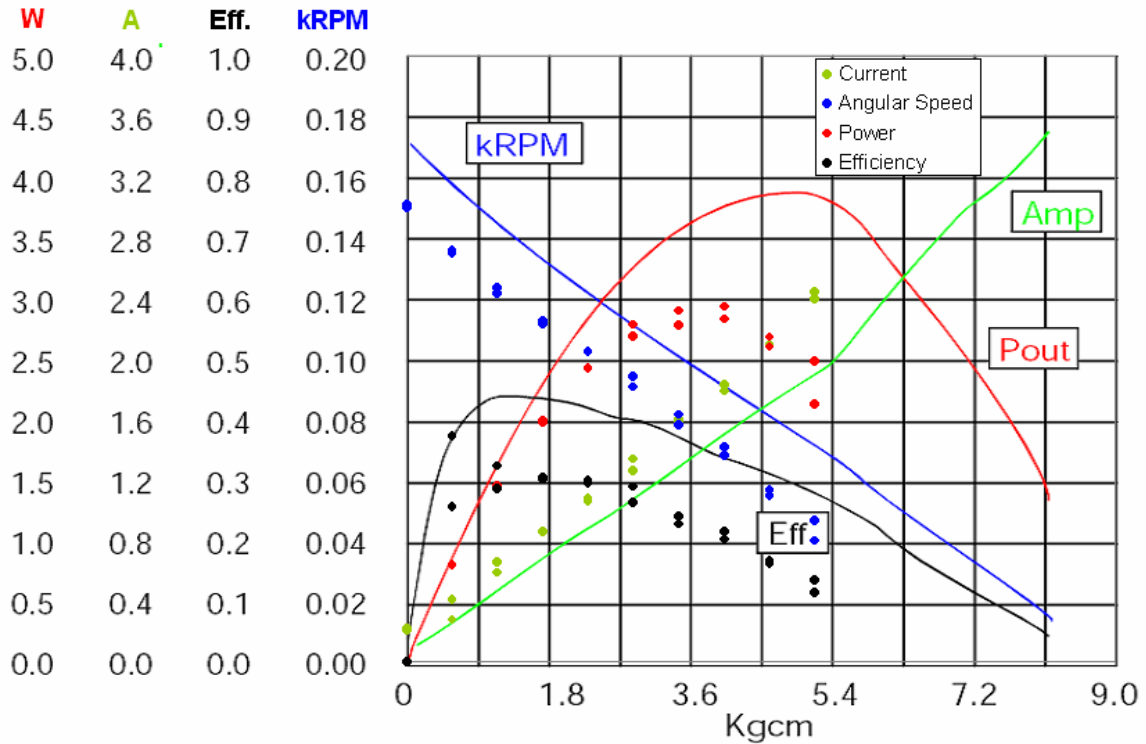


Figure 22: Dynamometer Experimental Results Superimposed with Manufacturer's Data [30]

The torque shown on the x axis of Figure 22 is given by the manufacturer in units of kg-cm. This unorthodox use of kilograms as force is assumed to be equivalent to the mass in kilograms multiplied by the acceleration due to gravity. The acceleration due to gravity is further assumed to be 9.80665 m/s^2 , resulting in a relationship of 1kg-cm being equivalent to 0.80665 N-cm. To simplify the analysis and discussion, this torque convention is used throughout this document.

The results of Figure 22 show that the motor specifications provided by the manufacturer are slightly better than those determined experimentally. While the curves follow the same

pattern, the experimental results are all approximately 10% lower. These losses are likely caused by energy escaping due to an imperfect connecting system between the motor and the dynamometer. Unfortunately, the dynamometer was unable to stall the motor, and reading could only be taken up to 4.5 in-lbs.

4.4.2 Efficiency

Once HAL was built and running, the actual efficiency of the entire system that raises and lowers the leg could be evaluated. Since the motor responsible for shoulder abduction can not be rotated continuously while installed, another method must be used. Knowing that the voltage remains constant, the torque constant can be used to determine the loss in efficiency. The torque constant is defined as the amount of torque the motor produces at a given level of current consumption [36]. Since the current versus torque is linear, a constant relationship can be derived. Using the experimental data collected, a linear trend line was added to the current values (Figure 23). This trend line gave a torque constant of 0.426 A/kg-cm.

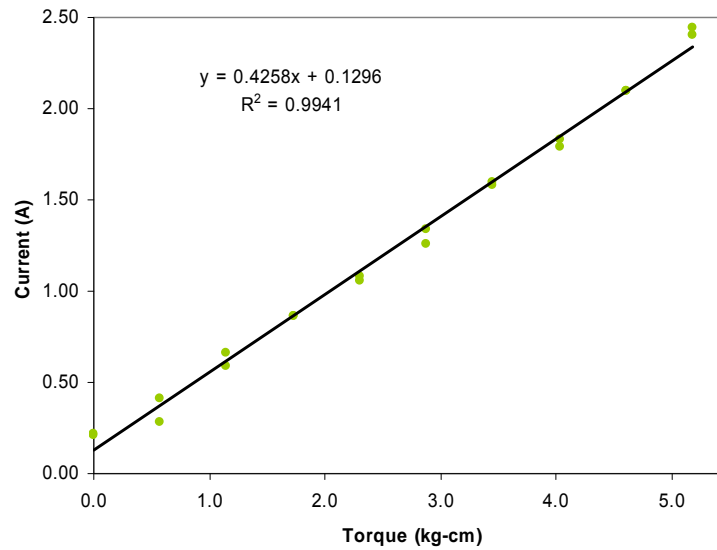


Figure 23: Motor Torque Constant Trend Line

To determine the torque constant for the shoulder abduction motor, HAL was suspended and held by the chassis. The leg was raised using the same velocity as that used for the dynamometer test. The torque was calculated by determining the moment of the leg by itself. The mass of the motor and encoder combination was measured to be 129.6 g, and the mass of the wheel and hub combination was measured to be 120.1 g. The remaining mass to be lifted can be attributed to the aluminum pieces. These mass (m) values can be calculated knowing the material density (ρ) and volume (v) by using the following equation:

$$m = \rho \cdot v \quad (4.4.4)$$

The masses must then be multiplied by the length of the lever arm (l) to determine the torque (T) required to lift the leg.

$$T = m \cdot l \quad (4.4.5)$$

The resulting torque (T) is 5.69 kg-cm. The current (I) required to lift the leg was experimentally determined to be 1.10 A. The torque constant (τ) can then be calculated.

$$\tau = \frac{I}{T} \quad (4.4.6)$$

The torque constant for the entire leg raising and lowering system is 0.193 A/kg-cm. The efficiency of this system can then be calculated by taking the ratio of the torque constant determined by actuating the leg (0.193) to the torque constant determined using the dynamometer (0.426); which comes out to 45.3 % efficient.

4.5 Conclusion

All sixteen motors on HAL have performed their function successfully. The worm and worm-gear combination used for shoulder abduction provides sufficient torque to raise the leg and to carry the weight of the entire robot. Although the efficiency of the entire leg raising and lowering system is below 50%, it is far from uncommonly low for worm-gears [29]. This value is likely significantly reduced because of the added support needed to keep the legs steady. The original design had much less friction, but there was too much slop (free play in the mechanical system) present.

5 Position Feedback

5.1 Needs

Position feedback is very important to HAL's locomotion. Since the torque experienced by each motor constantly varies, without feedback, there is no accurate way of telling how far a joint has moved. For successfully controlled locomotion, every movement has to be precise. Even when the motor is not energized, it is imperative to have a method for determining if a joint is moved due to outside forces. The relative position of each leg needs to be constantly updated.

Future work involving HAL may also include the need for mapping or global position sensing of the platform as a whole. Feedback on distance traveling, and in which direction, could make this possible.

5.2 Concepts

A large amount of research and testing has been done on robot position sensing. The most common methods, where motors are involved, use some sort of rotary displacement sensor. These sensors can come in many forms. Potentiometers are rotary variable resistors, whose resistance increases or decreases as a shaft is rotated. Most are not designed for continuous rotation, and have stops that prevent it from rotating further. They also have issues with wear and give non-linear output. For these reasons, potentiometers are often not as reliable as and harder to implement than other methods.

Rotary encoders are probably the most typical method for determining motor shaft position. There are two main types of rotary encoders: absolute and incremental. Absolute encoders produce a unique binary code for each distinct angle of the shaft, usually by using a disk with a set pattern of light and dark spots. Incremental encoders also use a disk, but are marked with a large number of radial lines – like the spokes of a wheel. Both types of encoders generally have an optical switch that generates an electrical pulse whenever one of the lines passes through its field of view [37].

Hall Effects sensors vary the output voltage in response to changes in the magnetic field density. Frequently, a Hall sensor is combined with circuitry that allows the device to act in a digital mode. They are commonly used in industrial applications in pneumatic cylinders, but can also be used on rotary shafts [38].

There are also many, more novel, approaches to determining robot extremity position. These tend to focus more on the overall location of the leg, rather than the position of each individual DOF. One method uses different forms of inertial navigation that implement Newton's laws of motion. Position sensing is achieved by utilizing inertial instruments, such as accelerometers and gyroscopes [39]. The main drawback is that typically the overall error grows with time. Inertial positioning systems are expensive, hard to implement, and hard to program/control.

Research has also been done with tracking robot legs using various forms of visual tracking. However, this is not yet a feasible approach for widespread use. Another hard to implement

method to improve position control is force control. A flexible gear system can be designed between the motor and load, by which the force on the gear can be measured [40]. This input can be used to characterize the robot's physical interaction with its environment.

5.3 Design

The complicated and/or expensive approaches were quickly ruled out for position sensing. Since encoders are the most common and simple method for keeping track of shaft position, that is the most obvious choice. The gear-motor that was selected also has a shaft protruding from the back, specially designed to attach to an encoder wheel. While absolute encoders would work, quadrature incremental encoders typically have a higher resolution and can be used for determining the direction the output shaft is rotating.



Figure 24: Encoder on Gear-motor

A quadrature encoder that can be easily implemented and used was selected. This encoder has a wheel containing 120 counts per revolution. With the 50:1 gear ratio, that gives 6000 total counts for each revolution of the gear-motor output. The resolution can then be

calculated to be 0.06° per encoder count. The readable incremental change in motor position is more sensitive, accurate, and repeatable than the system it is incorporated into. The amount of mechanical slop in the shoulder joint is significantly greater than 0.06° . As long as counts are not missed, this will give excellent position data.

Another nice feature about incremental encoders is the ability to easily implement speed or acceleration control. The frequency of the counts can be determined and used programmatically to decide to increase or decrease the voltage seen by the motor. This provides HAL with the ability to autonomously control all aspects of motion.

5.4 Theory

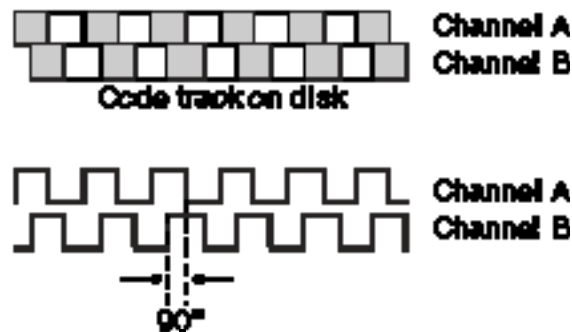


Figure 25: Quadrature Encoder Fundamentals [41]

The quadrature encoder uses two output channels (A and B shown in Figure 25) to sense position. The sensors read the code track 90° out of phase. This gives the ability to indicate both position and direction of rotation. If A leads B, the disk is rotating clockwise. If B leads A, the disk is rotating counter-clockwise.

A simple way to programmatically use a quadrature encoder to read position and direction is through the use of an interrupt. Channel A can be continuously monitored to count the number of pulses outputted by the encoder. Every time the value of Channel A switches from a low to high value, channel B can be checked. If, at that instant, Channel B is low, the disk is rotation clockwise; and a variable can be incremented. If Channel B is high, the disk is rotating counter clockwise; and the same variable can be decremented.

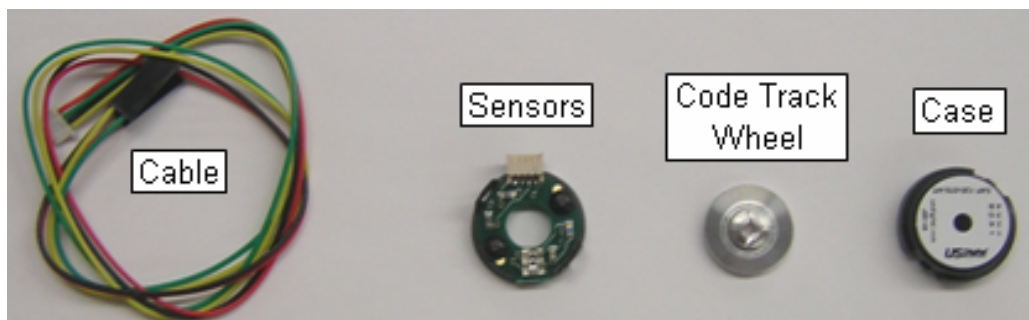


Figure 26: Encoder Components

Figure 26 shows the encoder components used on HAL. The encoder base (labeled “sensor”) is a circuit board that utilizes infrared sensors to read the code track light and dark spots. This version utilizes an innovative push-on hub disk assembly, meaning no set screw is required. A pre-applied transfer adhesive is used for mounting the encoder base onto the motor [42]. The kit also includes a snap-in polarized connector with color coded wires.

With the use of quadrature encoders, “dead reckoning” can be implemented. Dead reckoning is the process of estimating the current global position based upon a previously determined position and advancing that position based upon known speed, elapsed time, and course [43].

In HAL's case, the encoders can be used to give data about the movement of each motor. This data can be recorded and evaluated to give position estimates for each leg and for the robot as a whole. An analysis of HAL's dead reckoning abilities is presented in the next section.

5.5 Testing

5.5.1 Output

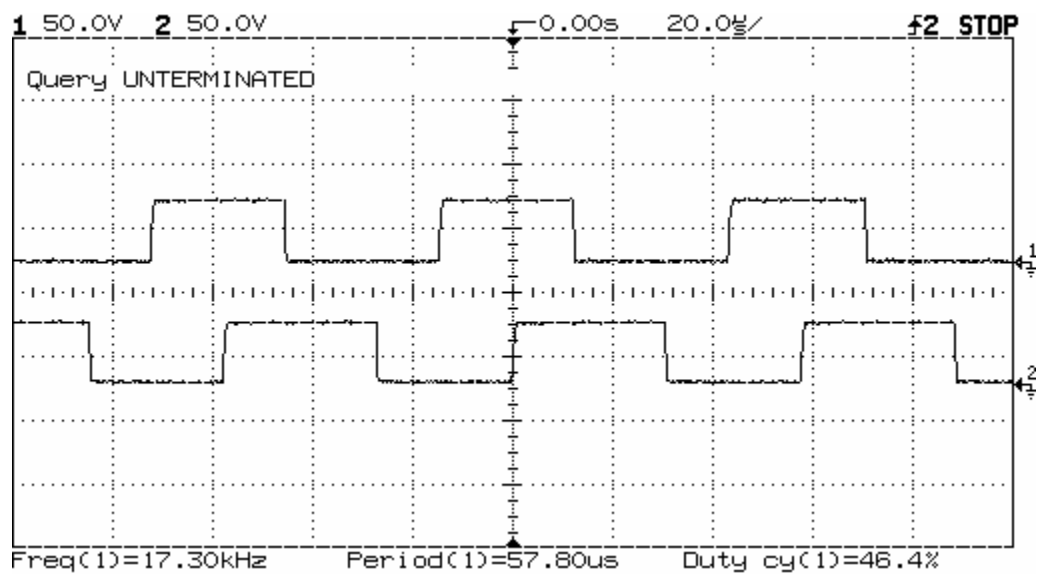


Figure 27: Encoder Output

To ensure proper operation, the output of both channels needs to be checked and characterized. Figure 27 shows the output of both channel A and B, as read on an oscilloscope (Agilent 54622D; 100 MHz). Both channels have nice square waves with a duty cycle of approximately 50% (high half of the time, and low half of the time). As

expected, the channels are 90° out of phase with each other, meaning they can effectively be used for determining motor direction.

For this experiment, one of HAL's wheel motors was run at full speed. The frequency was measured to be 17.30 kHz, which translates to a gear-motor speed of 2.88 RPM. The period of the pulses is $57.80 \mu\text{s}$. The high pulses give a value of 5V, and the low pulses are 0V.

5.5.2 Steering

The next test was meant to verify the displacement reading taken from the encoders. The steering motors were used to show that HAL can not only turn a motor to a given position, but also track the movement throughout the motion. A program was written utilizing internal data storage, described later in this document. This provided data in the form of angular position versus time.

HAL was programmed to turn a specific steering motor 90° counter-clockwise, then 270° clockwise, and finally 180° clockwise back to the starting point. HAL recorded the encoder positions approximately every half second (frequency of 2.007 Hz – due to microcontroller limitations). While this test was being conducted, a video was recorded (Figure 28) with a stop watch that was synchronized with the internal clock used in HAL's data collection. This video can be used as a truth model to determine the effectiveness of the encoders.

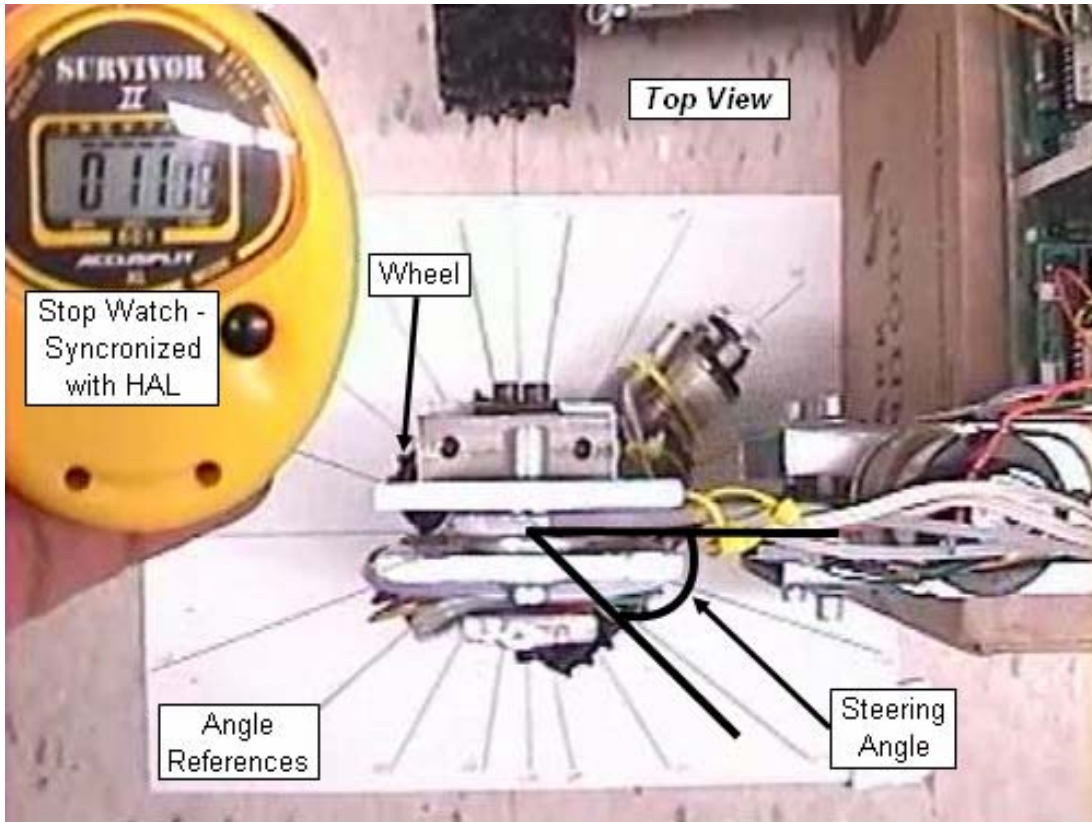


Figure 28: Steering Encoder Test Video Screen Shot

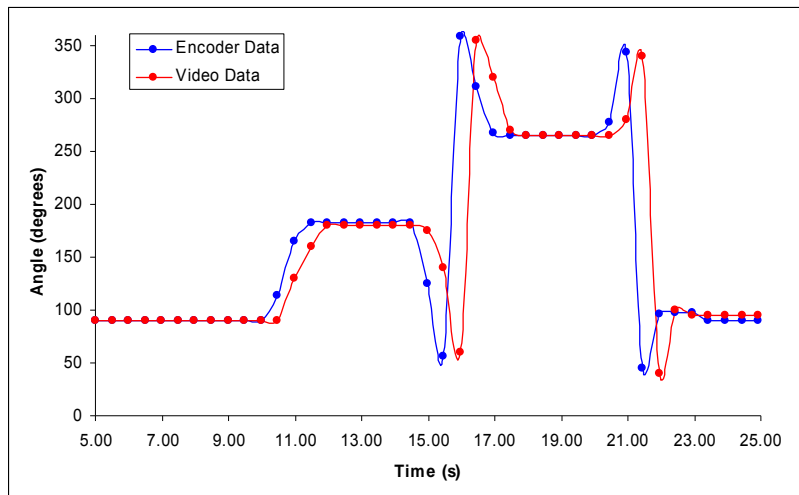


Figure 29: Steering Encoder Test Run 1 Data

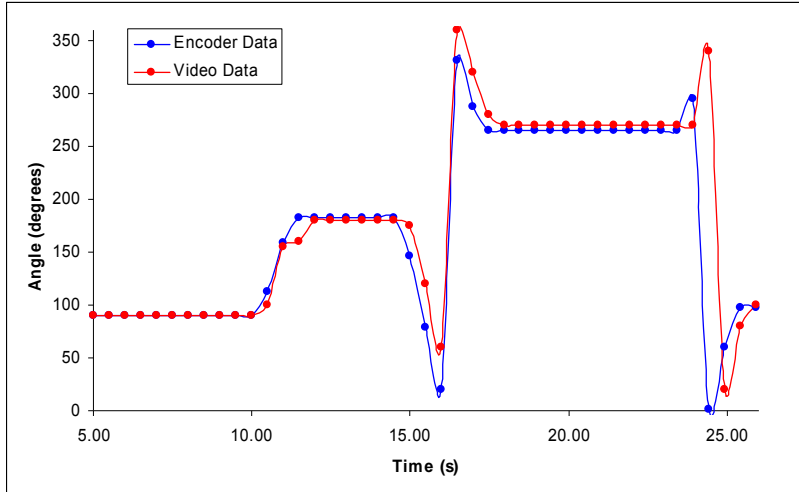


Figure 30: Steering Encoder Test Run 2 Data

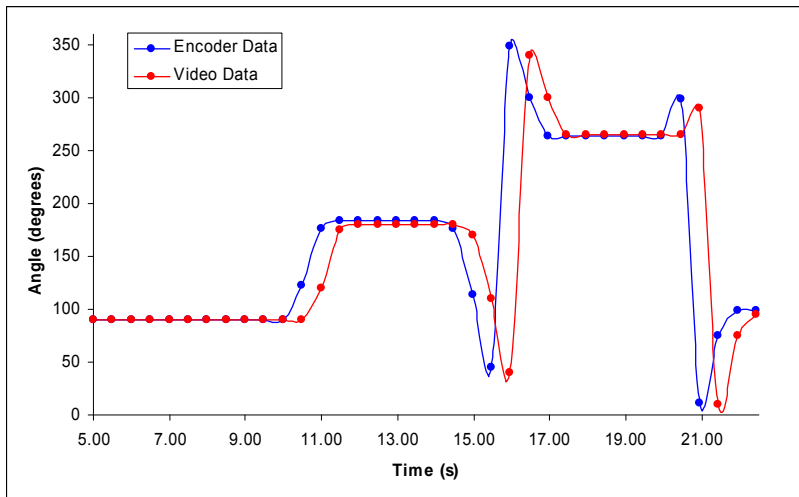


Figure 31: Steering Encoder Test Run 3 Data

The comparison of the data collected by HAL and that given in the video can be seen in Figure 29 – Figure 31. The two data series match up very well, with the exception of a small

phase shift along the x-axis (time). This can be explained by operator error when starting the stop watching, making the clocks slightly out of sync.

5.5.3 Dead Reckoning

Another test was performed at a much broader platform level. HAL's dead reckoning capabilities were put to the test. A program was written utilizing internal data storage. This time HAL rolled down a hallway, while simultaneously storing encoder data. A video recording was used in a similar fashion as in the previous test. The tiles in the hallway were used for the global coordinates (shown in Figure 32), and were measured to be 12 in in both dimension. The clock given by the camcorder (shown in Figure 33) was used to time the test.

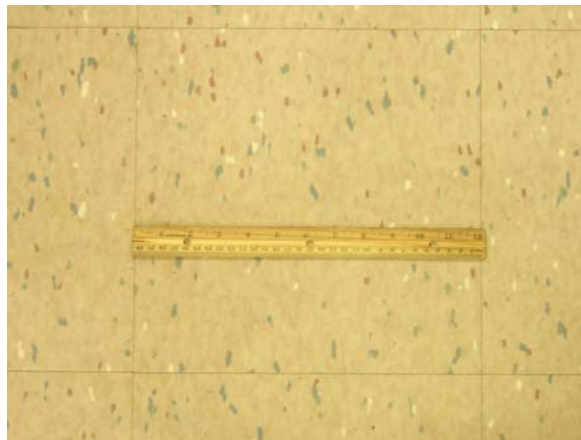


Figure 32: Tile Dimensions

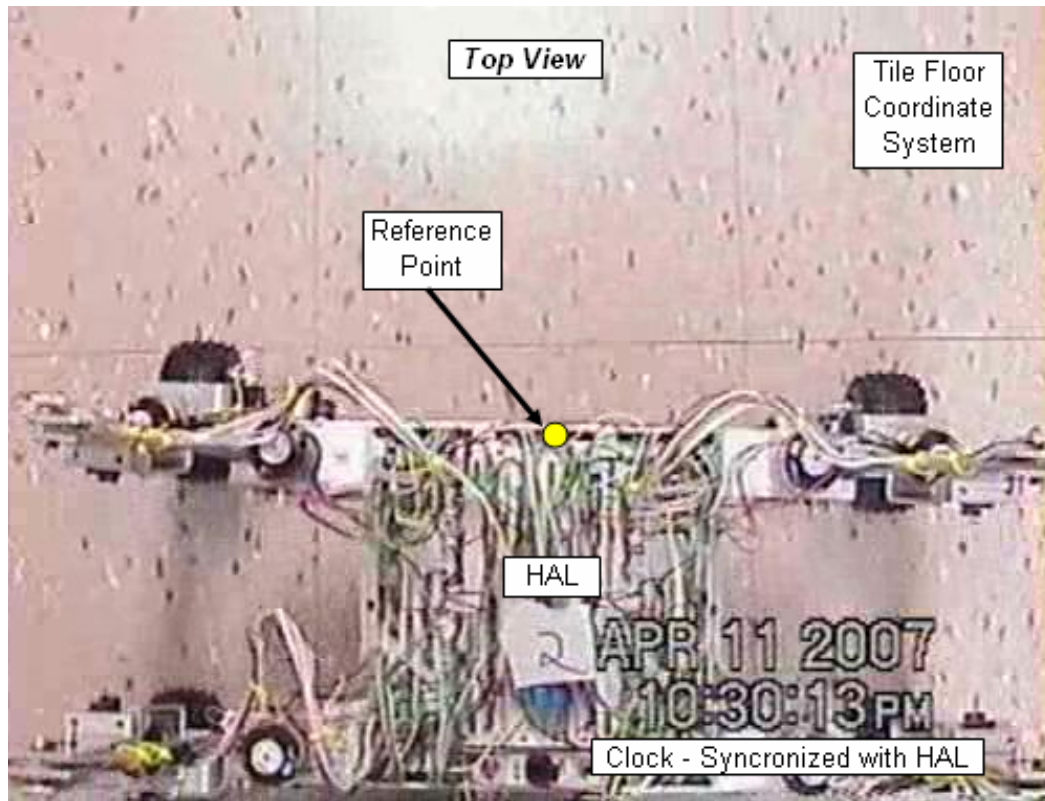


Figure 33: Dead Reckoning Test Video Screen Shot

The discrepancy between the encoder dead reckoning data and the actually video evidence must now be compared. The first step is to convert the stored encoder rotational displacement values into a meaningful form that give the global robot position. The following model is based on work done by a previous Rochester Institute of Technology student [39].

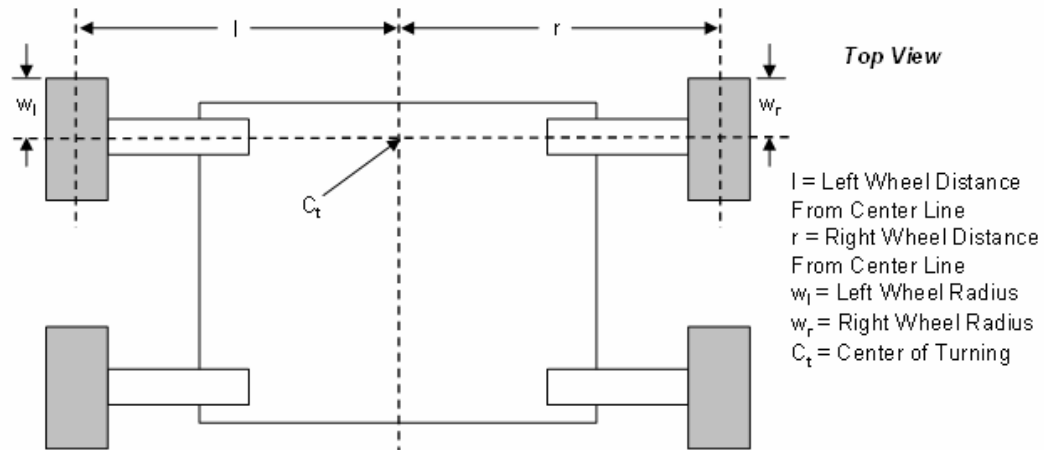


Figure 34: Robot Model

To simplify the analysis of HAL's dead reckoning to make it manageable, only the front two wheels will be taken into account. Assuming all four wheels remain parallel with the chassis and all four legs remain static, the position of the front two wheels are representative of the robot as a whole. Figure 34 shows the robot model and dimensions that will be used for the dead reckoning calculations. The center of turning (C_t) is a fixed point at the horizontal center of the chassis and directly between the centers of the front two wheels. The distances to the left and right wheels (l and r) and the left and right radii (w_l and w_r) are kept constant. The intent here is to track the path of C_t as the robot moves through its course. Further relationships will now be developed to achieve this goal.

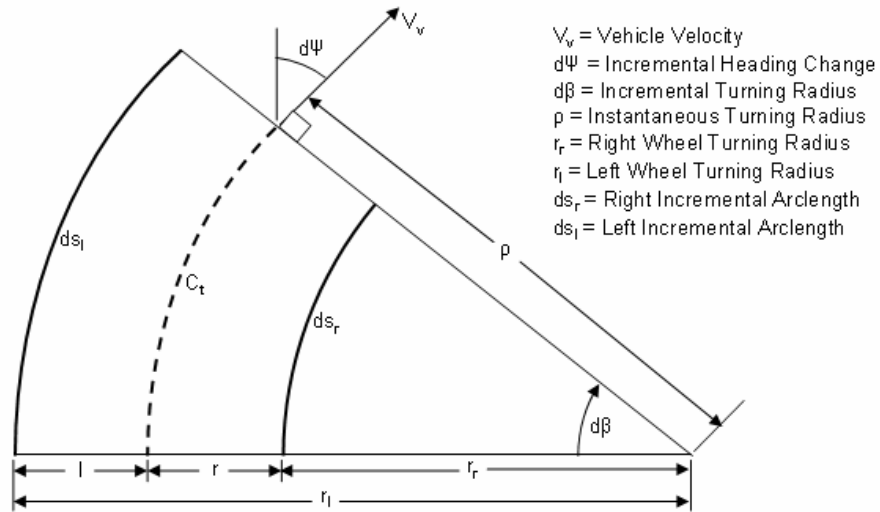


Figure 35: Incremental Turn

Figure 35 illustrates the path of the robot moving through an incremental turn ($d\beta$). The instantaneous vehicle velocity at the center of turning is given as V_v . The turning radius (ρ), incremental heading change ($d\Psi$), Turning radii (r_r and r_l), and incremental arc length (ds_r and ds_l) are also shown.

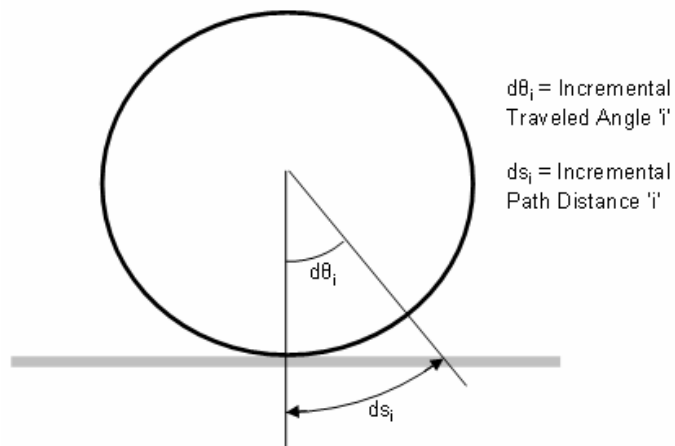


Figure 36: Wheel Model

The incremental travel angle ($d\theta_i$) and incremental path distance (ds_i) of the wheels is shown in Figure 36. This model assumes no wheel slip. The subscript i will be replaced with l for left and r for right.

By inspection of the geometry in Figure 35, the angles $d\Psi$ and $d\beta$ are equal. It can also be seen in Figure 35 that the arc length ds_l is equal to the radius r_l multiplied by the angle $d\beta$, which is in turn equivalent to the radius w_l multiplied by the incremental angle turned by the wheel $d\theta_l$.

$$\begin{aligned} ds_l &= r_l \cdot d\beta = w_l \cdot d\theta_l \\ ds_r &= r_r \cdot d\beta = w_r \cdot d\theta_r \end{aligned} \quad (5.5.1)$$

The wheel path turning radii are related to the instantaneous turning radii (ρ).

$$\begin{aligned} r_l &= \rho + l \\ r_r &= \rho - r \end{aligned} \quad (5.5.2)$$

Substituting Equation (5.5.1) into Equation (5.5.2) for r_l and recognizing that $d\beta$ equals $d\Psi$ as stated above, the left wheel equation can be solved for ρ .

$$\rho = \frac{w_l \cdot d\theta_l}{d\Psi} - l \quad (5.5.3)$$

Substituting this expression for ρ in the right wheel part of Equation (5.5.2), then substituting the resulting expression for r_r back into Equation (5.5.1) and finally solving for $d\Psi$ gives:

$$d\Psi = \frac{w_l \cdot d\theta_l - w_r \cdot d\theta_r}{l + r} \quad (5.5.4)$$

Integrating from zero to the current time step, gives an expression for vehicle heading Ψ_k .

$$\psi_k = \int_0^k d\psi = \int_0^k \left(\frac{w_l \cdot d\theta_l - w_r \cdot d\theta_r}{l+r} \right) = \frac{w_l \cdot \theta_{l,k} - w_r \cdot \theta_{r,k}}{l+r} \quad (5.5.5)$$

$\theta_{r,k}$ and $\theta_{l,k}$ are the respective wheel rotation angles recorded at time step k, and all the initial conditions are zeros.

Since the arc length of the wheel path is linearly related to the incremental turning angle $d\beta$ by the wheels turning radius (r_r or r_l), the following linear interpolation is made to find the value of the distance traveled by the center of turning:

$$ds = \frac{(ds_l - ds_r)}{(r_r - r_l)} (\rho - r_r) + ds_r \quad (5.5.6)$$

Substituting Equation (5.5.2) into Equation (5.5.6) for r_r and r_l gives:

$$ds = \frac{(ds_l - ds_r)}{(l+r)} \cdot r + ds_r \quad (5.5.7)$$

Substituting for ds_l and ds_r from Equation (5.5.1) gives:

$$ds = \frac{(w_l d\theta_l r + w_r d\theta_r l)}{(l+r)} \quad (5.5.8)$$

Integrating Equation (5.5.9) gives:

$$s_k = \int_0^k ds = \frac{(w_l \theta_{l,k} r + w_r \theta_{r,k} l)}{(l+r)} \quad (5.5.9)$$

The resulting value s_k is the linear distance traveled by the robot's center of turning at time step k.

Since the encoder data is given as wheel angular displacement values for each time step, further calculations must be done to determine HAL's global coordinates. It will be necessary to utilize Equation (5.5.9) to determine the linear displacement and Equations (5.5.5) to determine the angle of that displacement for each reading. Using the geometry from Figure 35, the global coordinates of C_t can be solved using the following technique:

$$\begin{aligned} X_k &= X_{k-1} + (s_k - s_{k-1})\sin(\psi_{k-1}) \\ Y_k &= Y_{k-1} + (s_k - s_{k-1})\cos(\psi_{k-1}) \end{aligned} \tag{5.5.10}$$

Where X_k and Y_k are the coordinates of C_t in the global plane, and X_{k-1} and Y_{k-1} are the coordinates from the previous time step. The robot moves forward a distance expressed by $(s_k - s_{k-1})$, while being oriented at angle Ψ_{k-1} .

Two separate runs were conducted to test HAL's dead reckoning abilities. The resulting position of the center of turning for these tests is shown in Figure 37 and Figure 38.

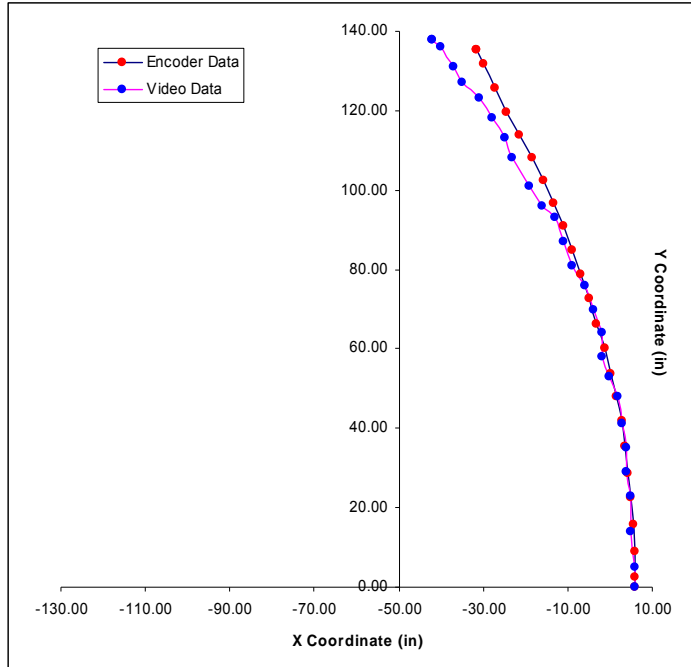


Figure 37: Run 1 Dead Reckoning Test

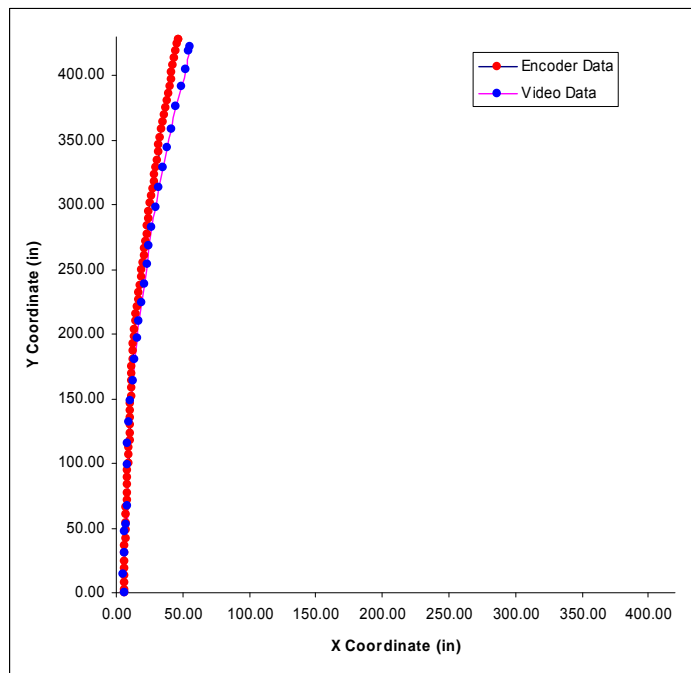


Figure 38: Run 2 Dead Reckoning Test

The accuracy of the encoders can be quantified by comparing the total distance traveled (D) of the given data in the video with the experimental data taken from the encoder readings.

This distance can be determined using Pythagorean's Theorem.

$$D = \sqrt{X^2 + Y^2} \quad (5.5.11)$$

Equation (5.5.11), for the first run, yields an encoder reading distance of 140.3 in. The video data gives a distance of 146.1 in, a difference of 4.0%. The second run yields an encoder reading distance of 429.5 in and a video data distance of 425.0 in, a difference of only 1.1%.

5.6 Conclusion

The encoders fulfilled all of the requirements needed for position sensing. They are used to control all sixteen joints, as well as for accurate dead reckoning. The data collected and presented in the previous section demonstrates the accuracy of the encoders. This is even more impressive knowing that “non-systematic” errors were not taken into account. Non-systematic errors are those not predicted in advance, e.g. wheel slippage and floor irregularities. If many of these errors are present, even small ones, they can build up extremely quickly – often referred to as “growth-rate” concept [44]. These results show that the versatility and robustness of the encoder feedback can be used for future needs.

Even more dead reckoning functionality can be added to HAL in the future. While all of the encoder data was stored internally on the robot itself, it had to have post-processing to be usable. The raw hexadecimal encoder counts were used in a spreadsheet to determine HAL's global coordinates. This set of mathematic equations could be implemented while running.

Future work with HAL could incorporate a Coordinate Rotation Digital Computer

(CORDIC) system. The CORDIC system is a simple and efficient way to perform the operations necessary for dead reckoning. CORDIC is an algorithm used to calculate trigonometric functions. It is commonly used if no hardware multiplier is available, since it only requires small lookup tables, bit shifts, and additions [45].

6 Power Electronics

6.1 Needs

A method for powering HAL's sixteen motors is essential for giving the ability to move. Not only is battery selection important, but also some way to control the voltage seen by the DC motors. An effective method for varying the voltage has the capability to effectively control the speed of each motor. Reversing the voltage is also imperative for allowing each joint to move in both directions.

6.1.1 Battery

All of the motors selected run with a maximum voltage of 7.2 V. This means the battery must also be rated at 7.2 V. The batteries must furthermore be able to handle the maximum sustained current draw. It can be assumed that the worst case current draw would be that if all four leg abduction motors were running, but unable to move. This would mean the maximum current is four times the stall current of an individual motor (3.5 A), resulting in a value of 14 A.

Some form of rechargeable battery is required. Non-rechargeable batteries of this magnitude are hard to find, and would not be cost effective. The ease of user operation would also be greatly enhanced by a rechargeable battery.

The size of the battery is not an imperative specification. However, the weight could have a great effect on the performance of the platform. The smaller the total payload carried by the legs, the better.

The total continuous runtime of HAL for testing purposes is most likely only going to be a few minutes at a time. However, future work may require it to run for prolonged periods. An arbitrary battery life specification was selected at one hour. It was estimated that HAL would certainly average less than 2 A continuously for this hour span, giving a needed battery rating of 2 A-hrs. At this rating, even when not being run continuously, the robot would only need to be recharged intermittently.

The final, possibly most overriding, factor is the cost. The cost of the battery must be kept to a minimum. The ideal battery for functionality may be cost prohibitive, and therefore not practical.

6.1.2 Motor Control

Once the power is supplied, something is needed to control the voltage seen by both sides of the motor. This device must also be able to both control and withstand the current drawn by the motor. These tasks must be able to be controlled with a typical microcontroller output – classically 0-5V and up to 25mA.

The speed should be able to be varied with reasonably good resolution. As mentioned before, this speed must also have the ability to be varied both clockwise and counter-

clockwise. Finally, like everything else on HAL, the size, weight, cost, and ease of implementation are all important.

6.2 Concepts

6.2.1 Battery

There are five main types of rechargeable batteries now in common use for powering electronic and electrical equipment: sealed lead-acid (SLA), rechargeable alkaline-manganese (RAM), nickel-cadmium (NiCd), nickel-metal hydride (NiMH), and lithium-ion (Li-Ion) [47].

SLA batteries are a development of the familiar “flooded” lead-acid battery used for many years in cars and trucks. It has a positive electrode of lead oxide, a negative electrode of porous metallic lead and sulphuric acid as the electrolyte. SLA batteries tend to have a relatively poor energy density, but are also the cheapest of the rechargeables. They are the best suited for application where low-cost power storage is the main consideration, and weight is not a problem. Since weight is a major issue in the design of HAL, SLA batteries are not suitable for this application [47]. Typical applications of SLAs include emergency lighting, solar power systems, and wheelchairs [46].

RAM batteries use a manganese dioxide positive electrode and a potassium hydroxide electrolyte, and the negative electrode is a special porous zinc gel designed to absorb hydrogen during the charging process. The separator is also laminated to prevent it being pierced by zinc dendrites. RAM batteries tend to have a shorter cycle life than other

rechargeables, especially when deeply cycled. This makes them mainly suitable for low-cost consumer applications where they are subjected to shallow cycling [47]. Typical applications of RAM's include portable emergency lighting, toys, portable radios, cassette and CD players, and testing instruments [46]. They are not commonly used in applications such as robotics, and are hard to find. For these reasons, they will not be investigated further.

NiCd batteries use nickel hydroxide as the positive electrode and cadmium metal/cadmium hydroxide as the negative electrode, with potassium hydroxide as the electrolyte. They have high energy density and relatively low cost, making them very popular for powering compact portable electronics. However, NiCd batteries suffer from something called the “memory effect” – meaning their performance per charge is diminished if they are not completely discharged before they are charged. NiCd batteries can provide very cost effective energy storage, and the longest working life of any of the rechargeables. That is why they are still the most popular, despite the appearance of the newer types [47]. Unfortunately, NiCd batteries are highly toxic, and must be handled with care and disposed of properly. Typical applications of NiCds include portable tools and appliances, model cars, data loggers, camcorders, and portable transceivers [46].

NiMH batteries use a nickel/nickel hydroxide positive electrode, a potassium hydroxide as the electrolyte, and a hydrogen-storage alloy such as lanthanum-nickel or zirconium-nickel for the negative electrode. NiMH batteries have high energy density, but are not as effective for deep discharge cycles. They tend to have a shorter working life. The main kinds of applications where NiMH batteries are most suitable are those which need a very compact

source of power, yet do not involve deep cycling [47]. Typical applications of NiMHs include cellular phones, cordless phones, compact camcorders, laptop computers, personal digital assistants, personal digital video disk players, and compact disk players [46].

Li-Ion batteries have a negative electrode of aluminum, coated with a lithium compound such as lithium-cobalt dioxide, lithium nickel dioxide or lithium-manganese dioxide. The positive electrode is generally copper, coated with carbon. The electrolyte is a lithium salt such as lithium-phosphorus hexafluoride, dissolved in an organic solvent such as a mixture of ethylene carbonate and dimethyl carbonate. Li-Ion batteries have an extremely high energy density. However, they are highly reactive and pose an explosion risk with rechargeable batteries. Unlike NiCd and NiMH batteries, Li-Ion batteries are not subject to memory effect, and have a relatively low self-discharge rate [47]. One major drawback is the cost, which is much higher than other types of rechargeable batteries. Typical applications of Li-Ion's include compact cellular phones, notebook personal computers, digital camera, and very small portable devices [46].

Table 1: Rechargeable Batter Comparison [46-48]

Type	Charge Life (cycles)	Operation Temperature		Storage Temperature		Self Discharge (%/day)	Discharge Slope	Energy Weight (MJ/kg)	Energy Density (W-h/kg)	Cycle Life	Charging Time (hrs)	Maximum Discharge Rate (% of A-hr rating)	Charge/Discharge Efficiency (%)	Cost
		Minimum (degrees F)	Maximum (degrees F)	Minimum (degrees F)	Maximum (degrees F)									
Lithium Ion	400	-4	140	-4	140	< 0.1	Flat	0.58	>100	Long	3-4	<100	99.9	Very High
Nickel-Cadmium	700	-4	113	-40	140	1	Flat	0.14-0.22	40-60	Long	14-16	>200	70-90	Medium
Nickel Metal-Hydride	400	-4	113	-40	140	4	Flat	0.11-0.29	30-80	Medium	2-4	20-50	66	Higher

Table 1 shows the comparison of the top three rechargeable competitors. While charge life and operation and storage temperatures are all well above the necessary values, all other criteria was taken into consideration. Table 2 shows a comparison of the current, weight, and cost of all three types of rechargeable batteries. The data was compiled by searching for 7.2 V batteries from random online retailers. Figure 39 shows a graph of the data presented in Table 2, in an effort to facilitate a better understanding.

Table 2: 7.2V Battery Values

Type	Li-Ion			NiCd			NiMH		
	Current Rating (mAh)	Weight (lbs)	Cost (\$)	Current Rating (mAh)	Weight (lbs)	Cost (\$)	Current Rating (mAh)	Weight (lbs)	Cost (\$)
	6600	0.70	117.88	1500	0.66	13.99	3200	0.70	23.95
	1460	1.50	129.99	1600	0.80	12.95	2000	0.60	11.00
	4140	0.40	118.59	1500	0.60	8.99	3300	0.85	13.95
	220	0.22	49.57	2400	0.85	29.90	2000	0.75	13.90
	2760	0.40	78.81	2000	0.68	24.99	3300	0.83	24.99
Median	2760	0.40	117.88	1600	0.68	13.99	3200	0.75	13.95
Mean	2990	0.60	102.12	1767	0.71	17.47	2833	0.75	16.96

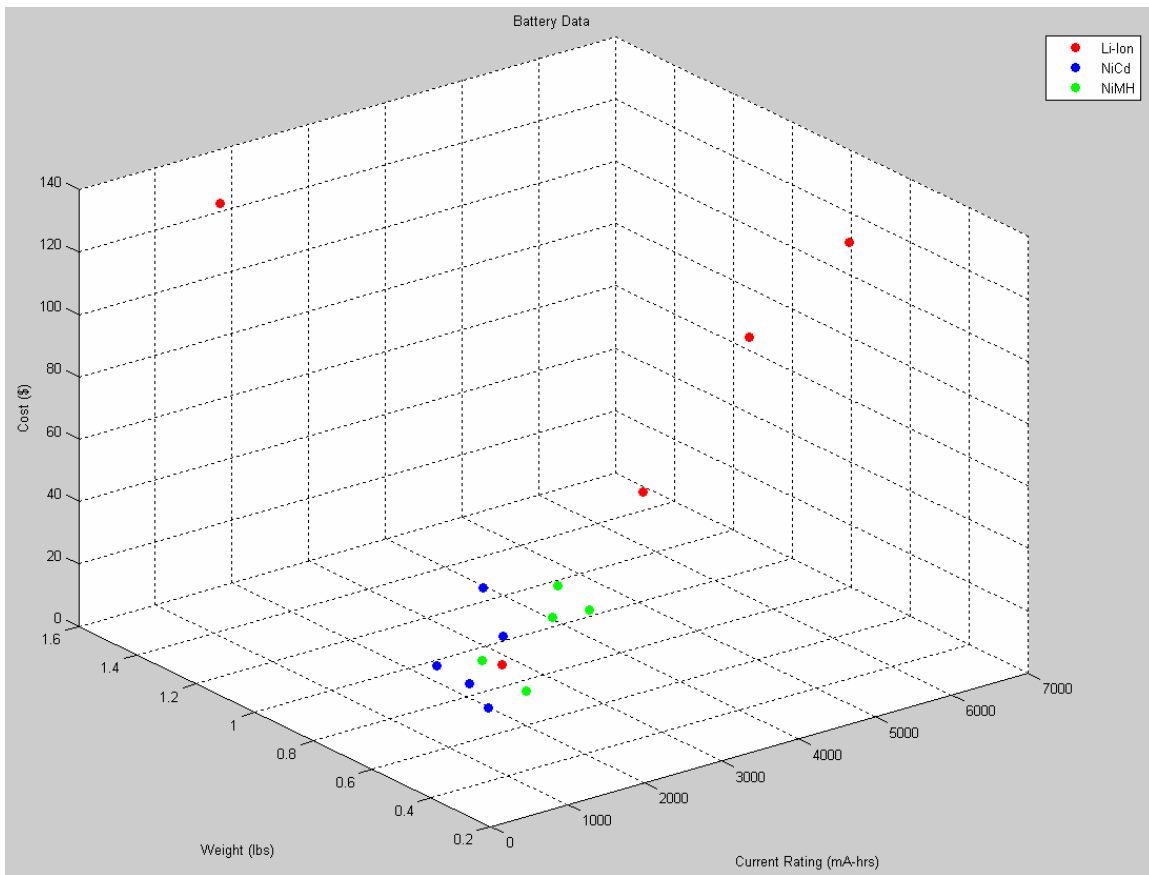


Figure 39: Battery Data

6.2.2 Motor Control

Generally, the rotational speed of a DC motor is proportional to the voltage applied to it. Speed control is achieved by varying the voltage to the motor by some method. There are four basic components used for controlling a DC motor: commercial motor controllers, relays, transistors, or H-Bridges. All four generally benefit from a microcontroller to provide control signals and utilize a secondary power supply for actually driving the motor.

There a vast number of commercial motor controllers for use with DC motors. There are also a large number of ways these controllers are designed to receive signals. Some use a pulse width modulation signal (PWM – explained later), some use serial communication, and others use a type of bus communication protocol (e.g. I²C or CAN – explained later). These controllers are usually very reliable and can sometimes be integrated directly to the encoders, which could in turn reduce the overhead in the microcontroller. Although much of the design work is already done for the user, commercial motor controllers tend to be large and costly. With the large currents that will be drawn by these motors, the use of commercial controllers quickly becomes infeasible.

Relays are a cost effective, and a relatively easy to implement, way of controlling the direction of a motor. The most appealing type of relay is a reed relay. The contacts of a reed relay are made of a magnetic material, allowing an electromagnet to act directly on them; rather than requiring an armature, like many other types of relays. Since the moving parts are small, reed relays are capable of faster switching than most others. Switching speed is a very important factor when using relays to control the speed of a motor. Since they only have two

states, open and closed, they have to pulse at high speeds to effectively control a motor. Slow switching could produce significant motor “chatter,” causing unsmooth motion. While reed relays can switch up to several hundred times per second, they can only switch low currents – usually in the mA range [49]. Since the motors used on HAL stall at around 3.5 A, relays would not be an effective means of controlling their motion.

Individual transistors can be used to effectively control the speed and direction of a motor. This would require a minimum of four transistors – two NPN and two PNP. Since the voltage levels and current required to control the motors would be too high for a microcontroller, buffers, diodes, and resistors are needed. Designing an effective circuit quickly becomes complicated and costly. This type of motor control design is commonly known as an H-bridge. Luckily, integrated circuits with this basic design already exist.

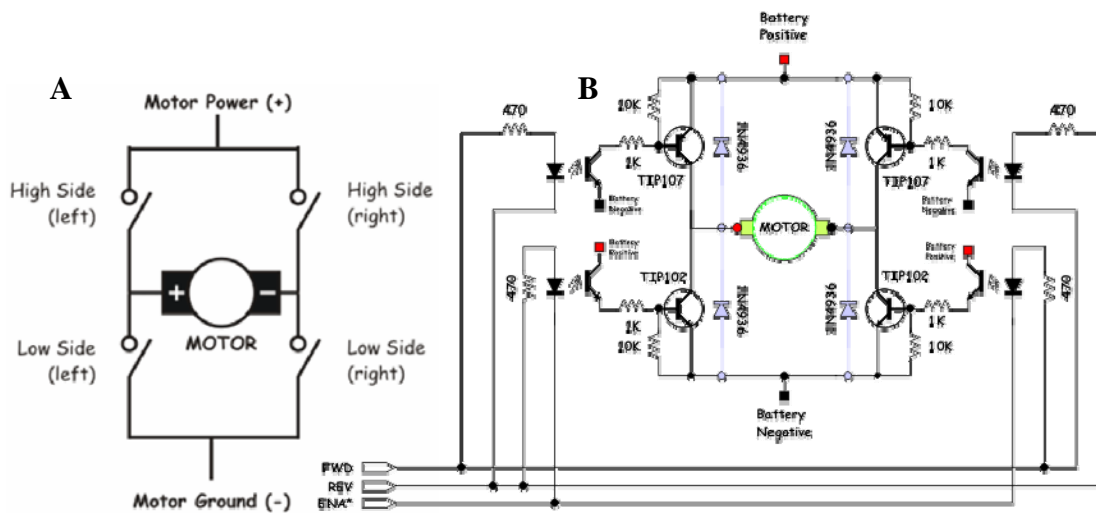


Figure 40: a) H-bridge Theory; b) Typical H-bridge Schematic [50]

Figure 40 shows the basic functionality of an H-bridge. When the *High Side (left)* and *Low Side (right)* portions are closed, the motor will turn forward. Inversely, when the *High Side (right)* and *Low Side (left)* portions are closed, the motor will turn in reverse. If all four virtual switches are closed, the motor has a high voltage on both sides and effectively brakes. Because they use transistors, these virtual switches can be cycled extremely fast; which can in turn be used to control the speed of the motor.

Commercial H-bridges are cheaper, smaller, and easier to implement than a “home-made” version. They can have ratings anywhere from the mA range to amperages in the high double digits. Generally, the higher the current rating, the more expensive the H-bridge. H-bridges are typical in robotics applications, and a large amount of documentation exists to assist the designer.

6.3 Theory

A voltage varying process, known as PWM, is the most efficient means by which a DC motor's speed can be controlled. The only way to control a DC motor's speed without varying the voltage is by controlling its current, which is highly wasteful of energy. The output pins of a microcontroller can only have a high and low state, and an H-bridge can only interpret the microcontroller data to switch the battery connection on and off. This makes it impossible to give a motor variable voltage, without including other components. PWM is a relatively simple method to get around this problem.

A suitable control signal can be generated in two ways: via a fixed frequency with a variable pulse width (PWM), or through a fixed pulse width with a variable frequency (pulse frequency modulation) [36]. The former is the most common way used by a microcontroller, since the latter generates many different frequencies and could cause some motors to resonate. The on and off pulses are fluctuated in such a way as to be able to give an average voltage that is a fraction of the battery voltage. Since these fluctuations happen very fast, the motor effectively sees the desired constant voltage.

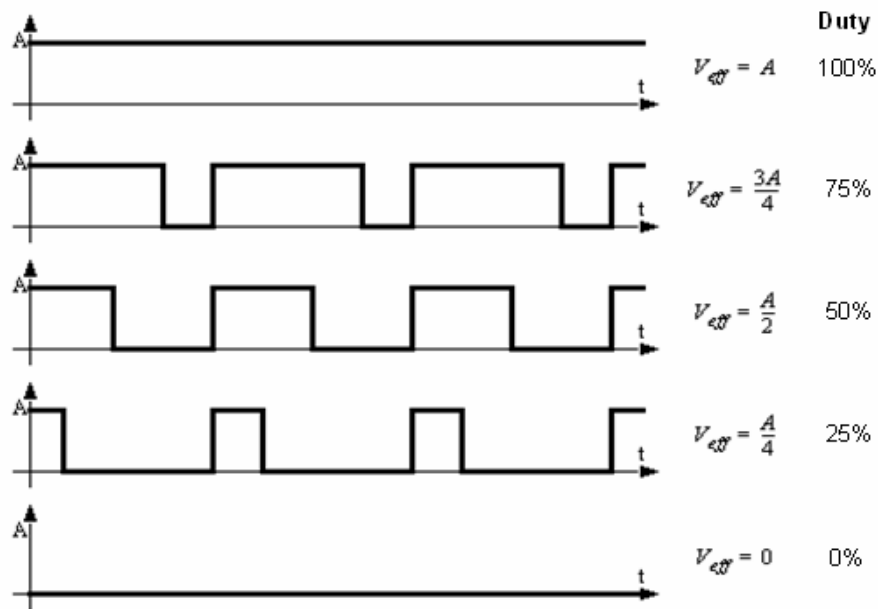


Figure 41: PWM Duty Cycles [51]

Figure 41 shows typical square waves that are produced using PWM, and its relationship to pulse frequency and duty cycle. Obviously, the higher the duty cycle, the faster the motor turns.

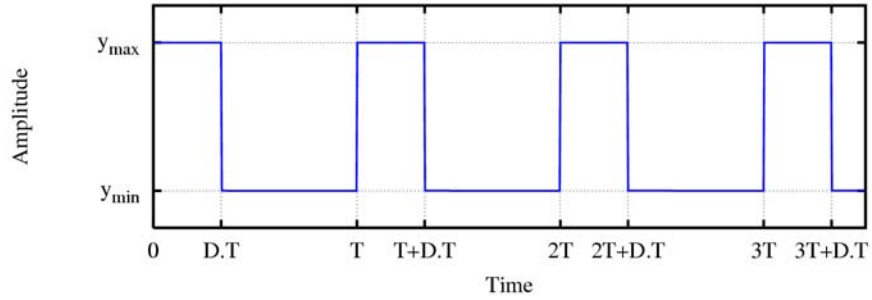


Figure 42: PWM Characterization [52]

If we consider a square waveform $f(t)$ with a low value y_{\min} , a high value y_{\max} , a duty cycle D , and a period T (see Figure 42), the average value of the waveform is given by:

$$\bar{y} = \frac{1}{T} \int_0^T f(t) dt \quad (6.3.1)$$

Since $f(t)$ is a square wave, the expression becomes:

$$\bar{y} = \frac{1}{T} \left(\int_0^{D.T} y_{\max} dt + \int_{D.T}^T y_{\min} dt \right) = \frac{D \cdot T \cdot y_{\max} + T(1-D)y_{\min}}{T} \quad (6.3.2)$$

Simplifying and assuming y_{\min} is zero gives:

$$\bar{y} = D \cdot y_{\max} \quad (6.3.3)$$

This shows that the average voltage (\bar{y}) is directly dependent on the duty cycle (D). This simple relationship can be used when programming the microcontroller.

6.4 Design

6.4.1 Battery

Using the data from Table 1, Table 2, and Figure 39, a battery type was chosen. Li-Ion was ruled out not only because of its high cost, but also because it does not come in a package that is easy to implement on a robot. That left NiMH and NiCd as the contenders. Both types of batteries are approximately the same cheap price, and come in forms that are easy to use for robotics. In the end, NiCd was chosen because of its slightly better ratings in most areas (as shown in Table 1). The memory effect should not be a problem, as long as the battery is drained completely over time before recharging. Figure 43 shows the 7.2V 2000 mAh NiCd battery that was chosen.



Figure 43: Battery

Another positive about the battery chosen is the accessories that are included. The wires have an industry standard connector that prevents inadvertently reversing the polarity. A charger is included that simply plugs into a standard outlet. An inexpensive connector designed to mate with the one on the battery allows for a simple way of connecting and disconnecting the battery to HAL.

At a rating of 2000mAh, this battery should provide more than enough current for the run times required for testing HAL. The connections used allow for easy upgrades to the battery if a higher rating becomes necessary for future applications. A 25 A switch is also included in series with the battery to provide easy control and safety functionality.

6.4.2 H-Bridge

After an exhaustive search of the H-bridges available for purchasing, one was selected. This H-bridge has a logic supply voltage of 5 V, supply voltage range of -0.3 – 33 V, and peak current of 5 A – all well within the values need for controlling HAL. It also includes features such as protection against over-voltage, over-current, over-temperature, and cross conduction faults. Fault diagnostics can be obtained by monitoring the two status terminals provided and the two input control lines [53]. The H-bridge is controlled using a direction input (Dir) and a PWM input (PWM). The direction state can be set high for clockwise rotation and low for counter-clockwise rotation, while the PWM line controls the voltage duty. Table 3 shows the functionality of the H-bridge. Out1 and Out2 are connected to the motor leads. On HAL, a high state (HS) is 7.2 V and a low state (LS) is 0 V.

Table 3: H-Bridge Function Table [53]

Dir	PWM	Out1	Out2	Mode
0	0	HS	HS	Brake
0	1	HS	LS	CCW
1	0	HS	HS	Brake
1	1	LS	HS	CW

One drawback of the H-bridge selected is that it only comes in a 20 pin small outline integrated circuit (SOIC) package. Since a dual in-line package (DIP) format is ideal for use in prototyping, a method for converting the outputs is necessary. This is most easily achieved by soldering the integrated circuit on a surface mount prototyping board, commonly referred to as a “surfboard.” A photograph of one of the sixteen H-bridge/surfboard construct is shown in Figure 44.

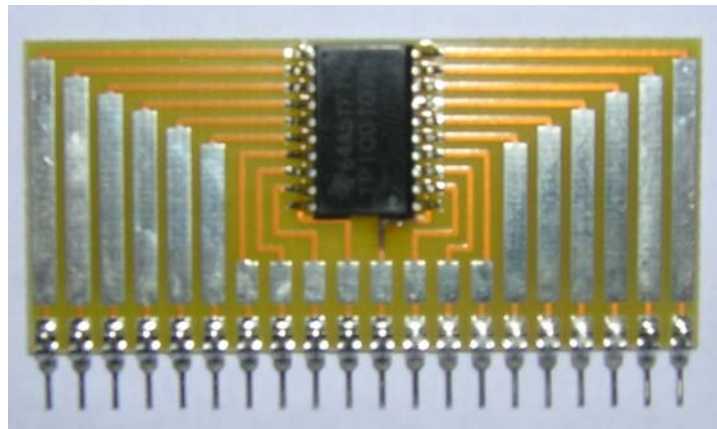


Figure 44: H-Bridge/ Surfboard Assembly

6.5 Test

Throughout preliminary testing, the H-bridges functioned admirably. However, when extensive use of the leg abduction motors began, a problem arose. The H-bridge was unable to handle the sustained high current draw needed to move the legs when a significant load

was applied. It was overlooked that although the maximum peak current the H-bridge can handle is 5 A, the continuous power dissipation is only 1.29 W. At 7.2 V, this provides a mere 0.18 A of continuous current. This is still enough for the motors on the other three joints, but the four shoulder abduction motors needed something with a higher rating. Figure 45 shows the comparison of the back of a good and a destroyed H-Bridge/Surfboard assembly. The bad H-bridge shown physically smoked when overheated.

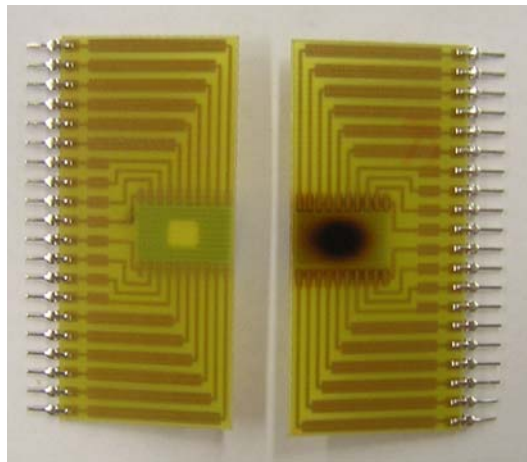


Figure 45: Good H-Bridge versus Bad H-Bridge

6.6 Redesign

A new method for controlling the four shoulder abduction motors became necessary. The first, most obvious choice was to find another H-bridge with a higher current rating. This posed a challenge, since the cost, size, and complexity of the H-bridges increase with size. As a larger H-bridge implementation became infeasible, other solutions were evaluated.

After reevaluating the needs of the shoulder abduction motors, it was determined that the ability to vary the voltage was not necessary. This is mainly due to the fact the worm and worm-gear combination reduces the angular velocity to less than 5 RPM. Two solutions became apparent: the use of transistors or the use of relays.

It quickly becomes cumbersome to successfully turn on and off and control the direction of a motor with transistors. A large number of other components are needed, such as diodes and buffers.

Motor direction can be controlled using just two relays. A double-pole double-throw (DPDT) relay can reverse the voltage and change the direction of the motor. This can be used in conjunction with a single-pole single-throw (SPST) relay that connects or disconnects the system to the battery.

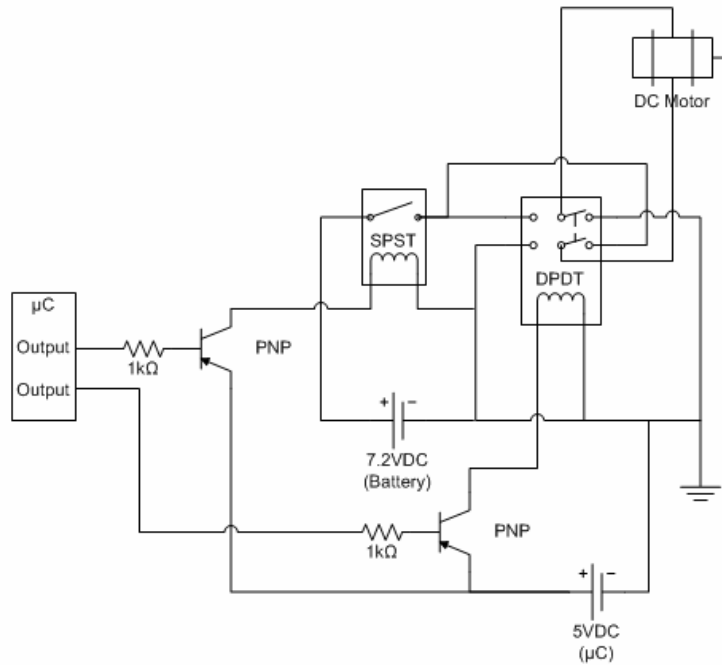


Figure 46: Motor Control Redesign Wiring Diagram

While it is relatively easy to find cheap relays suitable for the continuous currents needed, they require larger coil currents than can be supplied by most microcontrollers. To work around this, transistors can be used in conjunction with the internal microcontroller voltage regulator to boost the current to the relay coils. The setup used for each shoulder abduction joint is shown in Figure 46 and Figure 47.

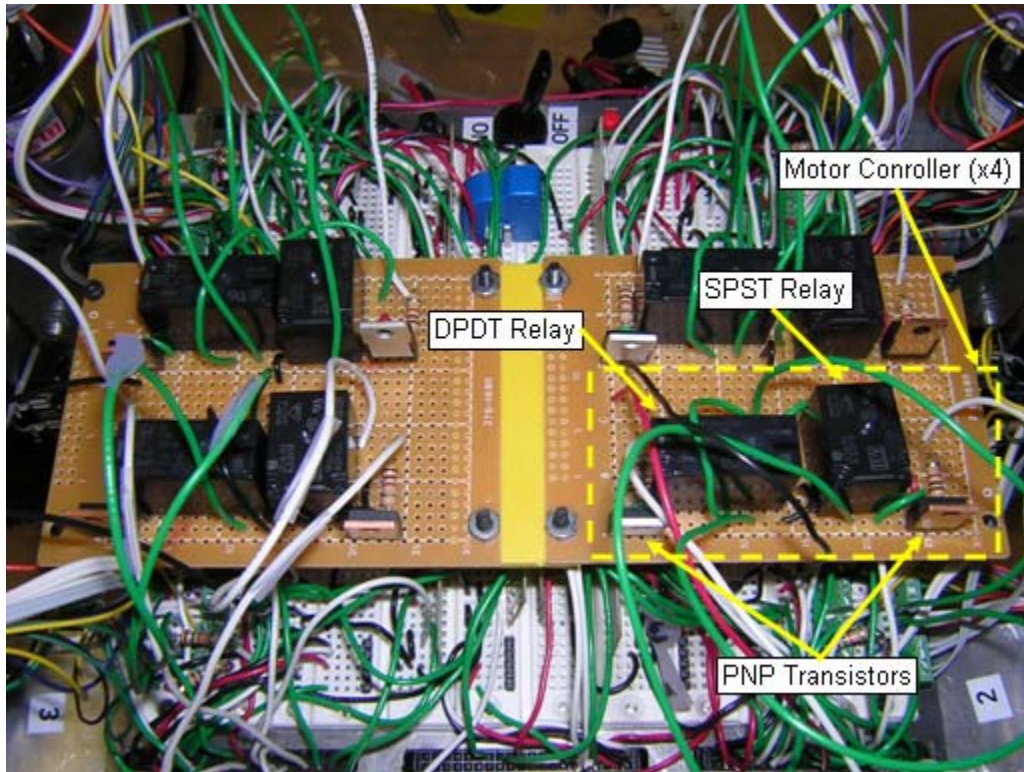


Figure 47: Shoulder Abduction Motor Controller

6.7 Conclusion

The battery selected is very effective for the needs of HAL. One charge was able to last through weeks of testing. The H-bridges are also very successful in controlling the speed and direction of the motors, excluding those connected to the shoulder abduction motors.

However, an effective solution was found. The relay/transistor motor control system has performed well under the extreme continuous current conditions.

7 Sensors

7.1 Needs

A various number of sensors are needed on HAL to help with motion control, gather information about the environment, and to help characterize locomotion. All sensors must be able to send and/or receive data from a microcontroller. While the encoders used on HAL's motors are sensors, they were discussed in detail in Chapter 5 and will therefore not be elaborated on here.

7.1.1 Motion Control

Two types of inputs are needed for HAL to achieve successful motion control. With variable terrain can come many robot stability problems. HAL could easily tip over if one or more of his legs are higher than the others. A hybrid locomotion form of active suspension can counteract this problem, but there needs to be some way of telling when and how far to move each leg. The first input must be a way of determining if HAL's chassis is level. If the legs are moved in such a way as to keep the chassis level on two planes, HAL should remain stable. However, even if the chassis is level, all four legs may not be touching the ground. In order to attain proper traction and stability, it is important to have a way of sensing whether or not each wheel is making contact with the ground.

7.1.2 Environmental Information

The only type of environmental information needed for the scope of this project is object detection. While object avoidance is not necessary for locomotion testing, a way of

determining there is an object present is. When HAL comes into contact with an object, it can try to step over it.

7.1.3 Locomotion Characterization

In order to quantifiably compare the advantages of traditional forms of locomotion with hybrid locomotion, efficiency will need to be determined. Measuring the efficiency of electrical systems is most easily accomplished by comparing the power used. Since the voltage being supplied to HAL always remains constant, the changes in current is directly proportional to the power being used. Therefore, a current sensor is needed to show the benefits and/or drawbacks of rolling, walking, and hybrid locomotion.

7.2 Concepts

7.2.1 Tilt Sensor

One of the most common types of tilt sensors is an electrolytic sensor. This type of sensor is cheap and easy to implement. They work using inherent liquid properties. As the sensor tilts, the surface of the fluid remains level due to gravity. The fluid is electrically conductive, and the conductivity between the two electrodes is proportional to the length of the electrode that is immersed in fluid [54]. Using five pins, dual axis tilt can be accurately determined. Electrolytic sensors offer good reliability and repeatability. The only problem for use on HAL is the fact that electrolytic sensors require AC current to operate. If DC power is used instead, electrolysis will occur and ruin the sensor.

Some ideas were brainstormed for different designs that could be made in-house, but all were eventually deemed unnecessarily complicated. The next step was to determine the best integrated circuit to accomplish dual axis tilt sensing.

7.2.2 Ground Contact

A few sensor types were considered for determining wheel ground contact. The use of a ranger was deemed too expensive and overly complex for this simple task. Any kind of contact switch would scrape on the ground, likely causing a short life. Pressure sensors were examined, and the most promising seemed to be a cheap and easy fix developed by a senior project at the University of Vermont [55]. The design of the pressure sensor is very simple. Conductive foam was used as a variable resistor in a simple voltage divider. As the foam is crushed, the resistance is reduced. A similar setup was created in the lab for possible use on HAL, but favorable results were never achieved.

7.2.3 Obstacle Detection

Object detection also had a number of possible solutions. Having a separate sensor for each leg is important, since only one leg is actuated at a time when traversing obstacles. Infrared or ultrasonic rangers were considered, but are expensive and overly complex. Other proximity sensors had similar characteristics as the rangers. A contact sensor, such as a switch or button, could be very easily implemented on HAL.

7.3 Design

7.3.1 Tilt Sensor

The tilt sensor chosen for use on HAL is a dual axis integrated circuit. It is very small, light weight, and is cost effective. The inclinometer has excellent reliability and stability over time and temperature. The manufacturer also states it has “instrumentation grade performance, high resolution and low noise, and outstanding overload and shock durability [56].” The measurement range is -90° to $+90^{\circ}$ for both axes, with a resolution of 0.003° . One of the most appealing aspects of this particular inclinometer is the ease of integration into systems being controlled by a microcontroller. Data can be read from the inclinometer using either a serial peripheral interface (SPI) or by reading a variable voltage output.

7.3.2 Ground Contact

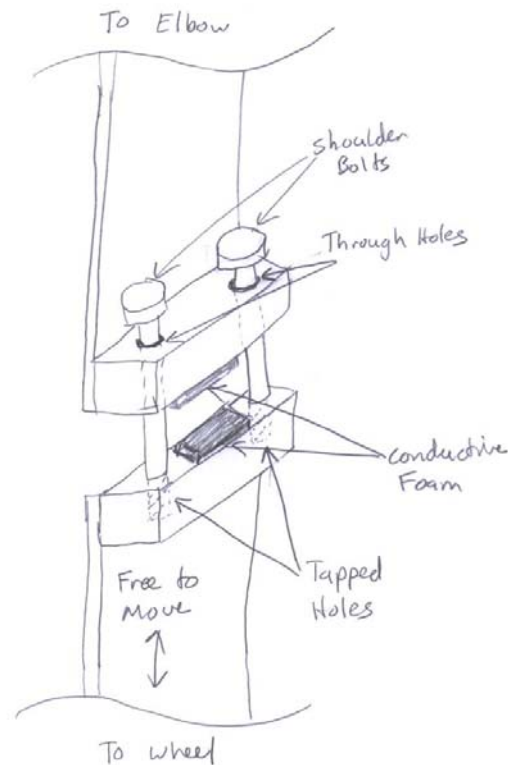


Figure 48: Ground Contact Sensor Design

It was decided that the best solution for determining ground contact was to design and build a sensor from scratch. The most simple and elegant solution consisted of a home made switch. The leg section between the elbow and steering joints was cut in half. Shoulder screws and small aluminum blocks are used to allow the cut section to come apart when there is no ground pressure. When the ground is contacted by the wheel, the two sections press together. These shoulder screws allow the leg section to slide axially (up and down), while preventing twisting or transverse movements. Conductive foam was used on both sides of the switch to absorb energy and to correct for any misalignments, while still allowing the circuit to be

completed. The design and implementation of this switch can be seen in Figure 48 and Figure 49.

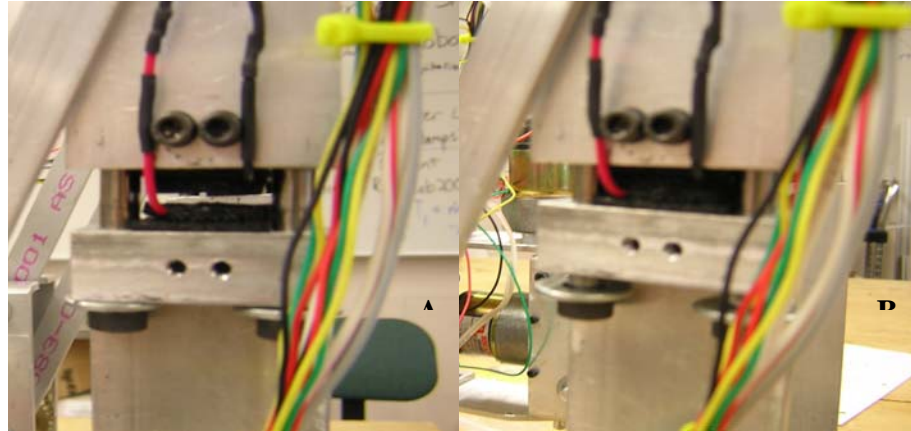


Figure 49: Ground Contact Sensor a) Off Ground; b) On Ground

7.3.3 Object Detection

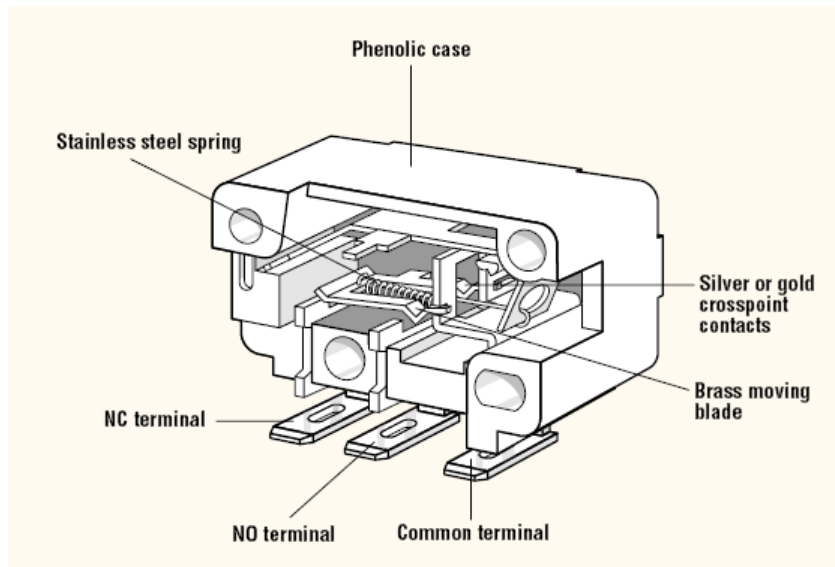


Figure 50: Limit Switch [57]

All four wheels need some form of obstacle detection in front of them, mainly for input when testing HAL's locomotion. This sensor needs to be cheap, simple, reliable, and repeatable. The style of sensor that fits these criteria the best is a simple limit switch. A low torque rotary actuation switch with a coil spring mechanism was selected (shown in Figure 50) and modified. The "wireform" actuators were removed and replaced with one designed to cover the entire area in front of the wheel (shown in Figure 51). When any part of the new contact arm presses against an obstacle, the switch is activated.

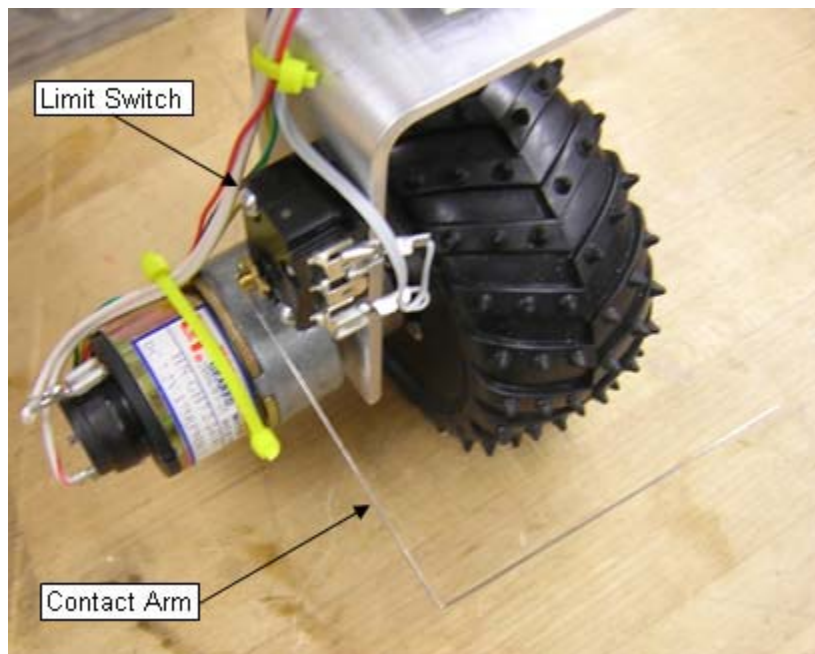


Figure 51: Limit Switch Assembly

The wiring diagram used for both the ground contact and object detection sensors is shown in Figure 52. The input to the microcontroller is kept high when the switch is open, and forced low when closed.

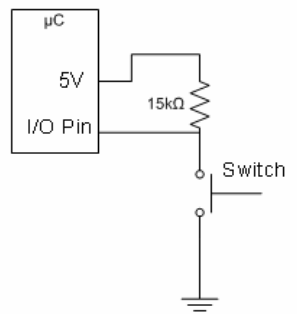


Figure 52: Switch Wiring Diagram

7.3.4 Current Sensor

A large DC current transducer is needed to be able to measure the large currents that can be drawn by the motors. A good worst case assumption is that all four shoulder abduction motors are stalled at the same time. This would mean 14 A would continuously be drawn from the battery. A closed loop multirange current transducer was found that is rated up to 25 A DC. This particular sensor uses a coil of wire and the Hall Effect to measure the current being drawn [58]. When placed in series with the line being measured, a variable voltage is outputted that is related to the current. This variable voltage can be easily read and interpreted by a standard microcontroller.

7.4 Test

7.4.1 Inclinometer

The inclinometer was tested through its entire rated range on both axes (see Figure 53). A protractor was used to measure the angle of the sensor, and a simple voltmeter was connected to the variable voltage output.

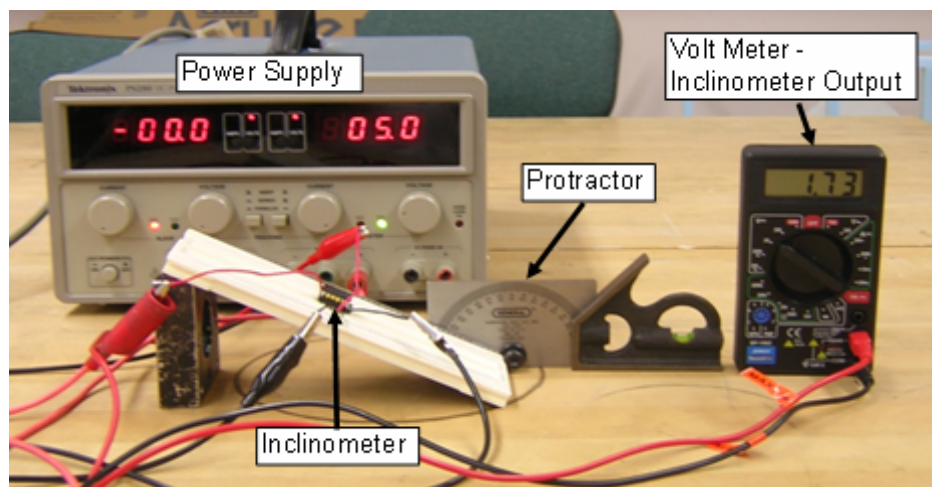


Figure 53: Inclinometer Test Setup

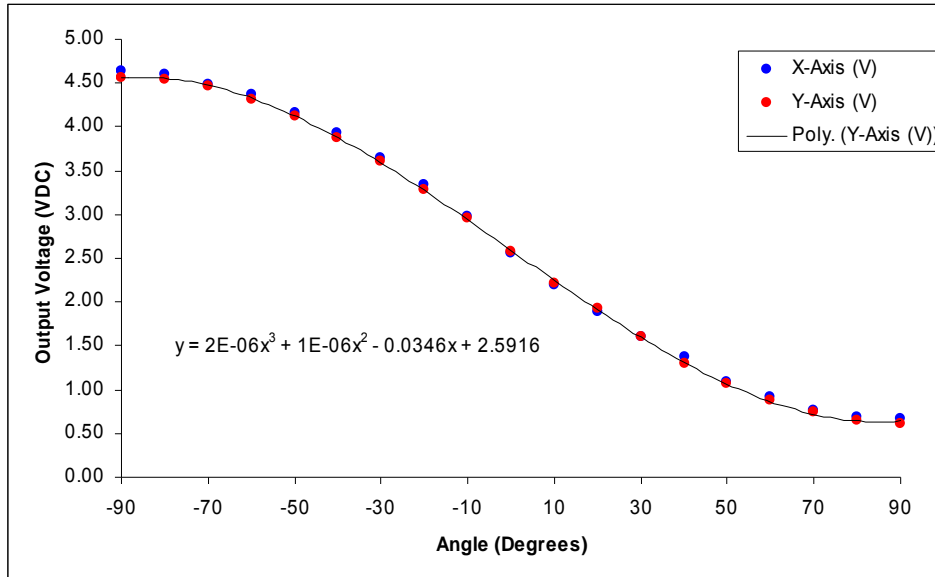


Figure 54: Inclinometer Test Results

The test results (see Figure 54) were virtually identical for both axes. A trend line is added to the data to be used in later testing. The variable voltage readings can easily be converted into dual axis incline values. This conversion will be discussed later.

7.4.2 Current Transducer

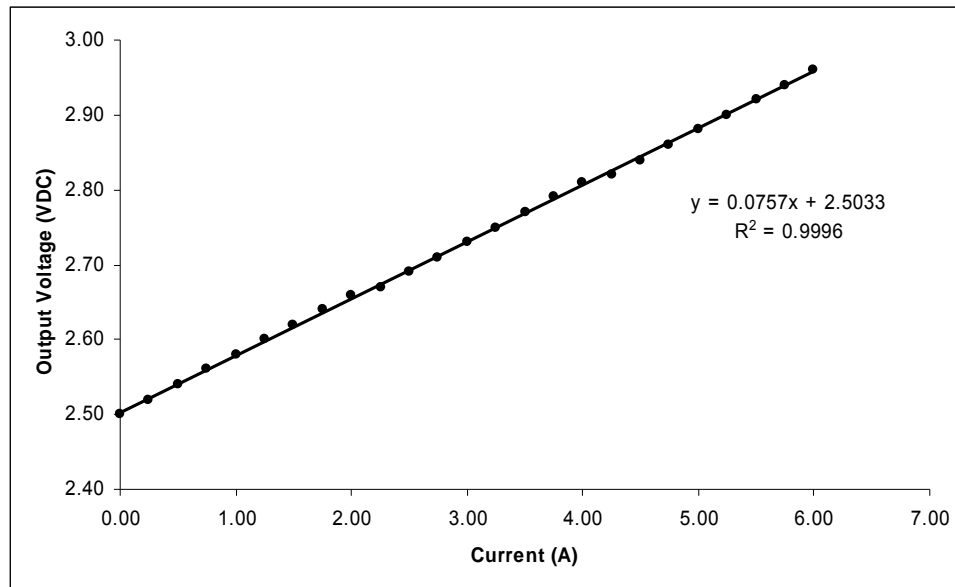


Figure 55: Current Transducer Test Results

The current transducer was tested using a laboratory power supply. The data presented in Figure 55 is very linear. Like the inclinometer, the trend line equation can be used for later testing.

7.5 Conclusion

All of the sensors selected more than sufficiently support HAL's needs. The level sensor and current transducer give accurate and reliable data. The limit switch used for obstacle detection is extremely simple and effective. The ground contact sensor does its job well, but adds a small amount of instability to the legs. Although this instability is not ideal, it is minor when compared to the slip in the leg system as a whole.

8 Microcontroller

8.1 Needs

The most obvious need for a microcontroller to control HAL is the ability to handle all of the inputs and outputs (I/O) made necessary by the subsystems. Table 4 shows the number of I/Os needed to control each leg, as well as the type of signal to be analyzed or produced. It is important to both have enough I/Os, and the ability to read and create the signals. Fifteen channels need to be able to read or produce digital signals, three need to be able to produce a PWM signal, and three need to be able to interpret an analog signal – most likely with an analog to digital converter (ADC). The digital input from the encoders will be switching very fast (up to 17.3 kHz), making a fast counter imperative the HAL’s success.

Table 4: Needed Inputs and Outputs

Leg Microcontroller (x4)				Central Micro controller			
	<i>Subsystem</i>	<i>Number of Channels</i>	<i>Type</i>		<i>Subsystem</i>	<i>Number of Channels</i>	<i>Type</i>
<i>Inputs</i>	Encoder Pulses	8	Digital	<i>Inputs</i>	Inclinometer	2	Analog
	Object Switch	1	Digital		Current Transducer	1	Analog
	Ground Sensor	1	Digital				
<i>Outputs</i>	H-Bridge Speed	3	PWM				
	H-Bridge Direction	3	Digital				
	Power Relay	1	Digital				
	Direction Relay	1	Digital				

It was determined early on to be beneficial to split up the huge number of tasks need to be performed among multiple microcontrollers. Each leg has its own controller that performs all of the tasks necessary to move and analyze the incoming data. These four leg microcontrollers are then connected to a central microcontroller that also reads platform sensors, but most importantly controls the overall robot and runs the motion algorithm.

The processing speed of the selected microcontroller is of the utmost importance. It has been previously shown that the encoders output pulses at a maximum speed of 17.3 kHz.

Determining the Nyquist Rate of this signal will give the maximum required controller speed. The Nyquist Rate is the minimum sampling rate required to avoid aliasing when sampling a continuous signal [59]. In other words, it is the minimum sampling rate required to allow unambiguous reconstruction of a band limited continuous signal from its samples. If the input signal is real and band limited, the Nyquist Rate is simply twice the highest frequency contained within the signal. This results in an encoder Nyquist Rate of 34.6 kHz.

Because HAL has five microcontrollers, communication is imperative for proper operation. Some choice of communication architecture needs to be implemented, i.e. RS232, SPI, I²C, or CAN. Ideally this would already be developed and implemented on the microcontroller itself, greatly reducing the complexity and development time required.

Other requirements may be considered external to the microcontroller itself, but are often included on the physical board. One is the need for some type of memory storage. There needs to be some method of storing the large number of data points required to do the testing

of different components (e.g. encoder position data). Another is the need for a 5 V regulator to provide power to some of the sensors (e.g. encoders, inclinometer, current transducer, and switches).

For the types of activities continually being performed by HAL, some variety of event driven programming with interrupts would be beneficial. Instead of waiting for a complete command to process information, the microcontroller can look repeatedly for information to process. In this way, batches of code can be triggered using interrupt handlers to react to hardware events. This style of programming would be especially helpful for reading the encoders. Otherwise, all encoder inputs would need to be polled continuously – detrimentally slowing down the program. Event driven programming gives the user the ability to do parallel programming (as apposed to linear programming) – doing different tasks at the same time.

With event driven programming, the microcontroller can perform other necessary tasks while it waits for an input from the encoder. Once the value of the encoder I/O line changes, an event portion of program can be run to check the other encoder channel. The value of the second encoder channel will be used to determine the direction of the motor, and in turn increment or decrement the variable counting the total pulses.

A familiar programming environment is always important when developing software.

HAL's programming is most familiar with languages similar to BASIC and C. To deviate from these would mean a long and tedious learning process.

As with all other aspects of HAL, cost is an important factor. However, this cannot be the overriding factor if detrimental to the required functionality, overall ease of implementation, or user friendliness.

8.2 Concepts

The cheapest and most basic microcontrollers are Peripheral Interface Controllers (PIC), made by Microchip Technology. There is a wide variety of this type of controller. However, they are not ideal for use on prototypes. A development board would need to be purchased for programming, and they do not include external memory or a voltage regulator.

Another popular category of microcontroller is the Stamp family, produced by Parallax. Although simple to use and with much of the necessary functionality, they are relatively expensive, have slow processing speed, do not have event driven or parallel programming, and/or do not use a familiar language.

PICs are often integrated on circuit boards to create other styles of microcontrollers. One such microcontroller, the Object Oriented PIC (OOPic), is produced by Savage Innovations. These are the most promising, and will be discussed in detail in the next section.

8.3 Design

The microcontroller selected for all five locations is the OOPic. According to the manufacturer: “Specially designed for robotics, the OOPic is a totally different approach to

microcontrollers that uses objects to control the attached hardware, while the application program focuses on controlling the objects [59].” The OOPic uses preprogrammed multitasking “objects” to interact with hardware. These objects control both peripherals, as well as all aspects of the OOPic itself. Scripts can be written in either BASIC, C, or Java to control these objects. During operation, the objects run continuously and simultaneously in the background, while the scripts run in the foreground to tell the objects what to do.

The OOPic includes a library of over 130 of these objects. Within this large library of objects, there are some specifically designed for the applications required by HAL. These include a PWM signal generator, ADC, quadrature encoder reader, communication link, button/switch reader, and of course digital I/Os. There are 31 I/O lines on each OOPic, more than enough for HAL’s needs.

Another unique feature of the OOPic is the capability of using “virtual circuits.” Virtual circuits can be thought of as the software equivalent of an electronic circuit connecting together objects in various ways. They allow objects to pass data to each other completely in the background, eliminating the need for certain scripts. Virtual circuits can handle the processing required for speed control, time-out events, limit switches, emergency breaking, and a while myriad of other functions, eliminating the need for the script to pole such tedious tasks.

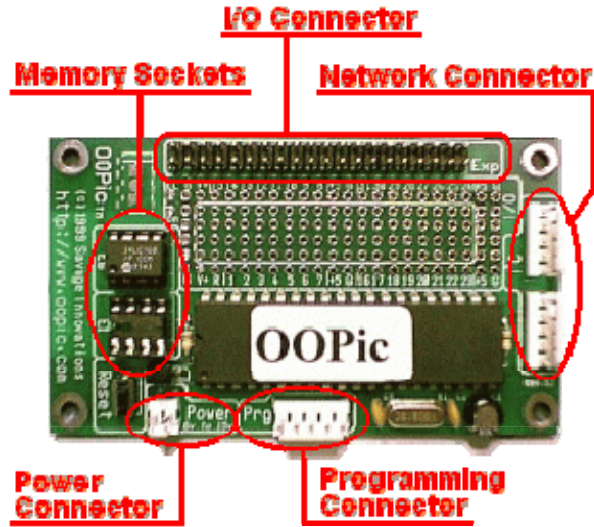


Figure 56: OOPic S-Board Layout [60]

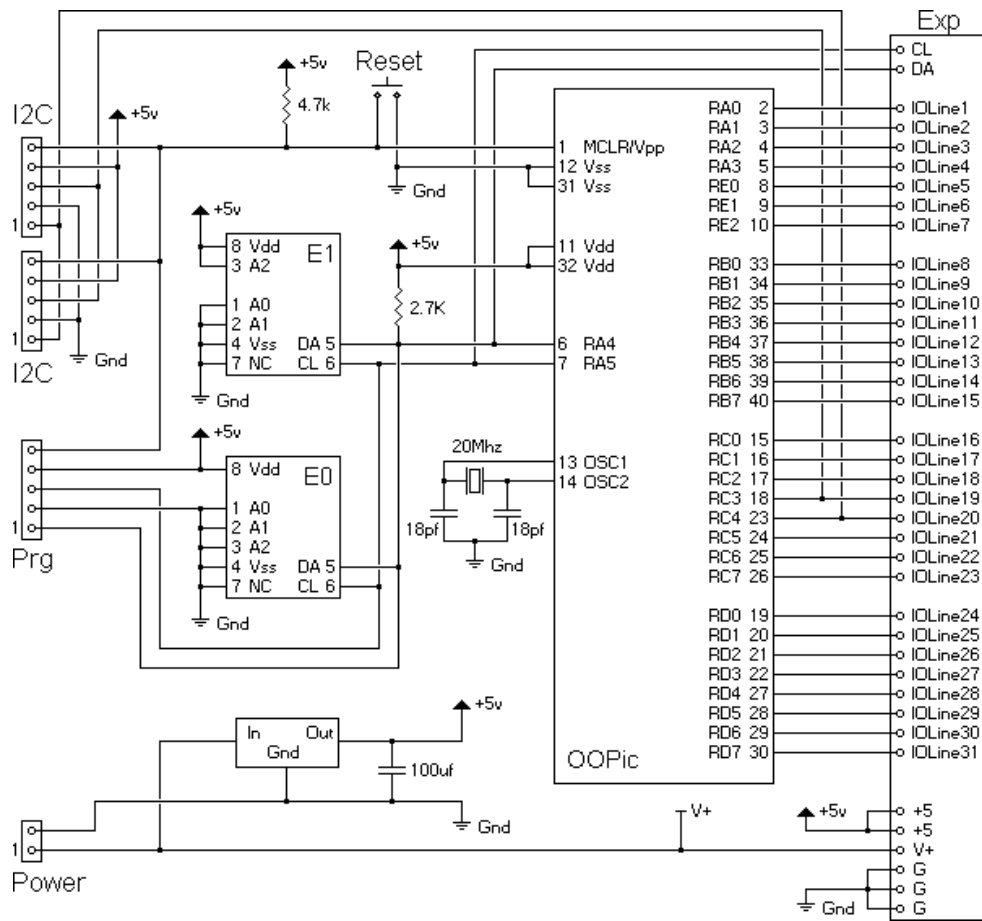


Figure 57: OOPic S-Board Wiring Diagram [6059]

OOPics include a built in network that can be used to communicate between all five controllers. An I²C bus network is used to communicate with other OOPics, store data in an electrically erasable programmable read-only memory chip (EEPROM), connect to a computer, or communicate with any other I²C devices. I²C devices have the nodes connected in parallel to a common communication bus, which eliminates a large amount of wire and connectors that are needed for other network types.

The OOPic comes standard with an external EEPROM, and also has an empty slot for another. This slot is utilized with the addition of a 1024 Kbit EEPROM, which was purchased separately. The OOPics are equipped with an object that can read and write values to the EEPROM in hexadecimal format. While virtually any size positive integer can be stored, anything above 255 requires additional processing.

The OOPic can be powered by a source with a voltage range of 6-15 V. Although the battery being used to power the motors is within this range, a separate standard 9 V battery grouping was implemented. This power design is to avoid problems that often arise in electrical systems that have power sinks that draw excessive amounts of current. The power provided to the microcontrollers will remain “clean” and unaffected by hardware. The power given to the OOPic is internally converted to 5 V, which can be used by the other devices located throughout the robot.

The main processor of the OOPic is a PIC16F877, with a clock speed of 20 MHz. When implemented on the OOPic, 2000 instruction per second and 100,000 virtual circuit operations per second can be run. With these specifications, it appeared that the OOPic would be able to keep up with all inputs using virtual circuits. The fastest of these inputs are those from the encoders. The OOPic should be able to run virtual circuit operations at almost three times the Nyquist Rate that is required to read the encoder inputs.

Table 5 shows the connection to the microcontrollers. Pins 1-5 are used for the programming cable connection to the computer. Pins 19 and 20 are dedicated to the I²C bus. On the leg microcontroller, the two dedicated PWM generation pins are utilized. While all I/O pins have the ability to produce a PWM signal, pins 27 and 29 have much better resolution (256 values versus 16 values). Dedicated ADC pins are utilized in the central microcontroller. These inputs convert the analog voltage to a digital value with a very high 10 bit resolution (0.0049 V per increment). All other I/O's used provide digital inputs and outputs.

Table 5: OOPic Connections

Leg Microcotroller (x4)			
<i>Pin</i>	<i>Name</i>	<i>Function</i>	<i>Direction</i>
1	LSDA	Local I ² C Serial Data	Bidirectional
2	GND	Ground	
3	LSCL	Local I ² C Serial Clock	Bidirectional
4	Power	+9V Power Supply	
5	Reset	Reset (Active Low)	Input
7	I/O 1	Wheel Encoder A	Input
8	I/O 14	Wheel Encoder B	Input
9	I/O 2	Steering Encoder A	Input
10	I/O 13	Steering Encoder B	Input
11	I/O 3	Shoulder Rotation Encoder A	Input
12	I/O 12	Shoulder Rotation Encoder B	Input
13	I/O 4	Shoulder Abduction Encoder A	Input
14	I/O 11	Shoulder Abduction Encoder B	Input
19	I/O 7	Object Detection Switch	Input
20	I/O 8	Ground Contact Switch	Input
21	+5V	+5V Regulated	
22	+5V	+5V Regulated	
23	GND	Ground	
24	GND	Ground	
27	I/O 17 (PWM-2)	Wheel PWM	Output
28	I/O 30	Shoulder Rotation PWM	Output
29	I/O 18 (PWM-1)	Steering PWM	Output
30	I/O 29	Shoulder Abduction On/Off	Output
31	I/O 19	I ² C Clock	Bidirectional
33	I/O 20	I ² C Data	Bidirectional
34	I/O 27	Shoulder Abduction Direction	Output
36	I/O 26	Shoulder Rotation Direction	Output
38	I/O 25	Steering Direction	Output
40	I/O 24	Wheel Direction	Output

Central Microcontroller			
<i>Pin</i>	<i>Name</i>	<i>Function</i>	<i>Direction</i>
1	LSDA	Local I ² C Serial Data	Bidirectional
2	GND	Ground	
3	LSCL	Local I ² C Serial Clock	Bidirectional
4	Power	+9V Power Supply	
5	Reset	Reset (Active Low)	Input
7	I/O 1 (A2D-0)	Current Transducer	Input
9	I/O 2 (A2D-1)	Inclinometer X-Axis	Input
11	I/O 3 (A2D-2)	Inclinometer Y-Axis	Input
21	+5V	+5V Regulated	
22	+5V	+5V Regulated	
23	GND	Ground	
24	GND	Ground	
26	I/O 31	Black Button	Input
28	I/O 30	Red Button	Input
31	I/O 19	I ² C Clock	Bidirectional
33	I/O 20	I ² C Data	Bidirectional

The functional decomposition showing the relationship of the microcontrollers to the other systems can be seen in Figure 7.

8.4 Test

Several tests were done using an oscilloscope to characterize the PWM output of the OOPics. The first, shown in Figure 58, uses one of the dedicated PWM generation pins at 50% duty (value of 127). The dedicated PWM I/Os produce a high frequency wave, so their output will be referred to as PWMH. The signal oscillates at a frequency of 19.65 kHz, producing a period of 50.90 μ s between pulses.

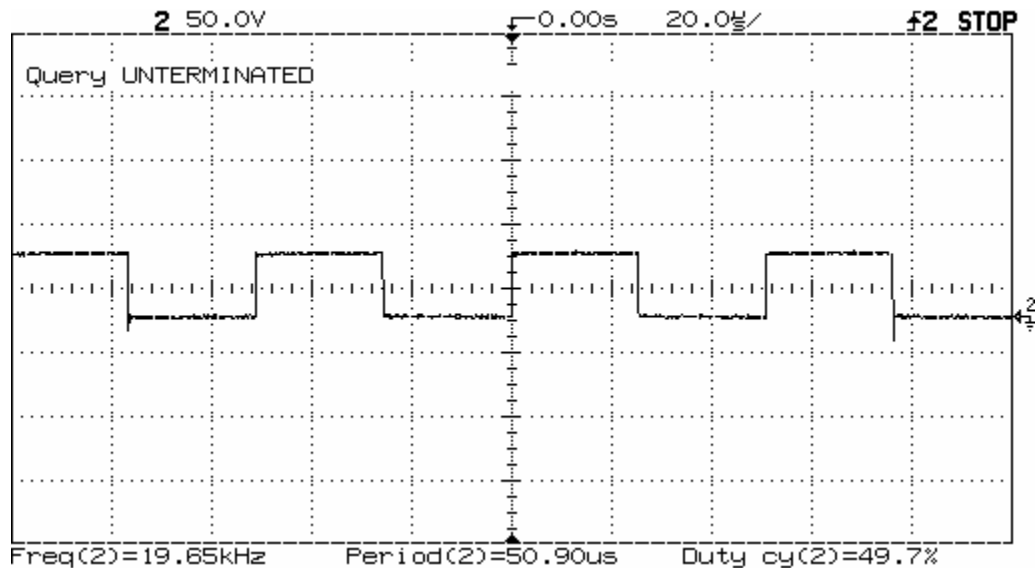


Figure 58: PWM High at 50% Duty

Next, the PWM output of a typical I/O with no dedicated PWM (PWML) was characterized. These I/Os produce a much lower frequency wave, so their output will be referred to as PWML. Figure 59 shows the signal produced at 50% duty (value of 7). As expected, the PWML gives less resolution than the dedicated PWM pins. The signal oscillates at a frequency of 560 Hz, producing a period of 1.79 ms.

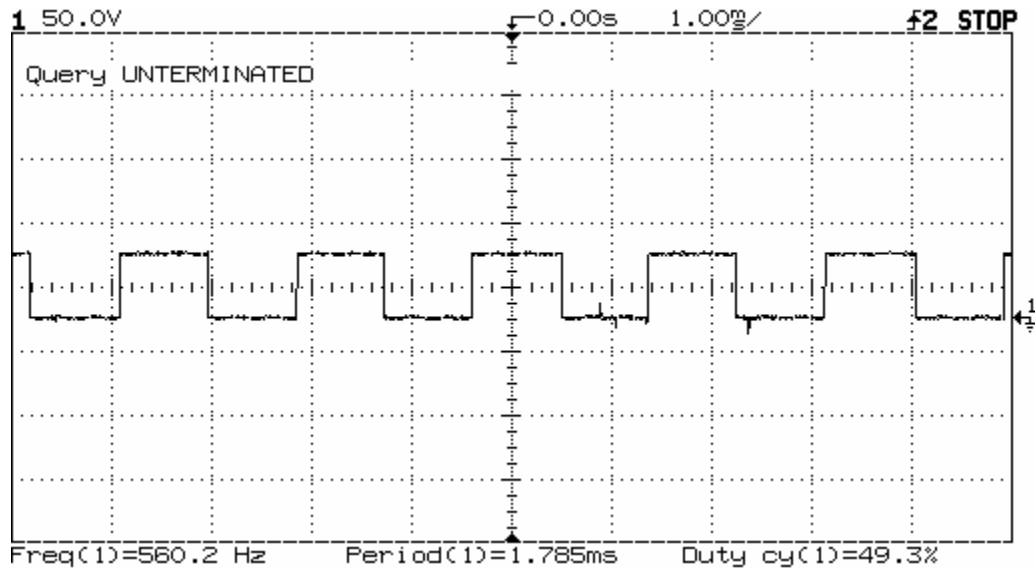


Figure 59: PWM Low at 50% Duty

Both PWM generation methods produce a nice square wave and give very favorable results when implemented into the motor control system. While still effective, a PWML pin produces a signal that is 2.8% as fast as a dedicated pin. Figure 60 physically shows the difference between these two methods. Channel 1 (upper) is the PWML output and Channel 2 (lower) is the PWMH output.

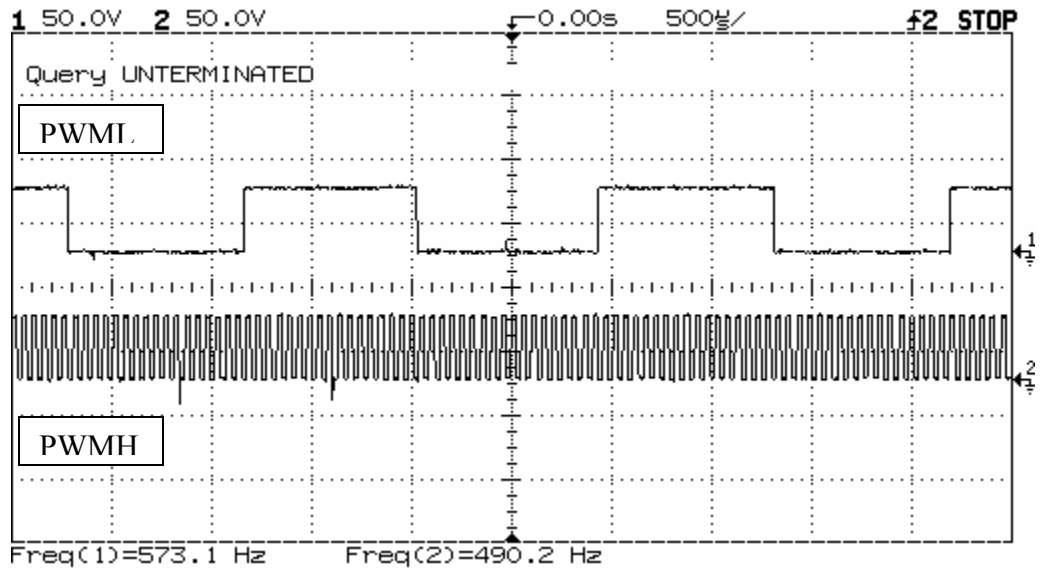


Figure 60: PWM High and PWM Low Output at 50% Duty

The OOPic's two types of PWM signals were analyzed at 100% duty (values of 255 and 15). Figure 61 proves that the signal does not oscillate at full duty, but gives a constant high value. This effectively uses the H-Bridge as a switch to give the motor the full 7.2 V from the battery.

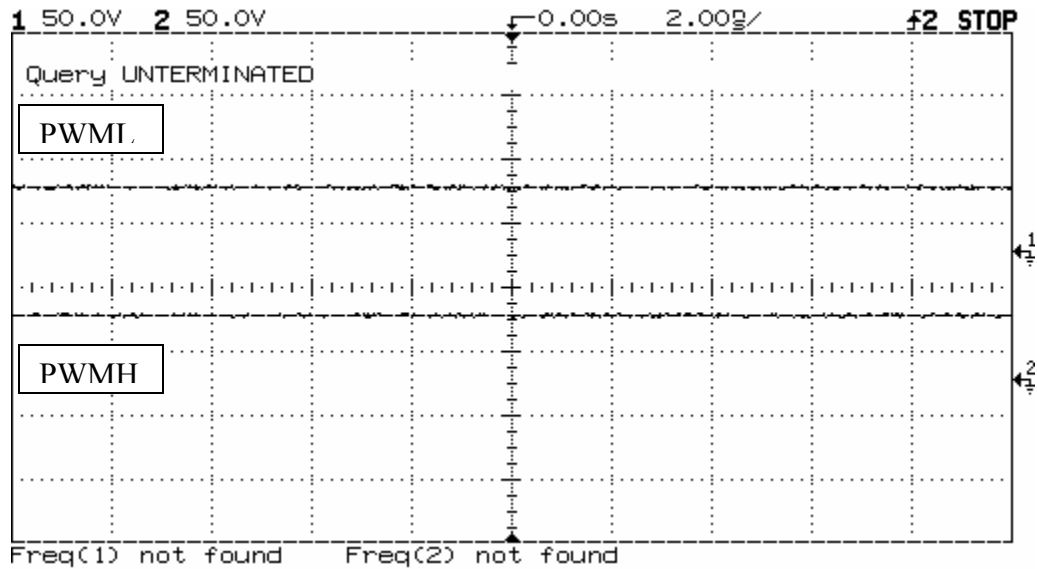


Figure 61: PWM High and PWM Low at 100% Duty

After implementing the OOPics into the motor control system, problems arose. It was discovered early on that the object created for the purpose of reading a quadrature encoder could not keep up with the high frequency of the encoder pulses. Even when the motors are significantly slowed, the data is extremely flawed. It became apparent a new method for counting pulses was needed.

Two methods for counting the encoder inputs were tested. The first attempt was to write a program that used an “If” statement in the code to increment a variable every time a pulse was detected. An oscilloscope was used to physically test the effectiveness of this method. One encoder channel was inputted into an I/O pin, while a second I/O pin was used to output the signal read. The “If” statement set the value of the output high if the value of the input

was also high, and conversely low if the input was low. A “Do” loop continuously ran this program.

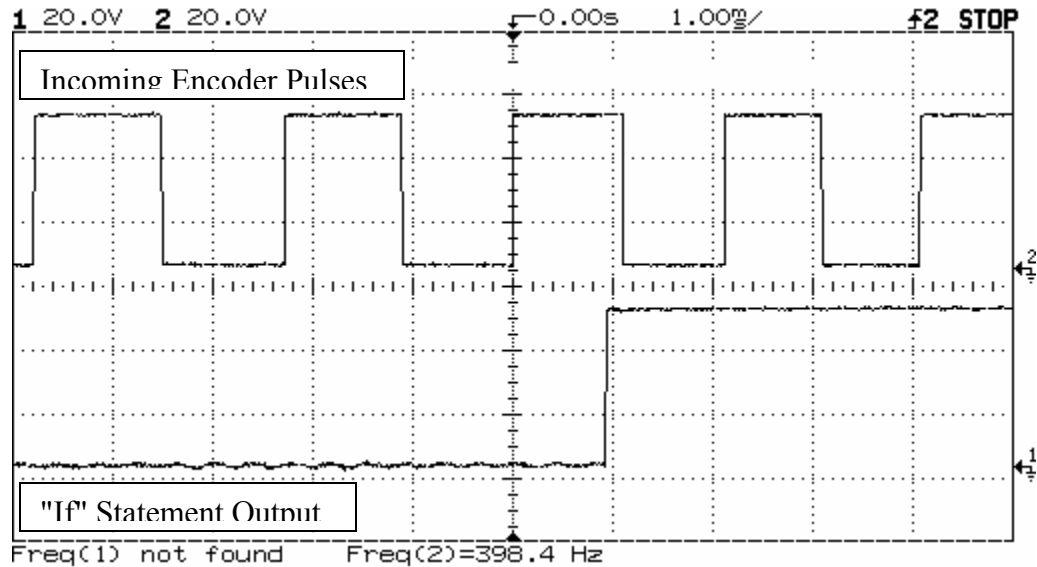


Figure 62: If Statement Test

Figure 62 shows the inability of the “If” statement to keep up with the encoder input. The program could not give favorable results, even at the slowest possible speeds.

The next test used a faster running virtual circuit to attempt to read the encoder input. The experiment was set up in the same manor as the previous one that used the “If” statement. The difference being that a virtual circuit was created (shown in Figure 63) that linked the input and output pins together and ran in the background. The results of this test were much more favorable and can be seen in Figure 64. Channel 2 (upper) is the true output of the encoder and Channel 1 (lower) is connected to the output pin.

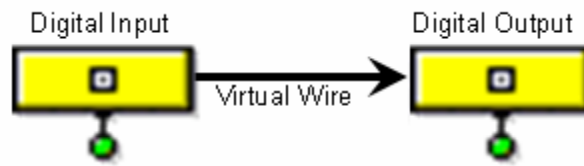


Figure 63: Encoder Test Virtual Circuit

The virtual circuit is able to follow the encoder input up to a value of approximately 1.5 kHz.

The upper chart in Figure 64 shows the virtual circuit successfully following an encoder input of 595 Hz, while the lower chart shows it breaking down above 1.5 kHz.

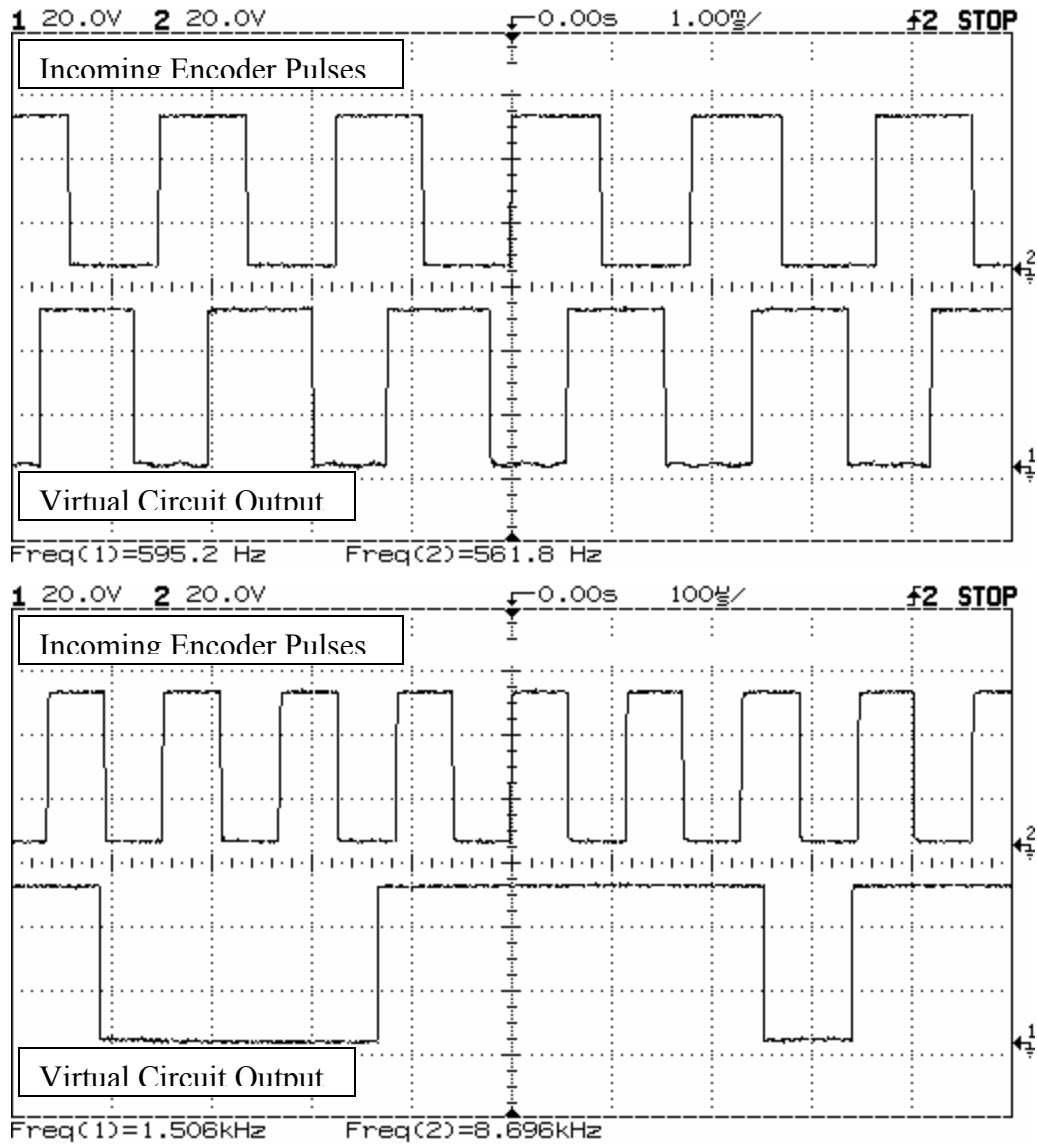


Figure 64: Virtual Circuit Test

Using this data and the properties of the gear-motor/encoder assembly, the maximum motor speed at which the encoders can be read is:

$$\frac{1500 \text{ cycles}}{1 \text{ sec}} \times \frac{1 \text{ Rev}}{6000 \text{ cycles}} \times \frac{60 \text{ sec}}{1 \text{ min}} = 15 \text{ RPM} = 90^\circ / \text{s} \quad (8.4.1)$$

This is acceptable for the angular velocity used on all of the joints except for shoulder abduction. Since they include further speed reduction through the worm and worm-gear combination, they must turn at much greater speeds. The solution to the problem will be discussed in the next section.

Using the same principles as the test, a new virtual circuit can be created to determine motor position. Figure 65 shows the virtual circuit used to accomplish this task. One channel on the encoder is used to input a signal into an object called “counter.” When this signal changes from a low to high pulse, the count command modifies the value of a word variable. The second encoder channel is wired to a function of the counter that determines whether to increment or decrement the output variable. In this way, the position of each motor can be kept up to date at all times in the background of the program.

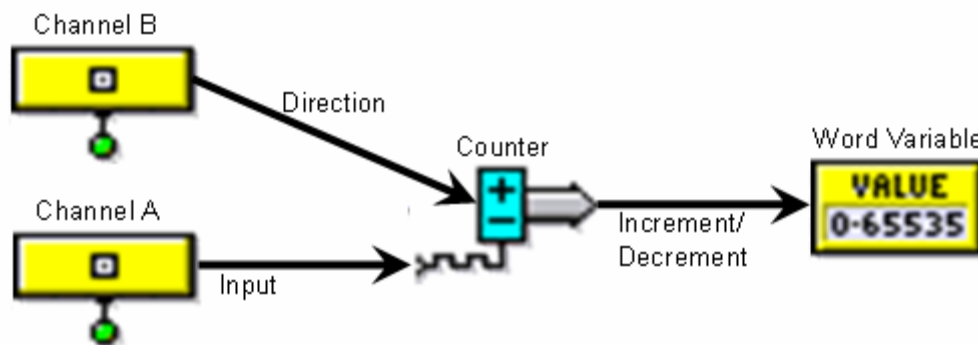


Figure 65: Quadrature Encoder Virtual Circuit

8.5 Redesign

The encoders located on the motors, used for the four shoulder abduction joints, output data at a much faster rate than can be handled by the OOPics. A few solutions to this problem were considered:

1. Quadrature decoders could be purchased to convert the encoder data into a form usable by the microcontrollers. These are usually expensive and would take up valuable real-estate on the chassis.
2. Another microcontroller, probably a PIC, could be implemented with the sole purpose of counting and interpreting encoder data. This method seemed promising at first and was researched further. After some research and testing, it was determined that the learning curve was too great and implementing this idea would be much too time consuming. Adding four more microcontrollers also seemed overly complex for the simplicity of the problem.
3. A different sensor could be implemented in place of the encoder. While it would be easy to use another sensor to determine the top and bottom of the full shoulder stroke, it is infinitely more difficult to keep track of the incremental position in-between.
4. The most simple, cheapest, and fastest solution to this problem was initially overlooked. A new encoder wheel could be bought or made with a smaller resolution. Since a suitable wheel could not be found on the market, the existing wheel was modified.



Figure 66: Encoder Wheel Comparison

Figure 66 shows a comparison of the original encoder wheel, with 120 counts, to the modified encoder wheel, with one count. The resolution of the shoulder abduction joint then becomes 50 counts per revolution, as compared to 6000 counts per revolution on all other joints. Even this significantly lower resolution is more than enough for HAL's purposes.

The output of both channels of a modified encoder is shown in Figure 67. While Channel 1 (upper) gives the expected square wave, Channel 2 (lower) gives an unexpected pattern. The same channel characteristics can be seen by all four modified encoders. It has not been determined why this occurs, but it is also not important to this project. Since the worm-gear prevents motion unless the motor is actively driven, the joint will only move when told by the microcontroller. Because of this, HAL will always know which way the joint is moving.

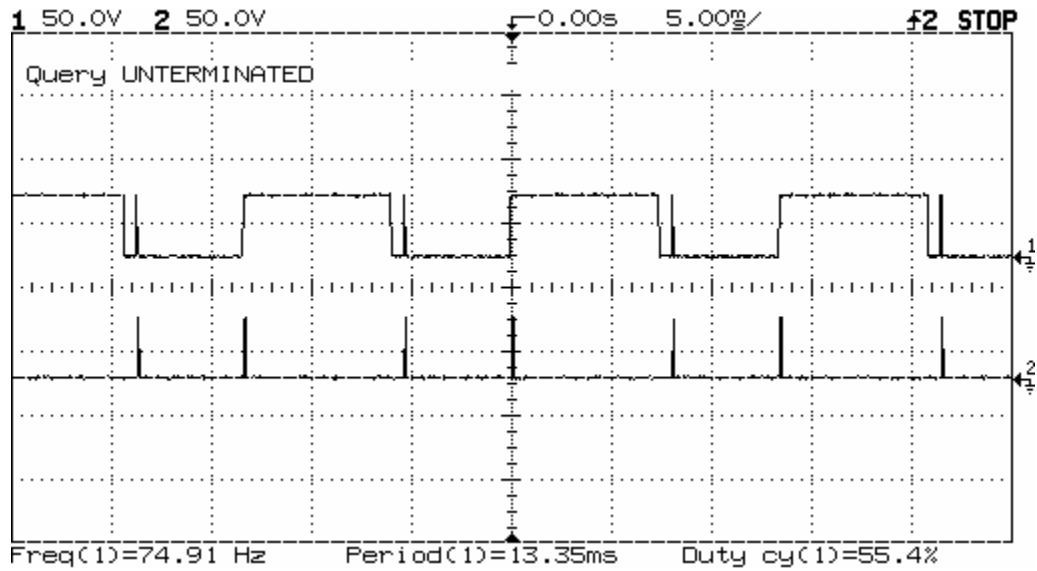


Figure 67: Modified Encoder Output

8.6 Conclusion

The OOPics are effective in all areas needed to control and test HAL, excluding reading the encoders. After some modifications, they can still be used to do this task. The documentation and debugging capabilities of the OOPic are also rather disappointing. Even with its drawbacks, the user friendliness, robustness, and included features make it a good choice for use in prototype robotic applications.

9 Chassis

9.1 Needs

9.1.1 Mechanical

HAL's chassis encompasses everything not directly connected to the legs itself. The first, and probably most obvious, role of this subsystem is to hold the shoulder joints. Not only must they be mechanically stable, but they also have to have enough space reserved for the motors and other components. Having enough area and volume is a major concern because of the vast number of components. The footprint has to be as small as possible, along with the weight. Connection points for components must also be taken into consideration. Some will never need to be accessed, while others need to be easy to get to.

9.1.2 Electrical

Some form of prototyping area is ideal for this first generation robot. A way to be able to easily connect and modify components is essential. Additions and changes are not planned, but must always be accounted for. Along these lines, access to the 40 pins located on the microcontrollers is important. Modifications should be able to be made without any disassembly.

The wires that run to the components located on the legs will need to be firmly attached. With the legs moving in so many different ways, a weak connection point could easily be compromised. They must also be kept from getting tangled or ensnared by any part of HAL.

9.2 Design

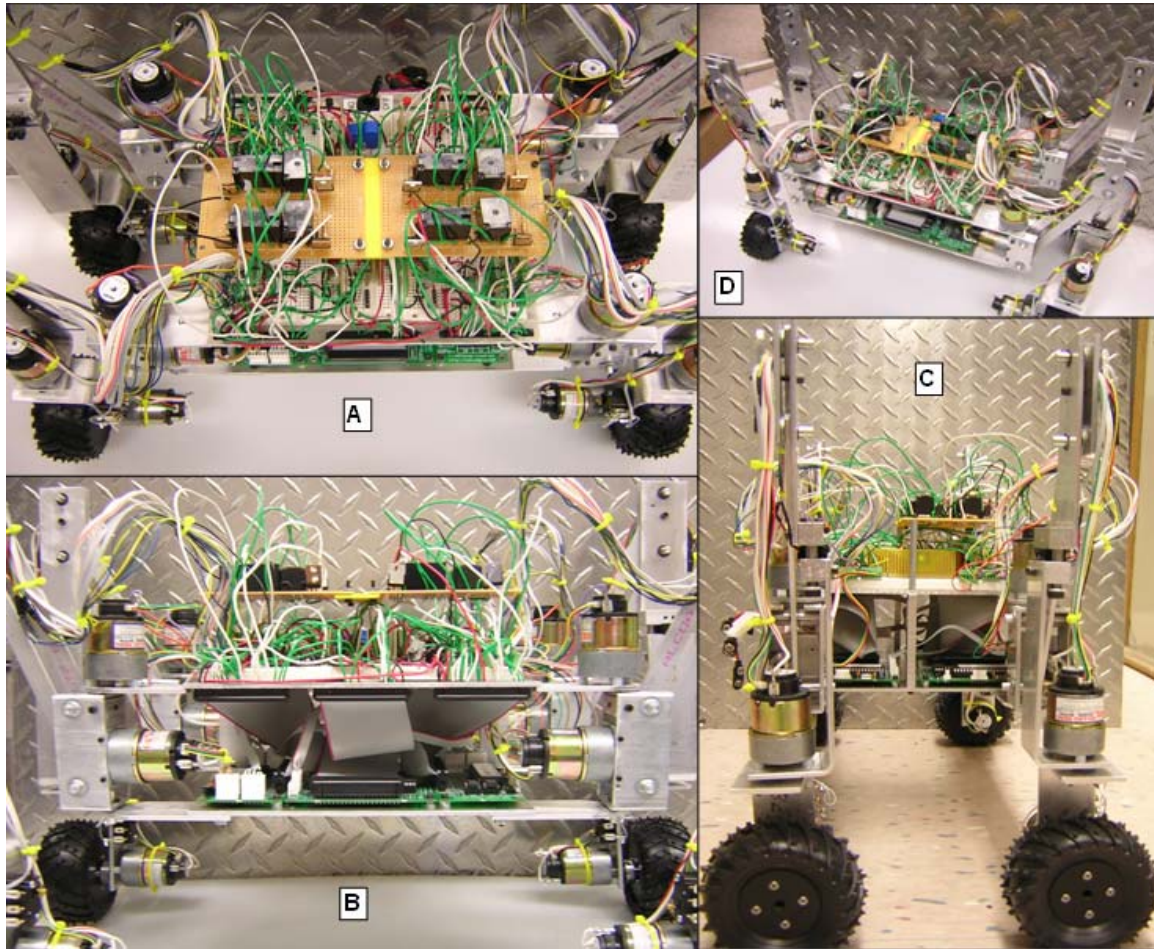


Figure 68: Chassis: a) Top View; b) Front View; c) Side View; d) Orthogonal View

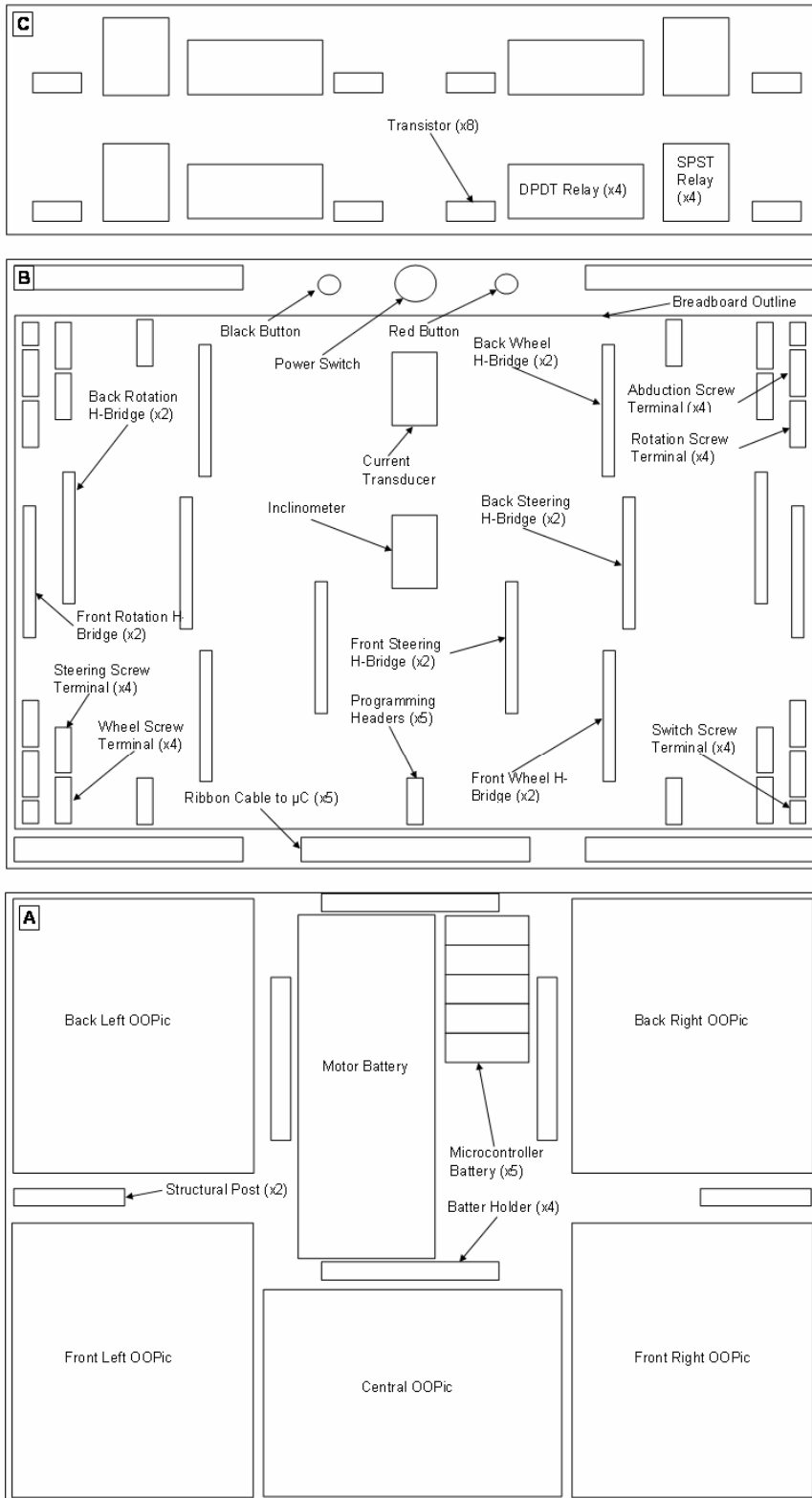


Figure 69: Chassis Diagram: a) Level 1; b) Level 2; c) Level 3

9.2.1 Mechanical

The material selected for HAL's chassis structure is aluminum. The reasons for this selection is the same as those for the legs – low weight, high specific strength, low cost, and ease of machining.

The chassis was originally designed with two levels. Trying to squeeze everything onto one level would make the robot extremely oversized. A two level design also simplifies the connections to the shoulder joint. A small third level was later added because of the redesign of the system controlling the shoulder abduction motor. The limited space required a whole new expansion to fit all of the parts required.

The basic layout of all three levels is shown in Figure 69. The first level can be considered HAL's brain – it holds all five microcontrollers and both battery sources. The Second and third levels can be considered HAL's heart – they hold all of the power electronics.

9.2.2 Electrical

For prototyping and modification simplicity, it was decided to make the vast majority of the second level one large breadboard assembly. Wires and components could be added and subtracted very easily and whenever needed.

40 pin ribbon cables were specified to give access to the microcontrollers. Since the microcontrollers were on the lowest level, access to their pins is very limited. The ribbon cable solves this problem by bringing all connections to second level. One end of the cable is

connected to the OOPic headers, while the other is permanently affixed to the base of the second level. The ends of the cable are in the same form as a 2x20 connection breadboard, allowing for easy connections.

A five pin programming header is located in one area of the OOPics that is not easily accessible in this design. The programming cable is meant to connect from the computer onto this location. Since the 40 pin connection also includes these programming connections, a new programming header was created on the second level breadboard. The programming cable can be connected directly to this header, virtually eliminating the need to ever get physical access to the OOPics again.

To keep the connections to the wires from leg components from pulling out, screw terminals were attached. These terminals hold strongly to the breadboard slots, while clamping onto the wire ends. This setup allows easy connection to all components, while still giving a sturdy hold.

The power switch bought for the motor battery was given a spot on the second level. Easy access to this switch is imperative in case of the need for emergency stopping. Two buttons were also added for programming purposes. They are used for starting or stopping routines in the microcontrollers.

The overall wiring diagram is shown in Figure 70, excluding those items whose diagram was shown earlier (i.e. switches and shoulder abduction control subsystem). Wire color

conventions were kept constant wherever possible. Power wires are mostly red, ground wires are mostly black, and signal wires are white and green.

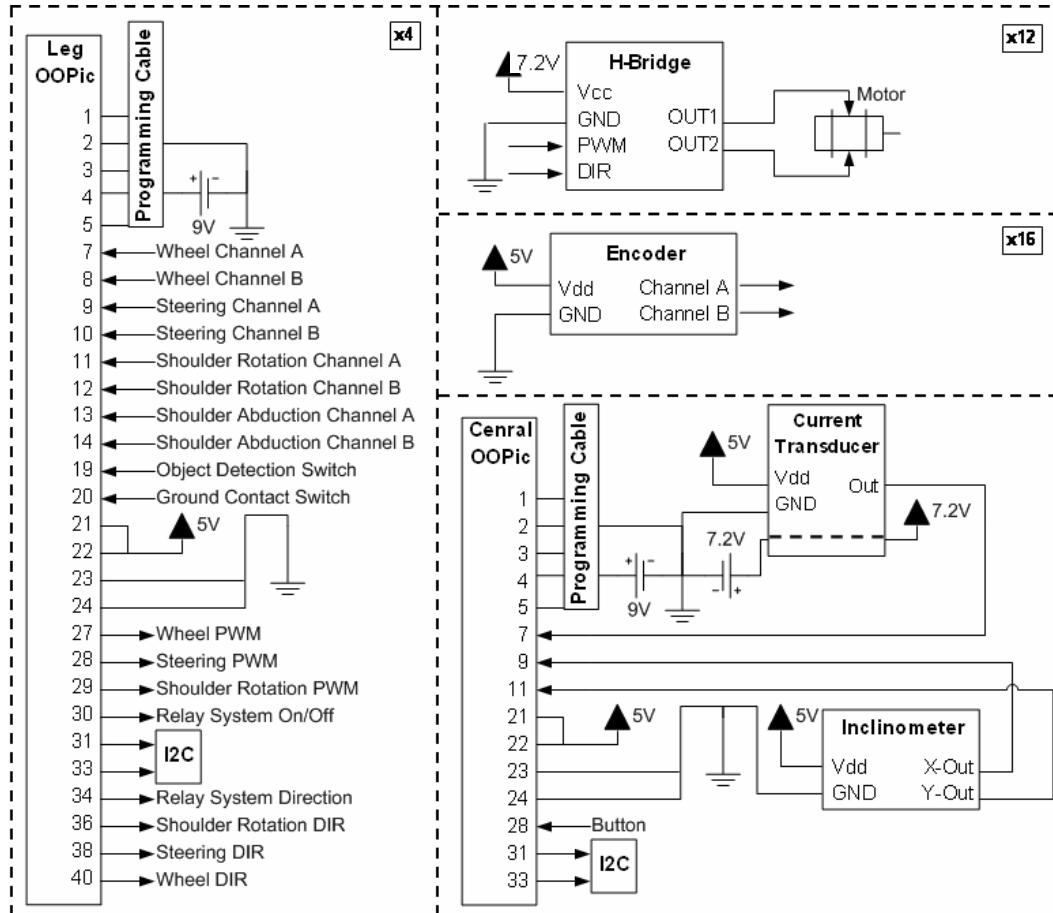


Figure 70: HAL Wiring Diagram

9.3 Conclusion

HAL's chassis suites all needs. Throughout the designing, building, and testing processes, different aspects of the wiring were modified. The breadboard style of wiring made it very easy to find any problems and make any necessary changes.

Although the current chassis design is successful, there are a few drawbacks. The vast number of wires makes certain changes hard to achieve. The wires easily become “buried” under others, making access difficult. While it has not been an issue on this robot, wires attached to breadboards can often pull out when unintended.

A future generation of HAL could be built that replaces the entire electrical part of the chassis with a single printed circuit board (PCB). This board would contain the microcontrollers, H-bridges, relays, and all other components in one compact form.

10 Hybrid Locomotion

A holistic platform discussion is needed to properly analyze the advantages of hybrid locomotion. HAL's overall functionality can be investigated in two ways: a posture control and an obstacle traversing evaluation.

10.1 Posture Control

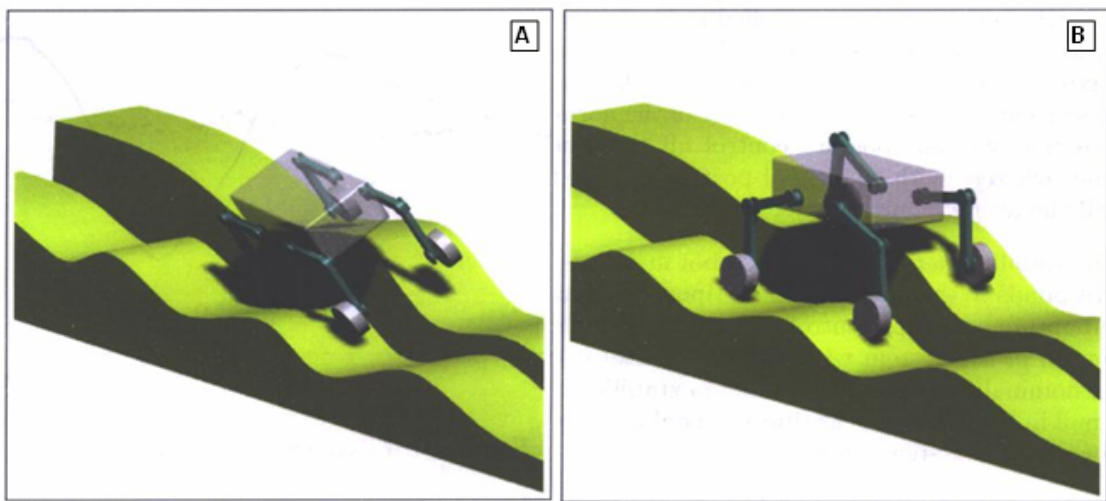


Figure 71: Posture Control Simulation [21]

One of the huge advantages of a hybrid locomotion platform over traditional types of locomotion is the ability to perform advanced posture control. Typical wheeled vehicles have an inherent instability when traveling over large terrain changes, e.g. the terrain shown in Figure 71. There are many types of passive suspension that can help account for this problem, but none as robust as driven legs. Walking robots have similar instability problems. The adjustments needed to modify a walking gait to achieve stability are extremely complex

and less reliable. The left side of Figure 71 illustrates a typical result of rolling or walking over rough terrain – the robot tipped over. The right side illustrates the more advantageous result of hybrid posture control.

With HAL's system of hybrid locomotion, it can easily, efficiently, effectively, and continuously compensate for changes in terrain. While the wheels provide the method for traveling along the ground, the legs act like an advanced form of active suspension. The inclinometer is used in conjunction with a motion algorithm (shown in Figure 72) to keep the chassis level. Motors can be constantly actuated to make corrections to leg position. HAL can relatively easily use the inclinometer to keep the chassis level, while also using the ground contact sensors to keep all four wheels on the ground. This not only keeps HAL stable, but also ensures constant four wheeled drive.

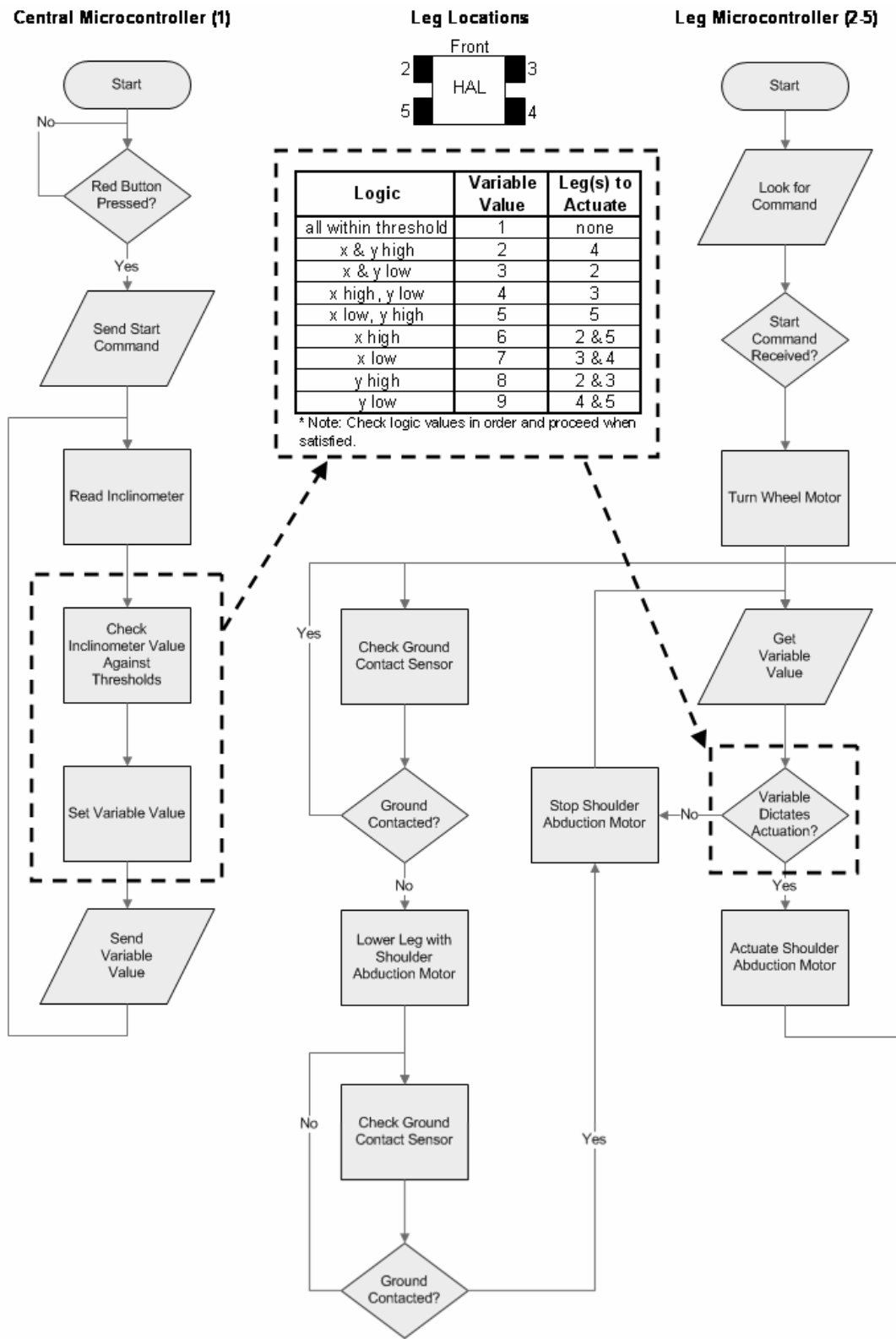


Figure 72: Posture Control Logic Flow Chart

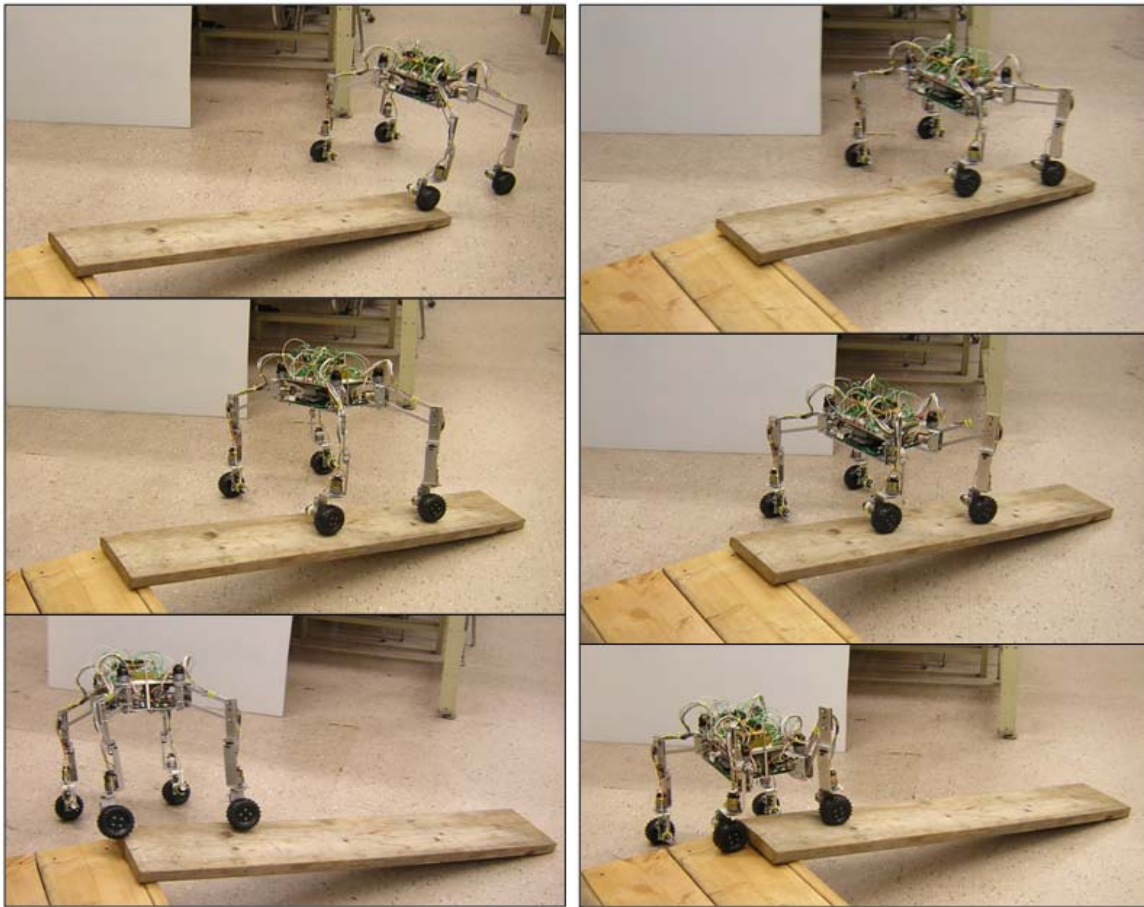


Figure 73: No Posture Control vs. Posture Control

Figure 73 shows half of HAL's wheels moving up a ramp, while the other two remain on flat ground with pure rolling and hybrid locomotion respectively. The last image in left column of Figure 73 was taken with HAL about to fall over. So much strain was placed on the two right legs and wheels, HAL was not able to move in a controlled manor. The advantages of hybrid locomotion posture control are made obvious by this figure.

10.2 Obstacle Traversing

One advantageous aspect of hybrid locomotion is the ability to traverse obstacles large in comparison to the size of the robot. Wheeled and tracked vehicles cannot overcome obstacles larger than the height of their wheels or tracks. Walking robots may be able to walk over larger objects, but much less efficiently and typically with more complications.

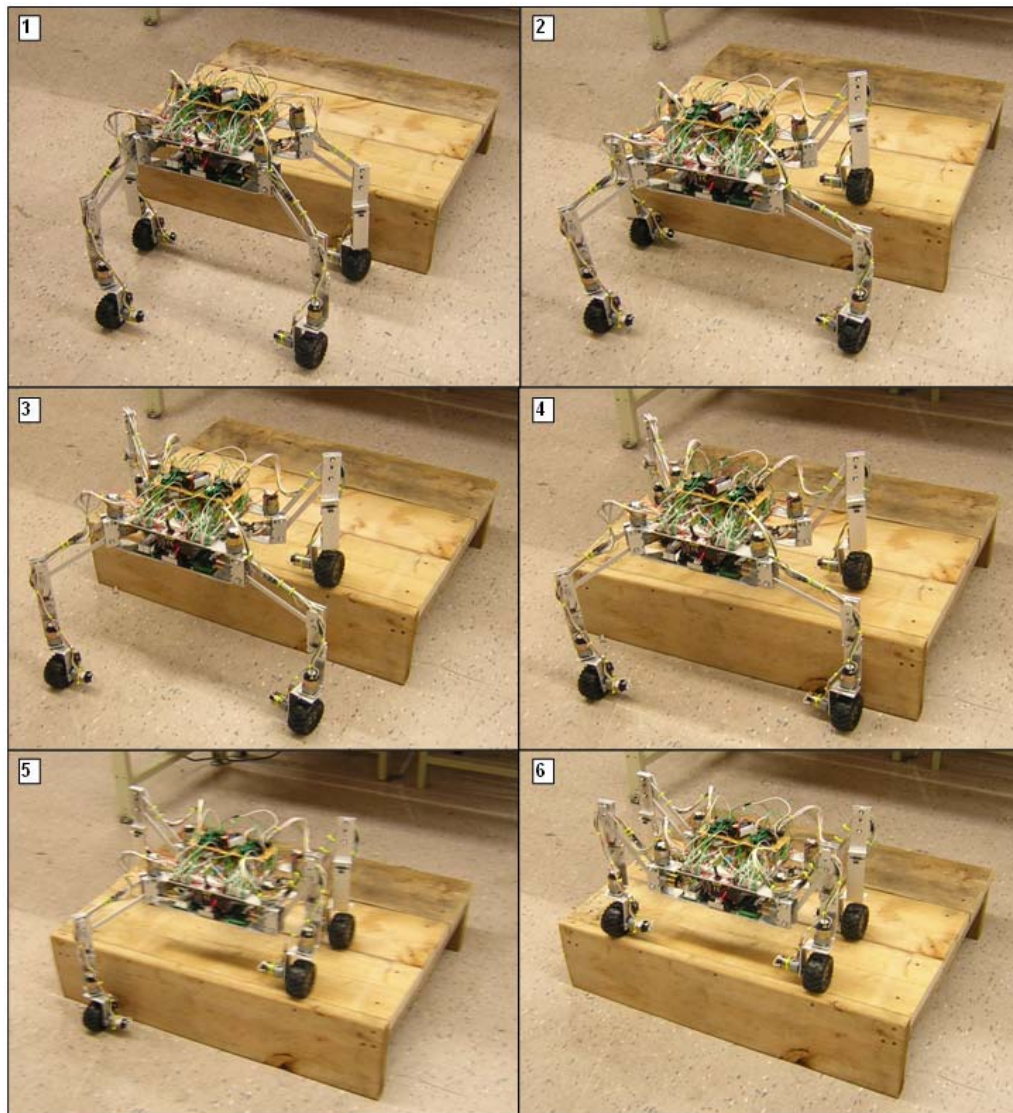


Figure 74: Step Traversing

Inherent mechanical instabilities in HAL prevented him from autonomously traversing an obstacle. However, an analysis was done to determine the most practical way to achieve hybrid locomotion onto a step. Figure 74 shows HAL stepping onto a step that is 9 in high. HAL accomplished this by doing the following:

1. Roll toward the step until the front right limit switch is pressed.
2. Raise the front right leg until the limit switch is released. Roll forward until the front left limit switch is pressed. Lower the front right leg until the ground contact sensor is activated.
3. Raise the front left leg until the limit switch is released. Roll forward and lower the front left leg until the ground contact sensor is activated.
4. Roll forward until the back right limit switch is pressed.
5. Raise the back right leg until the limit switch is released. Roll forward until the back left limit switch is pressed. Lower the back right leg until the ground contact sensor is activated.
6. Raise the back left leg until the limit switch is released. Roll forward and lower the back left leg until the ground contact sensor is activated.

The limit switches in front of each wheel is used to decide when to raise its respective leg. They can also be used in the opposite way to determine if the wheel has cleared the top of the step. Stability would be a major problem if the step was attempted to be traversed using pure walking. The high center of gravity could yield devastating results.

HAL's ability to traverse obstacles is not limited to a step. The same principles could be put into practice to overcome almost anything under the height of the full leg stroke.

11 Conclusions

11.1 Efficiency

One way of showing the vast difference between walking and rolling locomotion is through an efficiency analysis. The current transducer previously mentioned can be used to obtain data while HAL is moving. Figure 75 shows the difference between rolling and the motion of a walking gait. The data for rolling was recorded while HAL was traversing flat ground with a duty of 37% at each wheel motor. During this test, the speed averaged to about 6.5 in/sec.

Since true walking could not be successfully performed by HAL, current data was recorded during one full leg walk cycle. While performing this cycle, HAL was suspended by his chassis. This means the current recorded is tremendously smaller than it would be if the legs had to lift HAL's mass.

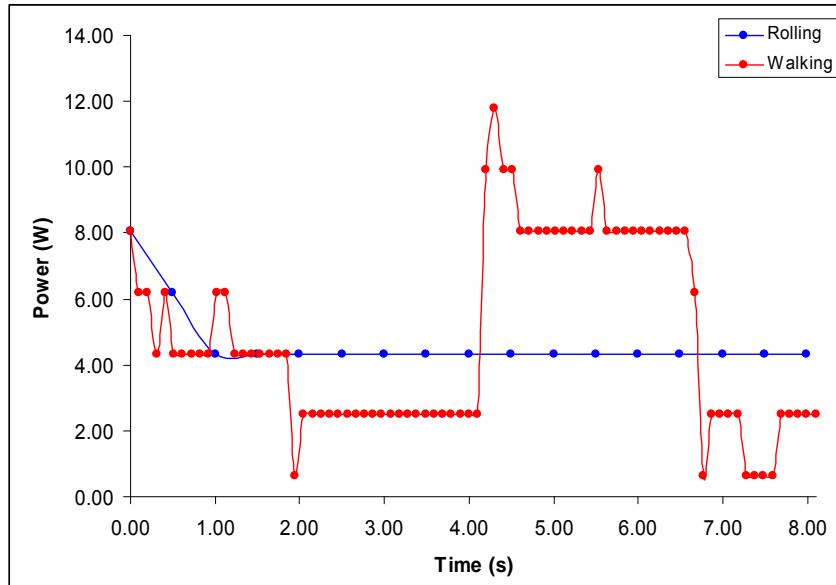


Figure 75: Instantaneous Power Usage

While the current transducer has fine resolution throughout the entire rating, both tests were within a small percentage of the total value span. This results in data with less resolution than would be ideal. However, the data is satisfactory to show efficiency benefits.

Now that the instantaneous power usage is found, the total work done throughout the entire experiment can be determined. This value is represented by the area under the curve (A) and is mathematically:

$$A = \int_a^b f(x)dx \quad (11.1.1)$$

Where a is the left most x value and b is the right most x value. Knowing the difference between each data point (h), the Trapezoid Rule can be used to approximate the value of this integral [61].

$$\int_a^b f(x)dx \approx \sum_{i=1}^n \frac{h}{2}(f(a + (i-1)h) + f(a + ih)) \quad (11.1.2)$$

Figure 76 shows the implementation of this approximation.

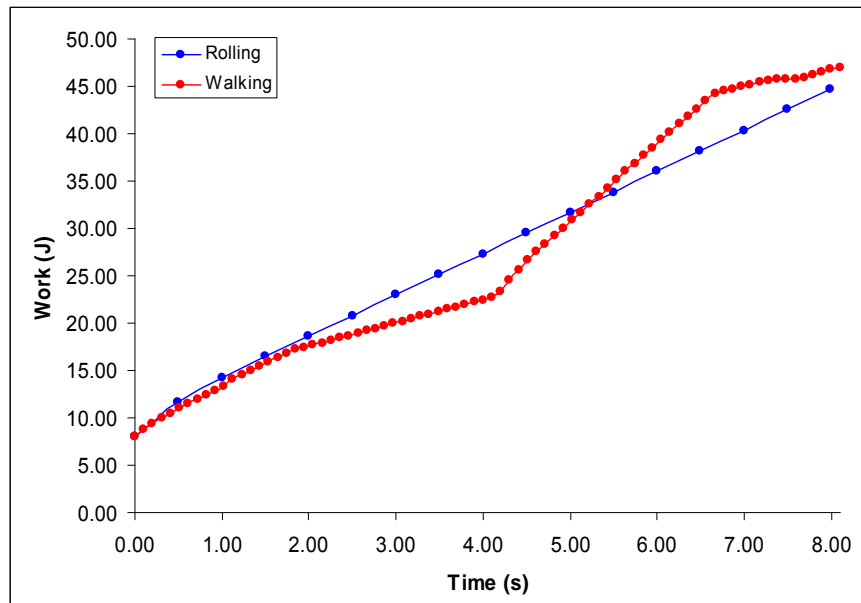


Figure 76: Total Work Done

The linear displacement caused by one walking actuation cycle is approximately 15 in. It takes about 8 sec to perform this maneuver. That extrapolates out to a platform speed of 1.9 in/sec, as compared to 6.5 in/sec for the rolling test. The total work done can also be related to the distance traveled, yielding values of 0.9 J/in for rolling and 3.1 J/in for walking.

With the data presented, it can easily be seen that rolling locomotion is much more efficient than walking. The power used by rolling locomotion comes out ahead in every category, even when walking is performed under unrealistically ideal conditions. Since the legs are

actuated much less during hybrid locomotion than during walking, it can be assumed to fall somewhere between the efficiencies calculated. As expected, the efficiencies of HAL's locomotion, from most efficient to least efficient, are rolling, hybrid, and lastly walking.

11.2 Effectiveness

11.2.1 Rolling

The effectiveness of controlled rolling motion was shown. HAL has the ability to use a sophisticated control system to roll with precision. The four wheeled steering methods implemented offer exciting results. HAL has the ability to not only turn with a zero turning radius, but also can change directions without changing the orientation of the chassis. The problem of trajectory planning and generation for four wheel steering systems has been previously researched [9], and can be implemented on HAL.

11.2.2 Walking

While pure walking was never achieved, due to the inherent instability found in mechanical quadruped platforms, an analysis was performed on the walking gate. Walking is at first very appealing for robotic locomotion, but can have many complications. Robots designs where navigation or dead reckoning is required will most likely want to steer away from this locomotion method.

11.2.3 Hybrid Locomotion

The capability of hybrid walking-rolling locomotion has been shown. The combined ability to traverse obstacles and implement posture control has very exciting possibilities. While there is room for improvement, the overall effectiveness can be seen. This robotic platform

is a good first generation design. The work performed in designing, building, and analyzing HAL became much more than just a proof of concept.

12 Recommendations

Modifications to the leg design could make HAL more stable and predictable. This could be greatly improved in two major areas: reduction of slop in the system and design of a different type of ground sensor. The tolerances for all leg joints should be tightened along with the implementation of a better design for the elbow joint. A quick fix was made with the addition of an aluminum plate to keep the joint in line. However, this added a significant amount of friction and reduced the efficiency of the shoulder abduction system.

Some leg instability is also added by the ground sensor. Since the hole for the shoulder bolts has to be large enough to allow them to slide axially, a noticeable amount of movement happens transversely. A different kind of pressure sensor could also help keep HAL's weight evenly distributed.

The ability of the shoulder abduction joint to passively hold its position may be ideally suited for all joints. While the quadrature encoders can keep track of the position of each joint when moved without powered, only moving when required would simplify the algorithms needed. The stability issues previously mentioned would furthermore benefit by this type of design.

A hexapod platform may provide more effective walking and could solve some problems encountered when trying to give HAL this ability. At least six legs are required to be able to

achieve static walking. This would expand the complication of the system, but would give more robust locomotion.

Probably the most frustrating part of this project was working with the OOPic microcontrollers. Although there are many positive features that made them a good choice for prototyping, they were found to be rather unreliable when implemented into the overall system. One did not operate at all when hooked up straight out of the box; another could not run programs that used events; and all had ghosts in the system that often could not be explained. Many times, the OOPics would stop running the program saved on the EEPROMs and inexplicably had to be reprogrammed. Unlike other microcontrollers, OOPics are also significantly harder to debug. The programmers guide, examples, and general information are extremely lacking. However, the most compelling reason to move away from OOPics is the inability to keep up with many electronic devices, i.e. encoders. They are exceptionally slow compared to other microcontrollers on the market.

The next generation of hybrid locomotion robot could take the work done on HAL and significantly reduce the size and weight in many areas. Electronically, a PCB can be created to eliminate the large and complicated breadboard/wire method currently used. A single board could be designed to include all microcontrollers, H-bridges, relays, sensors, and connection points. With a much smaller electrical system, the chassis size could in turn be significantly reduced. A single layer design could be feasibly.

Some form of remote control would also make debugging and testing more painless. It is hard to characterize a completely new electromechanical system when the user does not have direct control. While HAL displayed a large amount of aptitude in autonomy, the beginning trials could be more effective with direct control. Therefore, the ability to move both under direct control and with internal motion algorithms would be ideal

13 References

1. Goel, P., Roumeliotis, S. I., and Sukhatme, G. S. (1999). *Robust Localization Using Relative and Absolute Position Estimates*, pp. 1134-1140.
2. Jarvis, D. E. (1986). Paint Finishing Trends in the Automotive Industry. *Product Finishing (London)*, vol. 39, pp. 13-19.
3. Siegwart, R., and Nourbakhsh, I. (2004). *Introduction to Autonomous Mobile Robots*, MIT Press.
4. *The History and Workings of Robotics*. (April 18, 2007).
<http://www.thetech.org/exhibits/online/robotics/universal/page06.html>
5. *NSSDC Master Catalog: Spacecraft*. (April 18, 2007).
<http://nssdc.gsfc.nasa.gov/database/MasterCatalog?sc=1975-083C>
6. *Mars Exploration Rover Mission*. (April 19, 2007).
http://marsrovers.nasa.gov/technology/is_autonomous_mobility.html
7. *DARPA Grand Challenge*. (May 25, 2007).
<http://www.darpa.mil/grandchallenge/index.asp>
8. Shamah, B. (1999). *Experimental Comparison of Skid Steering Vs. Explicit Steering for a Wheeled Mobile Robot*. Masters Thesis, Carnegie Mellon University.
9. Wang, D. & Feng, Q. (2001). Trajectory Planning for a Four-Wheeled-Steering Vehicle. *Proceedings of the IEEE Conference on Robotics and Automation*, pp. 3320-3325.
10. Li, B., Shugen, M., Liu, J., & Wang, Y. (2005). Development of a Shape Shifting Robot for Search and Rescue. *Proceedings of the IEEE Conference on Safety, Security and Rescue Robots*, pp. 31-35.
11. *Robo-Rats Locomotion: Skid-Steer Drive*. (April 19, 2007).

<http://groups.csail.mit.edu/drl/courses/cs54-2001s/skidsteer.html>

12. Kimura, H., Fukuoka, Y., Hada, Y., & Takase, K. (2002). Three-Dimensional Adaptive Dynamic Walking of a Quadruped. *Proceedings of the IEEE Conference on Robotics and Automation*, pp. 2228-2233.
13. ASIMO. (April 20, 2007). <http://world.honda.com/ASIMO/new/>
14. CH3-R. (April 20, 2007). <http://www.lynxmotion.com/Category.aspx?CategoryID=101>
15. *Research on Quadruped Walking Machines*. (April 19, 2007). http://www-robot.mes.titech.ac.jp/robot/walking/walking_vehicle/walking_e.html
16. Hyon, S.H., & Mita, T. (May 2002). Development of a Biologically Inspired Hopping Robot – “Kenken”. *Proceedings of the 2002 IEEE International Conference on Robotics & Automation*, pp. 3984-3991.
17. Prautsch, P. and Mita, T. (1999). Control and Analysis of the Gait of Snake Robots. *Proceedings of the IEEE Conference on Control Applications*, pp. 502-507.
18. Michaud, S., Schneider, A., Bertrand, R., Lamon, P., Siegwart, R., Winnendael, M. & Schiele, A. (2007). *Solero: Solar-Powered Exploration Rover*. Autonomous Systems Lab, Swiss Federal Institute of Technology, Lausanne.
19. Guccione, S. & Muscato, G. (December 2003). The Wheelleg Robot. *IEEE Robotics and Automation Magazine*, pp. 33-43.
20. Endo, G. & Hirose, S. (May 1999). Study on Roller-Walker (Systems Integration and Basic Experiments). *Proceedings of the IEEE International Conference on Intelligent Robotics & Automation*, pp. 2032-2037.
21. Grand, C., BenAmar, F., & Bidaud, P. (October 2004). Stability and Traction Optimization of a Reconfigurable Wheel-Legged Robot. *The International Journal of Robotics Research*.

22. Adachi, H., Koyachi, N., Arai, T., Shimizu, A., & Nogami, Y. (1999). Mechanism and Control of a Leg-Wheel Hybrid Mobile Robot. *Proceedings of the 1999 IEEE/RSJ International Conference on Intelligent Robots and Systems*, pp. 1792-1797.
23. Halme, A., Leppanen, I., Montonen, M., & Ylonen, S. (2001) Robot Motion by Simultaneous Wheel and Leg Propulsion. *Proceedings of the 4th International Conference on Climbing and Walking*.
24. Boubakis, N. (June 1998). Kydonas – An Autonomous Hybrid Robot: Walking and Climbing. *IEEE Robotics & Automation Magazine*, pp. 52-59.
25. Quinn, Rogher D., et al. (2001). Insect Designs for Improved Robot Mobility. *Proceedings of the 4th International Conference on Climbing and Walking Robots*, pp. 69-76.
26. Bielmeier, C., & Walter, W. (2004). *Exploration of an Electroactive Plymer as an Actuator for Microrobotics*. Masters Thesis, Rochester Institute of Technology.
27. *Elements of Mechanical Design*. (April 25, 2007).
<http://ocw.mit.edu/OcwWeb/Mechanical-Engineering/2-72Spring-2006/CourseHome/index.htm>
28. Oberg, E., Jones, F., Horton, H., & Ryffel, H. (2004). *Twenty-Seventh Edition Machinery's Handbook*. New York: Industrial Press Inc.
29. *Worm Gear*. (April 25, 2007). http://en.wikipedia.org/wiki/Worm_gear
30. *Gear Head Motor – 7.2vdc 50:1 175rpm (6mm shaft)*. (April 26, 2007).
<http://www.lynxmotion.com/Product.aspx?productID=96&CategoryID=11>
31. Shingley, J., Mischke, R., & Budynas, R. (2004). *Mechanical Engineering Design – Seventh Edition*. New York: McGraw-Hill.
32. *Horse Power*. (May 14, 2007). http://en.wikipedia.org/wiki/Horse_power

33. Buckingham, E. (1949). *Analytical Mechaincs of Gears*. New York: McGraw-Hill.
34. Yu, H., Dubowsky, S., & Skwersky, A. *Omni-Directional Mobility Using Active Split Offset Castors*. Massachusetts Institute of Technology Department of Mechanical Engineering.
35. *Specifications, Product Testing and Terminology*. (April 28, 2007).
<http://www.johnsonite.com/en/specifications>
36. Clark, D. & Owings, M. (2003). *Building Robot Drive Trains*. New York: McGraw-Hill.
37. *Rotary Encoder*. (April 29, 2007). http://en.wikipedia.org/wiki/Rotary_encoder
38. *Hall Effect Sensor*. (April 29, 2007). http://en.wikipedia.org/wiki/Hall_effect_sensor
39. Carr, D. (September 2006). *Development and Test of a Kinematical Method for Estimating Rotation Using the Acceleration of a Rigid Body*. Masters Thesis, Rochester Institute of Technology.
40. Fun, W. (2002). Fuzzy Position/Force Control of a Robot Leg with a Flexible Gear System. *Proceedings of the IEEE Conference on Robotics and Automation*, pp. 2159-2164.
41. *Quadrature Encoder Fundamentals*. (May 1, 2007).
<http://zone.ni.com/devzone/cda/tut/p/id/4763>
42. E4P OEM Miniature Optical Kit Encoder. *US Digital Data Sheet*.
43. *Dead Reckoning*. (May 1, 2007). http://en.wikipedia.org/wiki/Dead_reckoning
44. Borenstein, J. (April 1995). Internal Correction of Dead-Reckoning Errors with a Dual-Drive Compliant Linkage Mobil Robot. *Journal of Robotic Systems*, Vol. 12, No. 4, pp. 257-273.

45. *CORDIC*. (October 4, 2006). <http://en.wikipedia.org/wiki/CORDIC>
46. *Battery*. (May 7, 2007). <http://en.wikipedia.org/wiki/Battery>
47. Choosing a Rechargeable Battery. (2001). *Electus Distribution Reference Data Sheet: RECHARGE.PDF (I)*.
48. *RadioShack's On-Line Battery Guidebook*. (May 7, 2007).
http://support.radioshack.com/support_tutorials/batteries/batgd-c01.htm
49. *Relays*. (May 8, 2007). <http://www.kpsec.freeuk.com/components/relay.htm>
50. *H-bridges: Theory and Practice*. (May 8, 2007).
<http://www.mcmanis.com/chuck/robotics/tutorial/h-bridge/index.html>
51. Jack, Hugh. (March 31, 2002). Automating Manufacturing Systems with PLCs. *Grand Valley State University*.
52. *Pulse-Width Modulation*. (May 8, 2007). http://en.wikipedia.org/wiki/Pulse-width_modulation
53. TPIC0107B PWM Control Intelligent H-Bridge. (2002). *Texas Instruments Data Sheet*.
54. Pheifer, D. & Powell, W. (May 1, 2000). The Electrolytic Tilt Sensor. *Sensors Weekly Newsletter*.
55. *Robot Arm Control System*. (May 8, 2007).
<http://www.cems.uvm.edu/~medialab/Spring04/mgauthie/project/pressureSensor.html>
56. SCA100T Series Inclinometer. *VTI Technologies Data Sheet*.
57. E Series Miniature Low Torque. *Cherry Data Sheet*.
58. Current Transducer LTS 25-NP. *LEM Components Data Sheet*.
59. *Nyquist Rate*. (May 21, 2007). http://en.wikipedia.org/wiki/Nyquist_rate

60. *OOPic*. (May 9, 2007). <http://oopic.com/>

61. *Trapezoidal Rule*. (May 15, 2007).

<http://metric.ma.ic.ac.uk/integration/techniques/definite/numerical-methods/trapezoidal-rule/>

14 Appendices

14.1 Appendix A – Bill of Materials

	Item	Name	Product Number	Supplier	Qty	Unit Cost (\$)	Line Cost (\$)
Purchased	Wheel	Rubber Moon Buggy Wheel (Large)	WHEEL-LGBUGGY	Budget Robotics	4	7.98	31.92
	OOPic I2C Connector Housing	CONN HOUS 5POS 100 W/RAMP/RIB	WM2003-ND	Digikey	10	0.40	4.04
	Inclinometer	Dual Output Inclinometer	551-1003-1-ND	Digikey	1	65.88	65.88
	H-Bridge	INTEL H-BRIDGE 180 MOHM 20-HSOP	296-10857-5-ND	Digikey	16	4.50	72.00
	Current Sensor	TRANSDUCER CURENT CLOSE LOOP 25A	398-1002-ND	Digikey	1	20.20	20.20
	Surfboard	PROTO-BRD 20 WIDE SOIC 20PIN SIP	9210CA-ND	Digikey	16	5.72	91.58
	6 Pin Screw Terminal Blocks	CONN TERM BLOCK 2.54MM 6POS	277-1277-ND	Digikey	16	2.94	47.09
	4 Pin Screw Terminal Blocks	CONN TERM BLOCK 2.54MM 4POS	277-1275-ND	Digikey	4	2.30	9.20
	Header-to-Header Ribbon Cable	IDC CABLE - ASC40H/AE40G/ASC40H	A3AAH-4006G-ND	Digikey	5	8.39	41.95
	SPST Relay	RELAY PWR 10A SPST 5VDC PC MNT	255-1106-ND	Digikey	4	1.15	4.60
	DPDT Relay	RELAY PWR DPDT 5A 5VDC PC MNT	255-1116-ND	Digikey	4	2.33	9.32
	Gear-Motor	Gear Head Motor	GHM-04	Lyrx motion	16	21.95	351.20
	Encoder	Quatrature Motor Encoder w/ Cable	QME-01	Lyrx motion	16	24.95	399.20
	Wheel Hub	Universal Hub - 6mm (pair)	HUB-02	Lyrx motion	2	8.00	16.00
	Aluminum Rod	Multipurpose Metric Aluminum (Alloy 6060)	1681T23	McMaster-Carr	1	9.46	9.46
	Aluminum Sheet	Machinable Marine-Grade Aluminum (Alloy 5086)	5865T31	McMaster-Carr	2	14.99	29.98
	Aluminum Rectangular Tube	Ultra Corrosion-Resistant Architectural Aluminum (Alloy6063)	88935K631	McMaster-Carr	1	10.17	10.17
	Aluminum Rectangular Bar	Multipurpose Aluminum (Alloy 6061)	8975K527	McMaster-Carr	1	3.85	3.85
	Aluminum Rectangular Bar	Multipurpose Aluminum (Alloy 6061)	8975K34	McMaster-Carr	1	10.62	10.62
	Retaining Ring	E-Style Retaining Rings	98543A113	McMaster-Carr	1	3.00	3.00
	Push Retainer	Retainers for Unthreaded Shafts	96415A128	McMaster-Carr	1	11.16	11.16
	Spacer	Unthreaded Round Spacer	93657A007	McMaster-Carr	36	0.80	28.80
	Shoulder Screw	Alloy Steel Standard Shoulder Screw	91259A542	McMaster-Carr	16	0.97	15.52
	Rubber	Natural Gum Foam Rubber	93625K45	McMaster-Carr	1	8.89	8.89
	Aluminum Bar	Alloy 2024 Aluminum Square Bar	86895K463	McMaster-Carr	1	18.50	18.50
	Thrust Bearing	Steel Ball Thrust Bearing Carbon Steel	6655K52	McMaster-Carr	4	2.26	9.04
	Gear Motor Machine Screw	Machine Screw (box of 100)	91420A122	McMaster-Carr	1	2.80	2.80
	Limit Switch Machine Screw	Round Head Slotted Machine Screw 4-40 Thread (box of 100)	90276A112	McMaster-Carr	1	1.77	1.77
	1024K bit EEPROM	CMOS Serial EEPROM	24FC1025-1/P	Microchip	7	3.86	27.02
	Clockwise Limit Switch	Low Torque Miniature Snap-Action Switch	29F2902	Newark in One	2	11.30	22.60
	Counter-Clockwise Limit Switch	Low Torque Miniature Snap-Action Switch	29F2903	Newark in One	2	8.54	17.08
	Female Disconnect	Female Disconnect Solderless Terminal	44F167	Newark in One	1	3.25	3.25
	Wire Mount Socket	Wire-To-Board Connector	48F3040	Newark in One	5	7.72	38.60
	Crimp Terminal	Solderless Terminal	35C4980	Newark in One	1	14.73	14.73
	Large Breadboard	PCB, Breadboard Prototyping board	17C6981	Newark in One	5	8.95	44.75
	Sm all Breadboard	PCB, Breadboard Prototyping board	17C6980	Newark in One	2	4.50	9.00
	Headers	Pin Headers	56H2242	Newark in One	5	0.68	3.40
	7.2VDC Battery	7.2V 2000mAh Ni-Cd Battery Pack and Charger Combo Pack	23-322	RadioShack	1	24.99	24.99
	Battery Connector	7.2V RC Connector	2300444	RadioShack	1	3.99	3.99
	Kill Switch	25A Kill Switch	275-708	RadioShack	1	2.99	2.99
	Sm all Button	FK4 P/B NO SWITCH	2751547	RadioShack	1	3.29	3.29
	PNP Transistor	TIP42 Transistor	276-2027	RadioShack	8	1.59	12.72
	NPN Transistor	TIP3055 Transistor	276-2020	RadioShack	8	1.79	14.32
	Prototyping Board	Multipurpose PC Board with 417 Holes	276-150	RadioShack	2	1.99	3.98
	Worm Gear	30:1 GEAR RATIO, 30 TEETH WORM GEAR	A1B 6-N32030	SDP/SI	4	20.25	81.00
Worm	32DP / 1 Lead / 0.438P.D., 4.08° Right Hand Worm	A1Q 5-N32	SDP/SI	4	20.77	83.08	
Microcontroller	OOPic II Plus	MCU-005-000	Superdroid Robots	4	59.00	236.00	
Microcontroller	OOPic II Plus Starter Kit	MCU-006-000	Superdroid Robots	1	69.95	69.95	
Bearing	10 Flanged Bearings 6x10x3 Sealed	kit720	VXB	4	29.95	119.80	
Robotics Lab	15 kΩ Resistor	-----	-----	-----	8	-----	-----
	2.7kΩ Resistor	-----	-----	-----	8	-----	-----
	9V Battery	-----	-----	-----	5	-----	-----
	Conductive Foam	-----	-----	-----	2	-----	-----
	Stand-off	-----	-----	-----	2	-----	-----
Machine Shop	Wire	-----	-----	-----	---	-----	-----
	Wire Tie	-----	-----	-----	40	-----	-----
Machine Shop	2-56 x 1/4 Machine Screw	-----	-----	-----	24	-----	-----
	4-40 Lock Washer	-----	-----	-----	16	-----	-----
	4-40 Machine Screw (various)	-----	-----	-----	30	-----	-----
	6-32 Machine Screw (various)	-----	-----	-----	24	-----	-----
	M2 Spring Pin	-----	-----	-----	12	-----	-----
	Piano Wire	-----	-----	-----	4	-----	-----
	Set Screw	-----	-----	-----	4	-----	-----
						Total	2164.28

14.2 Appendix B – Test Code

14.2.1 Steering Encoder Test

```
'Data storage objects
Dim Clock As New oClock
Dim Wire As New oWire
Dim Record As New oEvent
Dim E1 As New oEEProm

'PWM output to H-Bridge objects
Dim Steer_PWM As New oPWMH

'Output to H-Bridge direction objects
Dim Steer_Dir As New oDIO1

'Encoder count objects
Dim Steer_Encoder As New oCounter

'Encoder count input location objects
Dim Steer_Encoder_In As New oDIO1

'Encoder count input variable objects
Dim Steer_Encoder_Var As New oWord
Dim Steer_Encoder_High_Byte As New oByte
Dim Steer_Encoder_Low_Byte As New oByte

'Direction Variables
Dim wheel As New oBit
Dim steer As New oBit

'-----Start program-----
Sub Main()
Delay = 500 'Recommended for all programs

E1.Node = 84 'Use EEPROM slot E1
Clock.Rate = 115 'Set clock frequency
Wire.Input.Link(Clock.Result) 'Create virtual circuit
Wire.Output.Link(Record.Operate)
Wire.Operate = cvTrue
Clock.Operate = cvTrue
Steer_Encoder_Var = 10000 'Initialize encoder count variable
```

Delay = 500

'PWM outputs to H-Bridge setup
Steer_PWM.IOLine = 18

'Outputs to H-Bridge direction setup
Steer_Dir.IOLine = 25
Steer_Dir.Direction = cvOutput

'Encoder count input setup
Steer_Encoder.Operate = 1
Steer_Encoder.ClockIn1.Link(Steer_Encoder_In)
Steer_Encoder.Output.Link(Steer_Encoder_Var)

'Encoder count input location objects setup
Steer_Encoder_In.IOLine = 2
Steer_Encoder_In.Direction = cvInput

'H-bridge inputs
Steer_Dir.State = 0
Steer_PWM.DutyCycle = 73

'-----Begin Test-----
'Turn CCW 90 degrees
While Steer_Encoder_Var < 11500
Steer_PWM.Operate = 1
Wend
Steer_PWM.Operate = 0

'Hold
Delay = 100
Steer_Dir.State = 1
Steer_Encoder.Direction = 1
Delay = 200

'Turn CW 270 degrees
While Steer_Encoder_Var > 7000
Steer_PWM.Operate = 1
Wend
Steer_PWM.Operate = 0

'Hold
Delay = 100

```
Steer_Dir.State = 0
Steer_Encoder.Direction = 0
Delay = 200
```









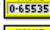
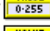
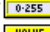
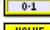
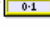
```
'Turn CCW 180 degrees
While Steer_Encoder_Var < 10000
Steer_PWM.Operate = 1
Wend
Steer_PWM.Operate = 0
```

```
'Stop recording data
Delay = 100
Clock.Operate = 0
```

```
End Sub
'-----End Program-----
```

```
'-----Record Encoder Output Subroutine-----
Sub Record_Code()
'Format data for storage
Steer_Encoder_High_Byte = Steer_Encoder_Var/256
Steer_Encoder_Low_Byte = Steer_Encoder_Var
'Store data
E1.Value = Steer_Encoder_High_Byte
E1.Value = Steer_Encoder_Low_Byte
'Reset variable
Record.Operate = 0
End Sub
'-----End Subroutine-----
```


Objects:

 Clock	oClock	An Object that provides a programmable logic clock
 Wire	oWire	An Object that copies the value of an oBoolean Object to another oBoolean Object.
 Record	oEvent	An Object that runs program code in response to an event.
 EEPROM	oEEProm	An Object that provides access to the non-volatile I2C EEPROM memory.
 Steer_PWM	oPMWH	An Object that provides a high-speed Pulse-Width-Modulated output using hardware specific I/O lines.
 Steer_Dir	oDI01	An Object that provides a 1 line digital I/O.
 Steer_Encoder	oCounter	An Object that provides counting functions.
 Steer_Encoder_In	oDI01	An Object that provides a 1 line digital I/O.
 Steer_Encoder_Var	oWord	An Object that manages a value with a range of 0 to 65,535.
 Steer_Encoder_High_Byte	oByte	An Object that manages a value with a range of 0 to 255.
 Steer_Encoder_Low_Byte	oByte	An Object that manages a value with a range of 0 to 255.
 wheel	oBit	An Object that manages a value with a range of 1 to 0.
 steer	oBit	An Object that manages a value with a range of 1 to 0.

14.2.2 Steering Encoder Test

Central Microcontroller:

'I2C Link object

Dim Master As New oDDELink

'Operate variable - begin leg programs

Dim operate As New oBit

'Button object

Dim Red As New oSwitch

'-----Start program-----

Sub Main()

Delay = 500 'Recommended for all programs

'I2C link setup

ooPIC.Node = 1

Master.Location = 41

Master.Direction = cvSend

Master.Input.Link(operate)

Master.Operate = cvTrue

'Button setup

Red.IOLine = 30

'Hold until button pressed

While Red.Position = 1

```
operate.Value = 0
Wend
```

```
'-----Begin Test-----
```

```
'Send start command to leg OOPics
```

```
operate.Value = 1
```

```
Master.Node = 2
```

```
Master.Sync = 1
```

```
Master.Node = 3
```

```
Master.Sync = 1
```

```
Master.Node = 4
```

```
Master.Sync = 1
```

```
Master.Node = 5
```

```
Master.Sync = 1
```




```
Delay = 100
```

```
Master.Sync = 0
```

```
End Sub
```

```
'-----End Program-----
```

Objects:

	Master	oDDELink	An Object that provides a Dynamic-Data-Exchange link over the I2C network.
	operate	oBit	An Object that manages a value with a range of 1 to 0.
	Red	oSwitch	An Object that reads the position of a switch.

Leg Microcontroller (1 of 4):

```
'I2C Link object
```

```
Dim Slave As New oDDELink
```

```
'Data storage objects
```

```
Dim Clock As New oClock
```

```
Dim Wire As New oWire
```

```
Dim Record As New oEvent
```

```
Dim E1 As New oEEProm
```

```
'Operate variable - begin leg programs
```

```
Dim operate As New oBit
```

```
'PWM output to H-Bridge objects
```

```
Dim Wheel_PWM As New oPWMH
```

```
'Output to H-Bridge direction objects
```

```

Dim Wheel_Dir As New oDIO1

'Encoder count objects
Dim Wheel_Encoder As New oCounter

'Encoder count input location objects
Dim Wheel_Encoder_In As New oDIO1

'Encoder count input variable objects
Dim Wheel_Encoder_Var As New oWord
Dim Wheel_Encoder_High_Byte As New oByte
Dim Wheel_Encoder_Low_Byte As New oByte

'-----Start program-----
Sub Main()
Delay = 500

'I2C Network Setup
ooPIC.Node = 3 '*****CHANGE FOR EACH LEG
Slave.Output.Link(operate.Value)
Slave.Operate = cvTrue

'Data storage setup
Clock.Operate = cvFalse
Clock.Rate = 1
Wire.Input.Link(Clock.Result)
Wire.Output.Link(Record.Operate)
Wire.Operate = cvTrue
E1.Node = 84

'PWM outputs to H-Bridge setup
Wheel_PWM.IOLine = 17

'Outputs to H-Bridge direction setup
Wheel_Dir.IOLine = 24
Wheel_Dir.Direction = cvOutput

'Encoder count input setup
Wheel_Encoder.Operate = 1
Wheel_Encoder.ClockIn1.Link(Wheel_Encoder_In)
Wheel_Encoder.Output.Link(Wheel_Encoder_Var)

'Encoder count input location objects setup
Wheel_Encoder_In.IOLine = 1

```

```

Wheel_Encoder_In.Direction = cvInput

'Set motor direction
Wheel_Dir.State = 0 '*****CHANGE FOR EACH LEG

operate = 0 'Initialize operate variable
Wheel_Encoder_Var = 0 'Initialize variable

Wheel_PWM.DutyCycle = 95 ' Set motor speed





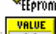




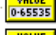
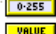
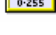

'-----Begin Test-----
'Hold until given start command
While operate = 0
Wheel_PWM.Operate = 0
Wend

'Start test
Clock.Operate = cvTrue
Wheel_PWM.Operate = 1
End Sub
'-----End Program-----

'-----Record Encoder Output Subroutine-----
Sub Record_Code()
'Format data for storage
Wheel_Encoder_High_Byte = Wheel_Encoder_Var/256
Wheel_Encoder_Low_Byte = Wheel_Encoder_Var
'Store data
E1.Value = Wheel_Encoder_High_Byte
E1.Value = Wheel_Encoder_Low_Byte
'Reset variable
Record.Operate = 0
End Sub
'-----End Subroutine-----

```

Objects:

 Slave	oDDELink	An Object that provides a Dynamic-Data-Exchange link over the I2C network.
 Clock	oClock	An Object that provides a programmable logic clock
 Wire	oWire	An Object that copies the value of an oBoolean Object to another oBoolean Object.
 Record	oEvent	An Object that runs program code in response to an event.
 EEPROM	oEEProm	An Object that provides access to the non-volatile I2C EEPROM memory.
 operate	oBit	An Object that manages a value with a range of 1 to 0.
 Wheel_PWM	oPWHM	An Object that provides a high-speed Pulse-Width-Modulated output using hardware specific I/O lines.
 Wheel_Dir	oDI01	An Object that provides a 1 line digital I/O.
 Wheel_Encoder	oCounter	An Object that provides counting functions.
 Wheel_Encoder_In	oDI01	An Object that provides a 1 line digital I/O.
 Wheel_Encoder_Var	oWord	An Object that manages a value with a range of 0 to 65,535.
 Wheel_Encoder_High_Byte	oByte	An Object that manages a value with a range of 0 to 255.
 Wheel_Encoder_Low_Byte	oByte	An Object that manages a value with a range of 0 to 255.

14.2.3 Posture Control Test

Central Microcontroller:

'I2C Link object

Dim Master As New oDDELink

'Operate variable - begin leg programs

Dim operate As New oNib

'Button objects

Dim Red As New oSwitch

'Inclinometer input objects

Dim x As New oA2D8

Dim y As New oA2D8

'-----Start program-----

Sub Main()

Delay = 500 'Recommended for all programs

'I2C link setup

ooPIC.Node = 1

Master.Location = 41

Master.Direction = cvSend

Master.Input.Link(operate)

Master.Operate = cvTrue

```
'Button setup  
Red.IOLine = 30
```

```
'Inclinometer setup  
x.IOLine = 2  
y.IOLine = 3  
x.Operate = cvTrue  
y.Operate = cvTrue
```

```
'-----Begin Test-----  
'Hold until button pressed  
While Red.Position = 1  
operate.Value = 0  
Wend
```

```
'Send start commmand  
operate.Value = 1  
Master.Node = 2  
Master.Sync = 1  
Master.Node = 3  
Master.Sync = 1  
Master.Node = 4  
Master.Sync = 1  
Master.Node = 5  
Master.Sync = 1  
Delay = 10  
Master.Sync = 0
```

```
'Set variable value to match inclinometer input  
Do  
If x < 116  
operate.Value = 3  
ElseIf y > 140  
operate.Value = 2  
Else  
operate.Value = 1  
EndIf
```






```
'Send variable value  
Master.Node = 3  
Master.Sync = 1  
Master.Node = 4  
Master.Sync = 1  
Delay = 10  
Master.Sync = 0
```

```

Loop 'Again
End Sub
'-----End Program-----

```

Objects:

	Master	oDDELink	An Object that provides a Dynamic-Data-Exchange link over the I2C network.
	operate	oNib	An Object that manages a value with a range of 0 to 15.
	Red	oSwitch	An Object that reads the position of a switch.
	x	oA2D8	An Object that measures the level of the voltage on an input line with an 8-bit result.
	y	oA2D8	An Object that measures the level of the voltage on an input line with an 8-bit result.

Leg Microcontroller (1 of 4):

```

'I2C Link object
Dim Slave As New oDDELink

'Operate variable - begin leg programs
Dim operate As New oNib

'PWM output to H-Bridge objects
Dim Wheel_PWM As New oPWMH

'Output to H-Bridge direction objects
Dim Wheel_Dir As New oDIO1

'Encoder count objects
Dim Wheel_Encoder As New oCounter

'Encoder count input location objects
Dim Wheel_Encoder_In As New oDIO1

'Shoulder abduction objects
Dim Shoulder_Direction As New oDIO1
Dim Shoulder_Power As New oDIO1

```

```

'-----Start program-----
Sub Main()
Delay = 500

'I2C Network Setup
oPIC.Node = 3 '*****CHANGE FOR EACH LEG
Slave.Output.Link(operate.Value)
Slave.Operate = cvTrue

```

```

'Shoulder control setup
Shoulder_Direction.IOLine = 27
Shoulder_Power.IOLine = 29
Shoulder_Direction.Direction = cvOutput
Shoulder_Power.Direction = cvOutput

'PWM outputs to H-Bridge setup
Wheel_PWM.IOLine = 17

'Outputs to H-Bridge direction setup
Wheel_Dir.IOLine = 24
Wheel_Dir.Direction = cvOutput

Wheel_Dir.State = 0 '*****CHANGE FOR EACH LEG

operate = 0 'Initialize operate variable

Wheel_PWM.DutyCycle = 125 'Set wheel speed



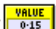

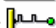








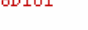


'-----Begin Test-----
'Hold until start command received
While operate = 0
Wheel_PWM.Operate = 0
Shoulder_Direction.Value = 0
Shoulder_Power.Value = 1
Wend

Wheel_PWM.Operate = 1 'Start wheel
Delay = 10

'Move shoulder when necessary
Do
If operate = 2 Or operate = 3
Shoulder_Power = 0
Else
Shoulder_Power = 1
EndIf
Loop
End Sub
'-----End Program-----

```


Objects:

 Slave	 oDDELink	An Object that provides a Dynamic-Data-Exchange link over the I2C network.
 operate	 oNib	An Object that manages a value with a range of 0 to 15.
 Wheel_PWM	 oPWML	An Object that provides a high-speed Pulse-Width-Modulated output using hardware specific I/O lines.
 Wheel_Dir	 oDIO1	An Object that provides a 1 line digital I/O.
 Wheel_Encoder	 oCounter	An Object that provides counting functions.
 Wheel_Encoder_In	 oDIO1	An Object that provides a 1 line digital I/O.
 Shoulder_Direction	 oDIO1	An Object that provides a 1 line digital I/O.
 Shoulder_Power	 oDIO1	An Object that provides a 1 line digital I/O.

14.2.4 Walking Gait Test

'PWM output to H-Bridge objects
Dim Swing_PWM As New oPWML

'Output to H-Bridge direction objects
Dim Swing_Dir As New oDIO1

'Shoulder abduction objects
Dim Shoulder_Direction As New oDIO1
Dim Shoulder_Power As New oDIO1

'-----Start program-----
Sub Main()
Delay = 1000

'Shoulder abduction setup
Shoulder_Direction.IOLine = 27
Shoulder_Power.IOLine = 29
Shoulder_Direction.Direction = cvOutput
Shoulder_Power.Direction = cvOutput

'PWM outputs to H-Bridge setup
Swing_PWM.IOLine = 30

'Outputs to H-Bridge direction setup
Swing_Dir.IOLine = 26
Swing_Dir.Direction = cvOutput
Swing_PWM.DutyCycle = 2

'-----Begin Test-----
Do
'Lower

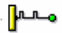



```
Shoulder_Direction.Value = 1
Delay = 5
Shoulder_Power.Value = 0
Delay = 185
Shoulder_Power.Value = 1
```

```
'Swing forward
Swing_Dir.State = 1
Swing_PWM.Operate = 1
Delay = 135
Swing_PWM.Operate = 0
```

```
'Raise
Shoulder_Direction.Value = 0
Delay = 10
Shoulder_Power.Value = 0
Delay = 275
Shoulder_Power.Value = 1
```

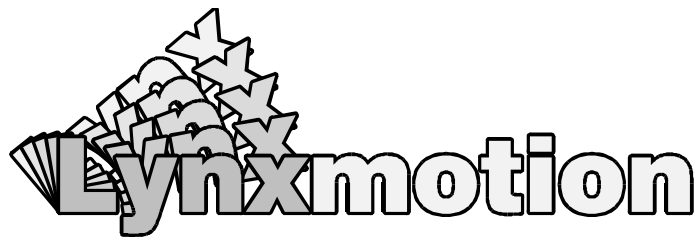
```
'Swing back
Swing_Dir.State = 0
Delay = 5
Swing_PWM.Operate = 1
Delay = 125
Swing_PWM.Operate = 0
Loop 'Again
End Sub
'-----End Program-----
```

Objects:

	Swing_PWM	oPWML	An Object that provides a low-speed Pulse-Width-Modulated output on any I/O line.
	Swing_Dir	oDI/O1	An Object that provides a 1 line digital I/O.
	Shoulder_Direction	oDI/O1	An Object that provides a 1 line digital I/O.
	Shoulder_Power	oDI/O1	An Object that provides a 1 line digital I/O.

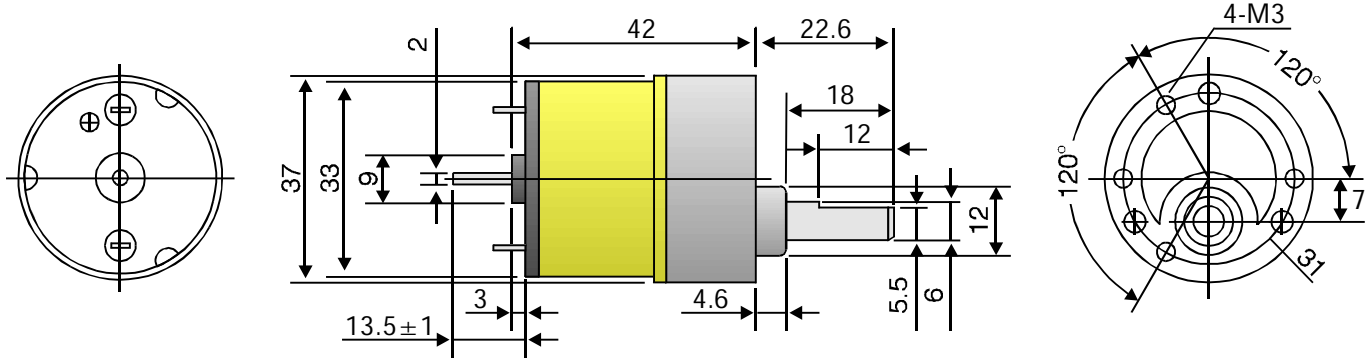
14.3 Appendix D – Select Manufacturer Specifications

Data sheet for:
 GHM-04
 7.2vdc 50:1 175rpm
 6mm shaft

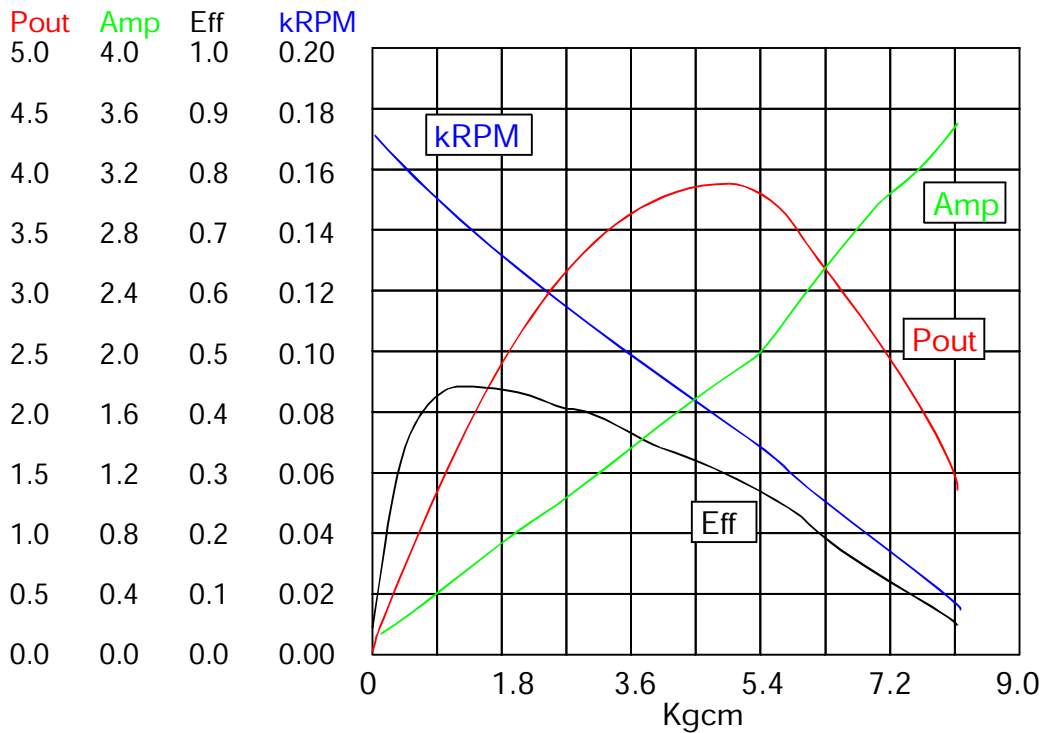


www.lynxmotion.com

I. OUTER DIMENSIONS



II. DRAWING OF CURVES



III. SPECIFICATIONS

Type: HN-GH35GMB
 Model: HN-GH7.2-2414T - 50:1

1. Testing Conditions:

Temp: 25° Celsius
 Humidity: 60%
 Motor Orientation: Horizontal

2. Rated Voltage: 7.2vdc

3. Voltage Operating Range: 6-7.2vdc

4. Rated Load at 7.2vdc: 1.0Kg-cm

Do not exceed rated load. Damage may occur!

5. No Load Speed at 7.2vdc: 175 RPM +/- 10%

6. Speed at Rated Load (1.0Kg-cm): 146 RPM +/- 10%

7. No Load Current at 7.2vdc: < 221mA

8. Current at Rated Load (1.0Kg-cm): < 556mA

9. Shaft End-Play: Maximum 0.8m/m

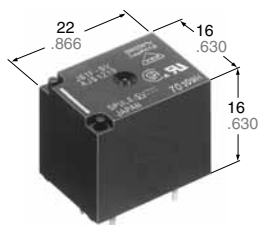
10. Insulation Resistance: 10M ohm at 300vdc

11. Withstand Voltage: 300vdc for 1 Second

12. The gear motor is not intended for instant reverse.

The gear motor must be stopped before reversing.

13. The gear motor does not include protection from water or dust etc.



mm inch

FEATURES

- **Miniature size with universal terminal footprint**
- **High contact capacity: 10 A**
- **TV-5 type available (Standard type)**
1 Form A type → TV-5
1 Form C type → TV-5 (N.O. side only)
- **VDE, TÜV also approved**
- **Sealed construction for automatic cleaning (Standard type)**
- **Class B and F coil insulation type also available.**
- **EN60335-1 GWT compliant (Tested by VDE) type available**
- **Surge voltage 6 kV type also available**

About Cd-free contacts

We have introduced Cadmium free type products to reduce Environmental Hazardous Substances. (The suffix "F" should be added to the part number)
Please replace parts containing Cadmium with Cadmium-free products and evaluate them with your actual application before use because the life of a relay depends on the contact material and load.

RoHS Directive compatibility information
<http://www.nais-e.com/>

SPECIFICATIONS

Contact

Types		Standard type	Long endurance type
Arrangement		1 Form A, 1 Form C	1 Form A
Initial contact resistance, max. (By voltage drop 6 V DC 1 A)		100 mΩ	
Contact material		AgSnO ₂ type	
Rating (resistive load)	Nominal switching capacity	10 A 250 V AC 10 A 125 V AC 6 A 277 V AC	10 A 250 V AC 10 A 125 V AC 10 A 277 V AC
	Max. switching power	2,500 VA	
	Max. switching voltage	250 V AC, 100 V DC	
	Max. switching current	10 A (AC), 5 A (DC)	
	Min. switching capacity*1	100 mA, 5 V DC	
Expected life (min. ope.)	Mechanical (at 180 cpm)	10 ⁷	
	Electrical at 10 A 125 V AC, 6 A 277 V AC resistive (standard) 10 A 277 V AC resistive (High power)	1×10 ⁵	2×10 ⁵
	10 A 250 V AC resistive (Standard: at 20 cpm) (High power: at 20 cpm, 105°C 221°F)**	5 × 10 ⁴ (No contact only)	1.2 × 10 ⁵

** Holding voltage should be 60% V of nominal voltage

Coil

Nominal operating power	360 mW
-------------------------	--------

#1 This value can change due to the switching frequency, environmental conditions, and desired reliability level, therefore it is recommended to check this with the actual load.

Remarks

*1 Detection current: 10mA

*2 Excluding contact bounce time

Characteristics

Max. operating speed		20 cpm	
Types		Standard type	Long endurance type
Initial insulation resistance		Min. 100 MΩ (at 500 V DC)	
Initial breakdown voltage*1	Between open contacts	750 Vrms for 1 min.	
	Between contacts and coil	1,500 Vrms for 1 min.	
Operate time*2 (at nominal voltage)		Max. 10 ms	
Release time (without diode)*2 (at nominal voltage)		Max. 10 ms	
Temperature rise (at nominal voltage)		Max. 35°C, resistive, nominal voltage applied to coil. Contact carrying current: 10A, at 70°C 158°F	
Shock resistance	Functional*3	98 m/s ² {10 G}	
	Destructive*4	980 m/s ² {100 G}	
Vibration resistance	Functional*5	10 to 55 Hz at double amplitude of 1.6 mm	
	Destructive	10 to 55 Hz at double amplitude of 2 mm	
Conditions for operation, transport and storage*6 (Not freezing and condensing at low temperature)	Ambient temp.*7	-40°C to +85°C -40°F to +185°F	-40°C to +105°C -40°F to +221°F
	Humidity	5 to 85% R.H.	
Unit weight		Approx. 12 g .423 oz	

*3 Half-wave pulse of sine wave: 11ms; detection time: 10μs

*4 Half-wave pulse of sine wave: 6ms

*5 Detection time: 10μs

*6 Refer to 6. Conditions for operation, transport and storage mentioned in AMBIENT ENVIRONMENT

*7 When using relays in a high ambient temperature, consider the pick-up voltage rise due to the high temperature (a rise of approx. 0.4% V for each 1°C 33.8°F with 20°C 68°F as a reference) and use a coil impressed voltage that is within the maximum allowable voltage range.

TYPICAL APPLICATIONS

1. Home appliances

Air conditioner, heater, etc.

2. Automotive

Power-window, car antenna, door-lock, etc.

3. Office machines

PPC, facsimile, etc.

4. Vending machines

ORDERING INFORMATION

Ex. JS 1a F — B — 12V — F —

Contact arrangement	Protective construction	Coil insulation class	Coil voltage (DC)	Contact material	Flame resistance and tracking resistance	Surge voltage
1: 1 Form C (Standard) 1a: 1 Form A (Standard) 1aP: 1 Form A (Long endurance type)	Nil: Sealed type F: Flux-resistant type	Nil: Class E insulation B: Class B insulation F: Class F insulation	5, 6, 9, 12, 18, 24, 48 V	F: AgSnO ₂ type	Nil: — T: EN60335-1 (Conform)	6K: 6kV type

Standard: UL/CSA, VDE, TÜV (Standard type)
UL/CSA, VDE (Long endurance type and EN60335-1 GWT compliant type)
UL/CSA (Surge voltage 6kV type)

- Notes: 1. Standard packing: Carton: 100 pcs. Case: 500 pcs.
2. When ordering TV rated (TV-5) types, please consult us.
3. Contact arrangement 1aP type is Flux-resistant type only (Class B insulation only).
4. Please inquire about the previous products (Cadmium containing parts).

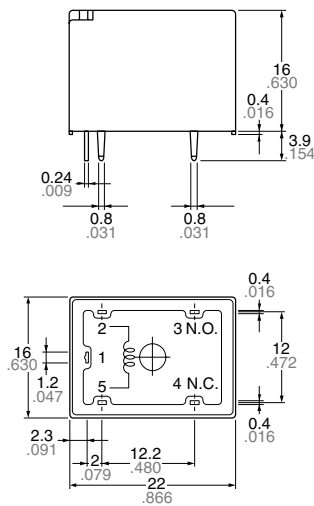
COIL DATA

Part No.					Nominal voltage, V DC	Pick-up voltage, V DC (max.) (at 20°C 68°F)	Drop-out voltage, V DC (min.) (at 20°C 68°F)	Coil resistance, Ω (±10%) (at 20°C 68°F)	Nominal operating current, mA (±10%) (at 20°C 68°F)	Nominal operating power, mW (at 20°C 68°F)	Max. allowable voltage (at 85°C 185°F)
Standard type		Long endurance type									
Sealed type		Flux-resistant type		Flux-resistant type							
1 Form A	1 Form C	1 Form A	1 Form C	1 Form A							
JS1a-5V-F	JS1-5V-F	JS1aF-5V-F	JS1F-5V-F	JS1aPF-B-5V-F	5	3.5	0.5	69.4	72	360	130%V of nominal voltage
JS1a-6V-F	JS1-6V-F	JS1aF-6V-F	JS1F-6V-F	JS1aPF-B-6V-F	6	4.2	0.6	100	60		
JS1a-9V-F	JS1-9V-F	JS1aF-9V-F	JS1F-9V-F	JS1aPF-B-9V-F	9	6.3	0.9	225	40		
JS1a-12V-F	JS1-12V-F	JS1aF-12V-F	JS1F-12V-F	JS1aPF-B-12V-F	12	8.4	1.2	400	30		
JS1a-18V-F	JS1-18V-F	JS1aF-18V-F	JS1F-18V-F	JS1aPF-B-18V-F	18	12.6	1.8	900	20		
JS1a-24V-F	JS1-24V-F	JS1aF-24V-F	JS1F-24V-F	JS1aPF-B-24V-F	24	16.8	2.4	1,600	15		
JS1a-48V-F	JS1-48V-F	JS1aF-48V-F	JS1F-48V-F	JS1aPF-B-48V-F	48	33.6	4.8	6,400	7.5		

- Notes) 1. Class B and F coil insulation types available.
Ex) JS1aF-B-12V-F
JS1aF-E-12V-F
2. EN60335-1 GWT compliant types available. When ordering, please add suffix "T".
Ex) JS1aF-B-12V-F-T
3. Surge voltage 6kV types available. When ordering, please add suffix "6K" (except for Long endurance type and EN60335-1 GWT compliant type).
Ex) JS1aF-B-12V-F-6K

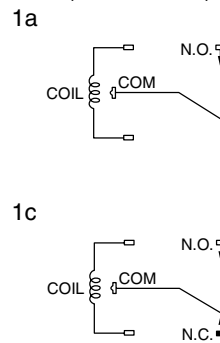
DIMENSIONS

mm inch

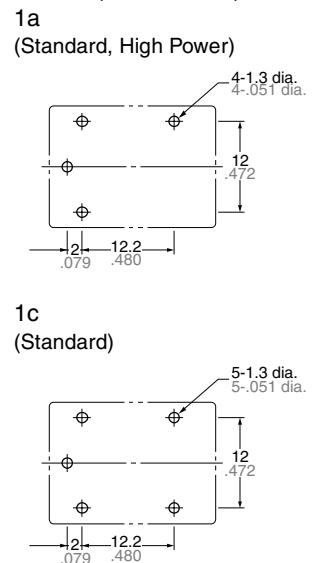


Note: Terminal No. 4 is only for Standard 1 Form C type
General tolerance: ±0.3 ±.012

Schematic (Bottom view)



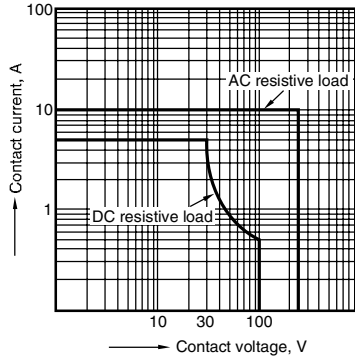
PC board pattern (Bottom view)



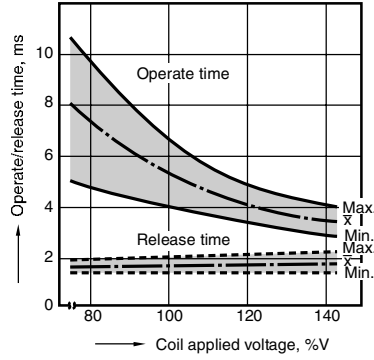
Tolerance: ±0.1 ±.004

REFERENCE DATA

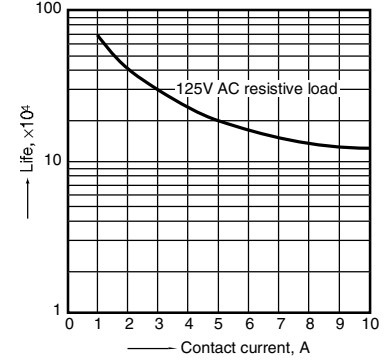
1. Maximum value for switching capacity



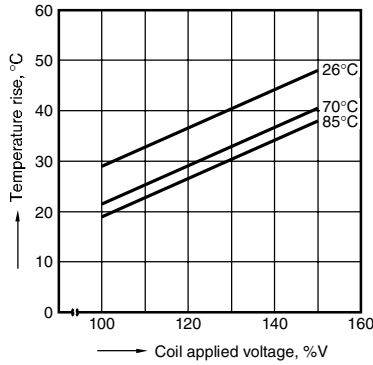
2. Operate/release time
Sample: 25 pcs., JS1-12V-F



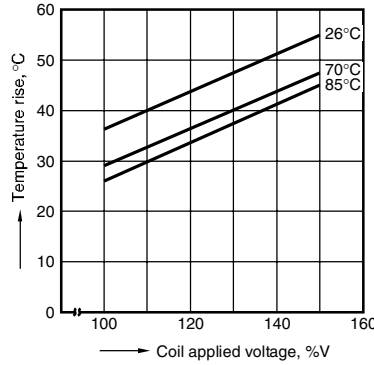
3. Life curve
Ambient temperature: Room temperature



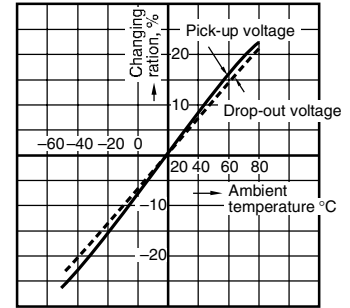
4-(1). Coil temperature rise
Sample: 5 pcs., JS1a-24V-F
Measured portion: Inside the coil
Contact current: 5 A



4-(2). Coil temperature rise
Sample: 5 pcs., JS1a-24V-F
Measured portion: Inside the coil
Contact current: 10 A



5. Ambient temperature characteristics
Sample: 6 pcs., JS1-12V-F

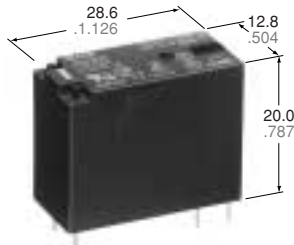


For Cautions for Use, see Relay Technical Information

Panasonic
ideas for life

**COMPACT PC BOARD
POWER RELAY**

JW RELAYS



mm inch

FEATURES

- Miniature package with universal terminal footprint
- High dielectric withstanding for transient protection: 10,000 V surge in μs between coil and contact
- Sealed construction
- Class B coil insulation types available
- TV rated (TV-5) types available (only for 1 Form A type)
- VDE, TÜV, SEMKO, SEV, FIMKO, TV-5 also approved

SPECIFICATIONS

Contact

		Standard type	High capacity type
Arrangement		1 Form A, 1 Form C, 2 Form A, 2 Form C	1 Form A, 1 Form C
Initial contact resistance, max. (By voltage drop 6 V DC 1 A)		100 m Ω	
Contact material		Silver alloy	
Rating (resistive load)	Nominal switching capacity	5 A 250 V AC, 5 A 30 V DC	10 A 250 V AC, 10 A 30 V DC
	Max. switching power	1,250 VA, 150 W	2,500 VA, 300 W
	Max. switching voltage	250 V AC, 30 V DC	
	Max. switching current	5 A	10 A
	Min. switching capacity ^{#1}	100 mA, 5 V DC	
Expected life (min. ope.)	Mechanical (at 180 cpm)	5 \times 10 ⁶	
	Electrical (at 6 cpm) (Resistive load)	10 ⁵	

Coil

Nominal operating power	530 mW
-------------------------	--------

#1 This value can change due to the switching frequency, environmental conditions, and desired reliability level, therefore it is recommended to check this with the actual load.

Remarks

- * Specifications will vary with foreign standards certification ratings.
- *1 Detection current: 10mA
- *2 Wave is standard shock voltage of $\pm 1.2 \times 50\mu\text{s}$ according to JEC-212-1981
- *3 Excluding contact bounce time
- *4 Half-wave pulse of sine wave: 11ms; detection time: 10 μs
- *5 Half-wave pulse of sine wave: 6ms
- *6 Detection time: 10 μs
- *7 Refer to 6. Conditions for operation, transport and storage mentioned in AMBIENT ENVIRONMENT
- *8 When using relays in a high ambient temperature, consider the pick-up voltage rise due to the high temperature (a rise of approx. 0.4% V for each 1°C 33.8°F with 20°C 68°F as a reference) and use a coil impressed voltage that is within the maximum allowable voltage range.

Characteristics

		Standard type	High capacity type
Max. operating speed (at rated load)		6 cpm	
Initial insulation resistance		Min. 1,000 M Ω at 500 V DC	
Initial breakdown voltage*1	Between open contacts	1,000 Vrms for 1 min.	
	Between contacts and coil	5,000 Vrms for 1 min.	
	Between contact sets	3,000 Vrms for 1 min. (2 Form A, 2 Form C)	
Initial surge voltage between contacts and coil*2		Min. 10,000 V	
Operate time*3 (at nominal voltage)		Max. 15 ms	
Release time (without diode)*3 (at nominal voltage)		Max. 5 ms	
Temperature rise (at 20°C) (at nominal voltage) (with nominal coil voltage and at nominal switching capacity)		1a: max. 39°C 1c, 2a, 2c: max. 55°C (resistance method)	1a: max. 45°C 1c: max. 55°C (resistance method)
Shock resistance	Functional*4	Min. 98 m/s ² {10 G}	
	Destructive*5	Min. 980 m/s ² {100 G}	
Vibration resistance	Functional*6	Approx. 98 m/s ² {10 G}, 10 to 55 Hz at double amplitude of 1.6 mm	
	Destructive	Approx. 117.6 m/s ² {12 G}, 10 to 55 Hz at double amplitude of 2.0 mm	
Conditions for operation, transport and storage*7 (Not freezing and condensing at low temperature)	Ambient temp.*8	-40°C to +85°C -40°F to +185°F	
	Humidity	5 to 85% R.H.	
Unit weight		Approx. 13 g .46 oz	

TYPICAL APPLICATIONS

1. Home appliances
TV sets, VCR, Microwave ovens
2. Office machines
Photocopiers, Vending machines
3. Industrial equipment
NC machines, Robots, Temperature controllers

ORDERING INFORMATION

Ex. JW 1 F S N B DC5V —

Contact arrangement	Contact capacity	Protective construction	Pick-up voltage	Coil insulation class	Coil voltage	Environmental support
1: 1 Form C 1a: 1 Form A 2: 2 Form C 2a: 2 Form A	Nil: Standard (5 A) F: High capacity (10 A)*	S: Sealed type	N: 70% of nominal voltage	Nil: Class E insulation B: Class B insulation	DC 5, 6, 9, 12, 18, 24, 48 V	<ul style="list-style-type: none"> RoHS Directive conforming type (AgSnO₂ type) F: 1a (Standard/High capacity) Nil: 1c (Standard/High capacity), 2a (Standard), 2c (Standard) RoHS Directive non-conforming type (AgCdO type) Nil: 1a (Standard/High capacity)

*Only for 1 Form A and 1 Form C type
UL/CSA, VDE, SEMKO, FIMKO, SEV approved type is standard.
Notes: 1. When ordering TV rated (TV-5) types, add suffix-TV (available only for 1 Form A type).
2. Standard packing: Carton: 100 pcs. Case: 500 pcs.

TYPES

Standard (5A) types

Contact arrangement	Coil voltage, V DC	Part No.	Contact arrangement	Coil voltage, V DC	Part No.
1 Form A	5	JW1aSN-DC5V (-F)	2 Form A	5	JW2aSN-DC5V
	6	JW1aSN-DC6V (-F)		6	JW2aSN-DC6V
	9	JW1aSN-DC9V (-F)		9	JW2aSN-DC9V
	12	JW1aSN-DC12V (-F)		12	JW2aSN-DC12V
	18	JW1aSN-DC18V (-F)		18	JW2aSN-DC18V
	24	JW1aSN-DC24V (-F)		24	JW2aSN-DC24V
	48	JW1aSN-DC48V (-F)		48	JW2aSN-DC48V
1 Form C	5	JW1SN-DC5V	2 Form C	5	JW2SN-DC5V
	6	JW1SN-DC6V		6	JW2SN-DC6V
	9	JW1SN-DC9V		9	JW2SN-DC9V
	12	JW1SN-DC12V		12	JW2SN-DC12V
	18	JW1SN-DC18V		18	JW2SN-DC18V
	24	JW1SN-DC24V		24	JW2SN-DC24V
	48	JW1SN-DC48V		48	JW2SN-DC48V

High capacity (10 A) types

Contact arrangement	Coil voltage, V DC	Part No.	Contact arrangement	Coil voltage, V DC	Part No.
1 Form A	5	JW1aFSN-DC5V (-F)	1 Form C	5	JW1FSN-DC5V
	6	JW1aFSN-DC6V (-F)		6	JW1FSN-DC6V
	9	JW1aFSN-DC9V (-F)		9	JW1FSN-DC9V
	12	JW1aFSN-DC12V (-F)		12	JW1FSN-DC12V
	18	JW1aFSN-DC18V (-F)		18	JW1FSN-DC18V
	24	JW1aFSN-DC24V (-F)		24	JW1FSN-DC24V
	48	JW1aFSN-DC48V (-F)		48	JW1FSN-DC48V

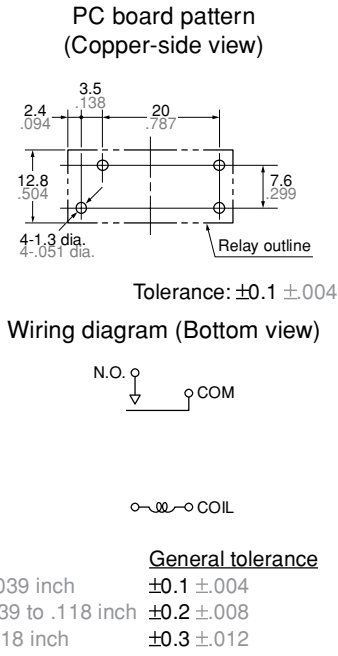
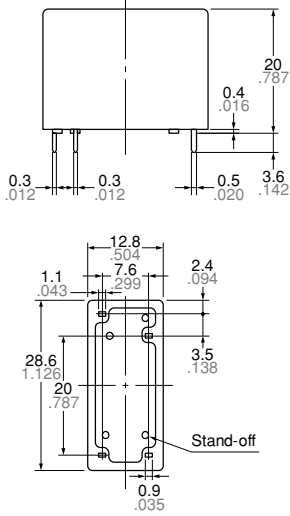
COIL DATA (at 20°C 68°F)

Nominal voltage, V DC	Pick-up voltage, V DC (max.) (Initial)	Drop-out voltage, V DC (min.) (Initial)	Nominal operating current, mA (±10%)	Coil resistance, W (±10%)	Nominal operating power, mW	Max. allowable voltage
5	3.5	0.5	106	47	530	130% V of Nominal Voltage (at 60°C 140°F) 120% V of Nominal Voltage (at 85°C 185°F)
6	4.2	0.6	88	68		
9	6.3	0.9	58	155		
12	8.4	1.2	44	270		
18	12.6	1.8	29	611		
24	16.8	2.4	22	1,100		
48	33.6	4.8	11	4,400		

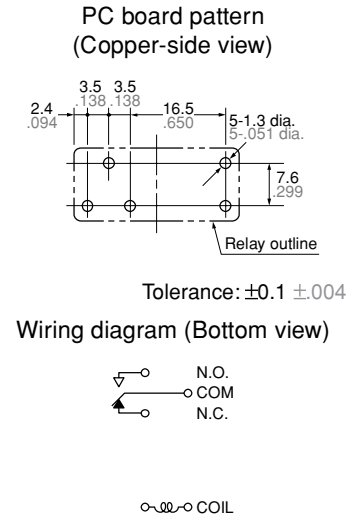
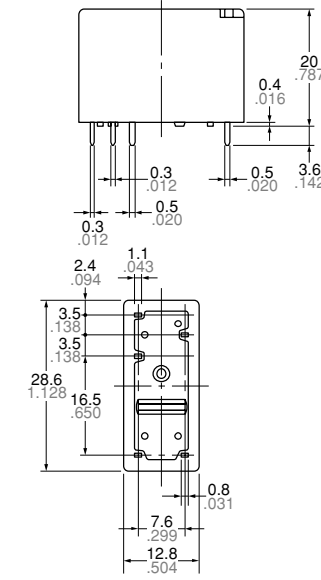
DIMENSIONS

mm inch

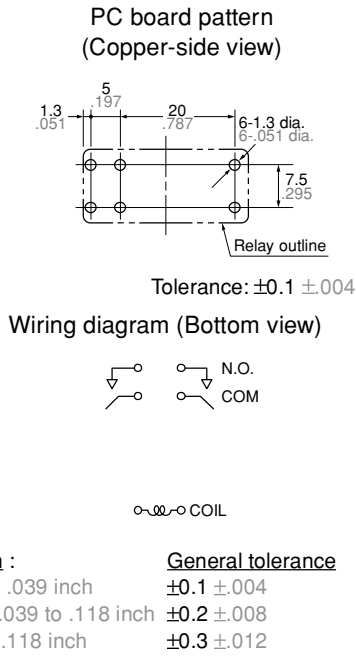
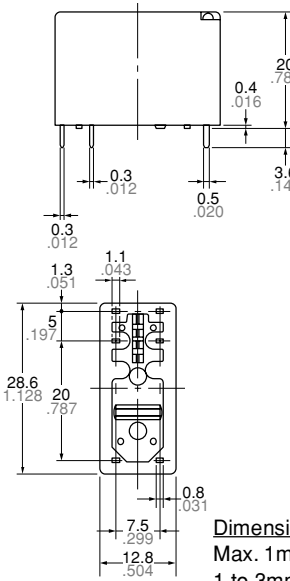
1 Form A



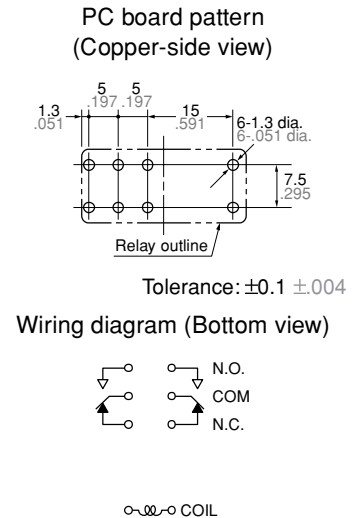
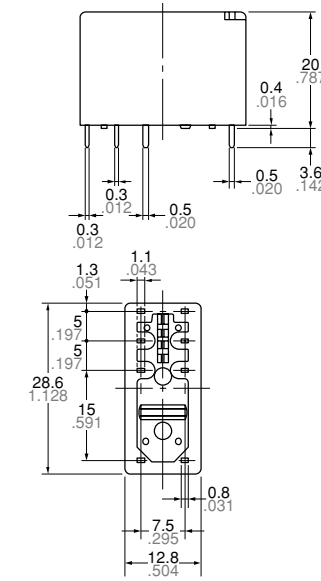
1 Form C



2 Form A

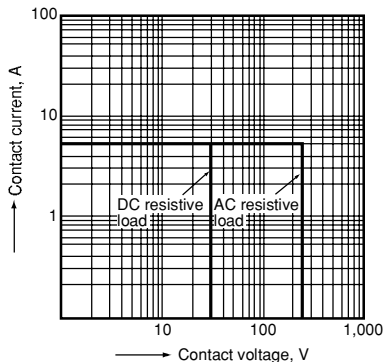


2 Form C

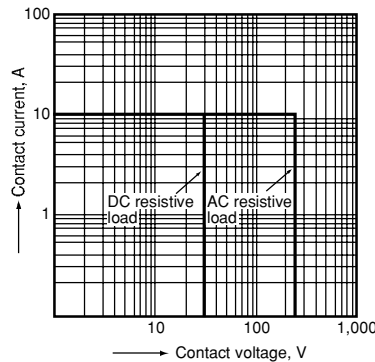


REFERENCE DATA

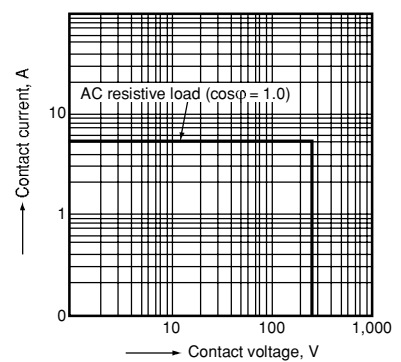
1-(1). Maximum operating power
1 Form A Standard (5 A) type



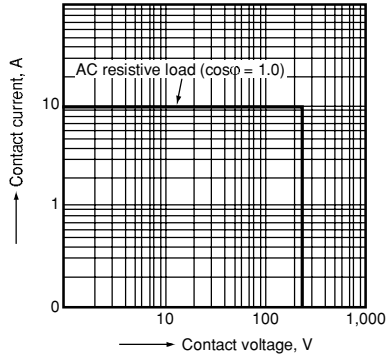
1-(2). Maximum operating power
1 Form A High Capacity (10 A) type



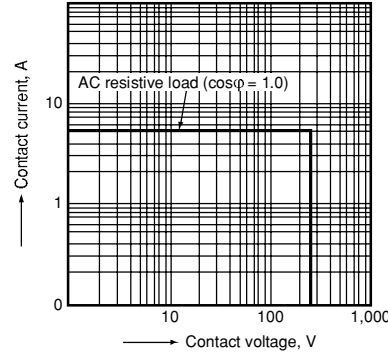
1-(3). Maximum operating power
1 Form C Standard (5 A) type



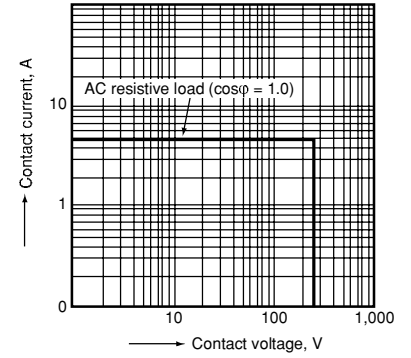
1-(4). Maximum operating power
1 Form C High Capacity (10 A) type



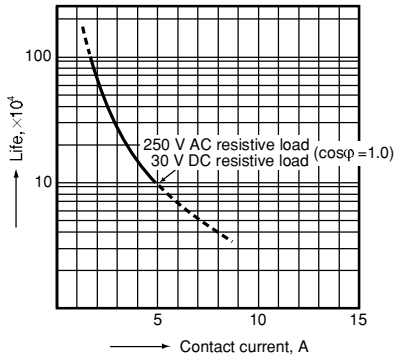
1-(5). Maximum operating power
2 Form A Standard (5 A) type



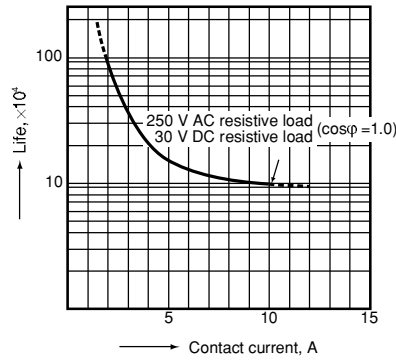
1-(6). Maximum operating power
2 Form C Standard (5 A) type



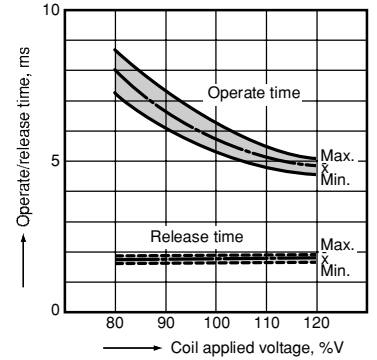
2-(1). Life curve
1 Form A Standard (5 A) type



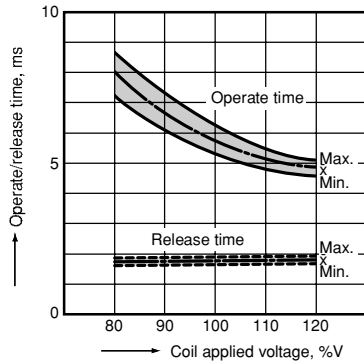
2-(2). Life curve
1 Form A High Capacity (10 A) type



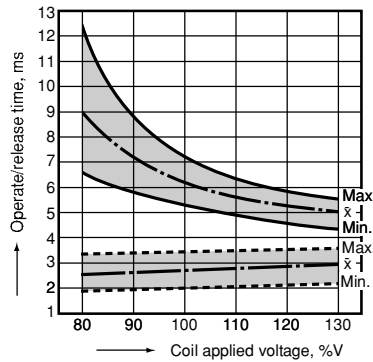
3-(1). Operate/release time
Sample: JW1aSN-DC12V, 10 pcs.
Ambient temperature: 20°C 68°F



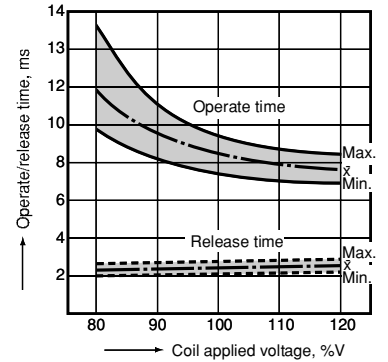
3-(2). Operate/release time
Sample: JW1aFSN-DC12V, 10 pcs.
Ambient temperature: 20°C 68°F



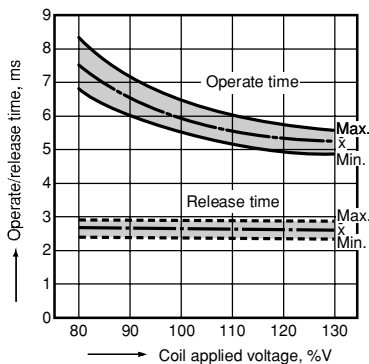
3-(3). Operate/release time
Sample: JW1SN-DC12V, 6 pcs.
Ambient temperature: 20°C 68°F



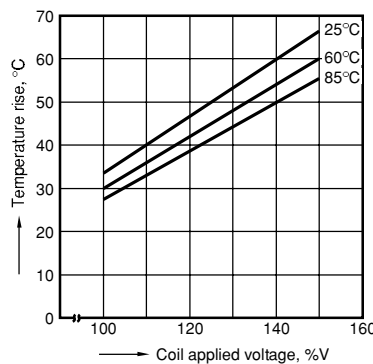
3-(4). Operate/release time
Sample: JW2aSN-DC24V, 6 pcs.
Ambient temperature: 20°C 68°F



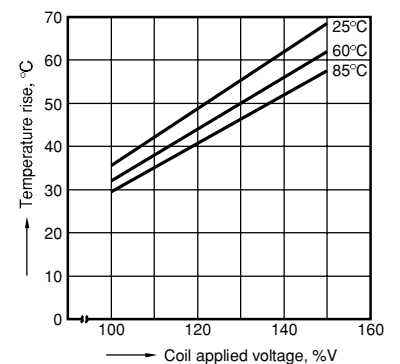
3-(5). Operate/release time
Sample: JW2SN-DC12V, 6 pcs.
Ambient temperature: 20°C 68°F



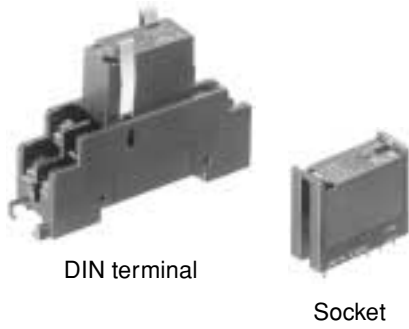
4-(1). Coil temperature rise
(Contact carrying current: 5A)
Sample JW1aFSN-DC12V, 6 pcs.
Point measured: Inside the coil



4-(2). Coil temperature rise
(Contact carrying current: 10 A)
Sample: JW1aFSN-DC12V, 6 pcs.
Point measured: Inside the coil



ACCESSORIES

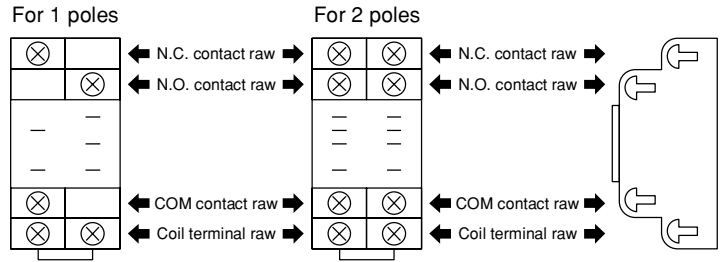


DIN terminal

Socket

FEATURES

1. Space saving design
2. Wiring can be done with ease (DIN terminal)



TYPES

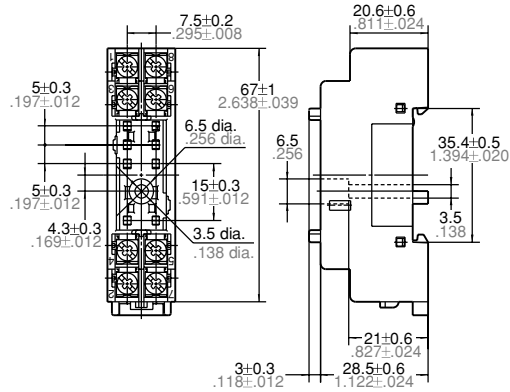
Product name	Number of poles	Part No.	Applicable relay type				Standard packing	
			1 Form A	1 Form C	2 Form A	2 Form C	Inner carton	Outer case
JW1 DIN terminal socket (with hold-down clip)	1	JW1-SFD	•	•			10 pcs.	100 pcs.
JW2 DIN terminal socket (with hold-down clip)	2	JW2-SFD			•	•		
JW1 PC board socket	1	JW1-PS	•	•				
JW2 PC board socket	2	JW2-PS			•	•		
JW1 Plug-in socket	1	JW1-SS	•	•				
JW2 Plug-in socket	2	JW2-SS			•	•		

SPECIFICATIONS

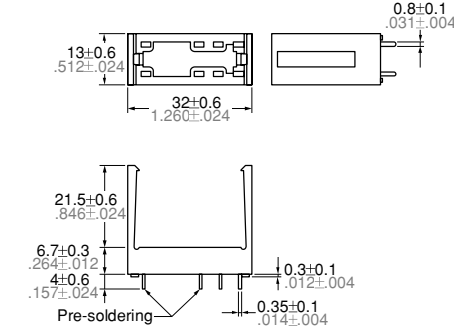
Item	Type	PC board socket/Plug-in socket		DIN terminal socket	
		1 pole	2 poles	1 pole	2 poles
Breakdown voltage		1,500 vrms for 1 minute		1,500 Vrms for 1 minute	1,000 Vrms for 1 minute
Insulation resistance		Min. 100 MΩ		Min. 100 MΩ	

DIMENSIONS

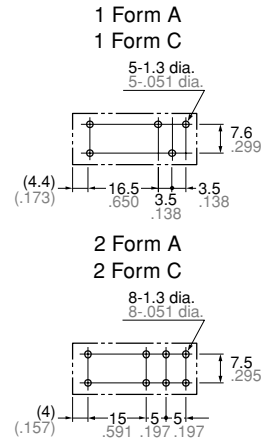
1. DIN terminal socket



2. PC board socket

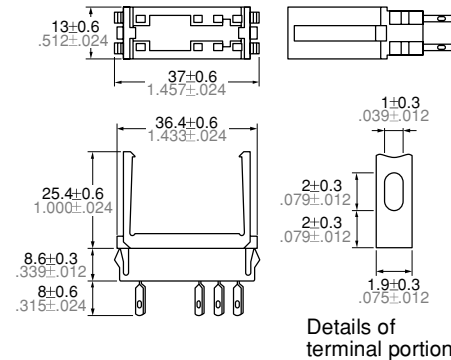


PC board pattern (Bottom view)

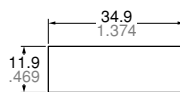


Tolerance: ±0.1 ±.004

3. Plug-in socket



Panel cut-out
(Thickness: 1.0 to 2.0 .039 to .079)



Tolerance: ±0.1 ±.004

For Cautions for Use, see Relay Technical Information

Current Transducer LTS 25-NP

$I_{PN} = 8 - 12 - 25 \text{ A}$

For the electronic measurement of currents : DC, AC, pulsed, mixed, with a galvanic isolation between the primary circuit (high power) and the secondary circuit (electronic circuit).



Electrical data

I_{PN}	Primary nominal r.m.s. current	25	At
I_p	Primary current, measuring range	0 .. ± 80	At
V_{OUT}	Analog output voltage @ I_p	$2.5 \pm (0.625 \cdot I_p / I_{PN}) \text{ V}$	
	$I_p = 0$	$2.5^{1)}$	V
N_S	Number of secondary turns ($\pm 0.1 \%$)	2000	
R_L	Load resistance	≥ 2	k Ω
R_{IM}	Internal measuring resistance ($\pm 0.5 \%$)	50	Ω
TCR_{IM}	Thermal drift of R_{IM}	< 50	ppm/K
V_C	Supply voltage ($\pm 5 \%$)	5	V
I_C	Current consumption @ $V_C = 5 \text{ V}$	Typ $23 + I_S^{2} + (V_{OUT} / R_L) \text{ mA}$	
V_d	R.m.s. voltage for AC isolation test, 50/60 Hz, 1 mn	3	kV
V_e	R.m.s. voltage for partial discharge extinction @ 10 pC	> 1.5	kV
\hat{V}_w	Impulse withstand voltage 1.2/50 μs	> 8	kV

Accuracy - Dynamic performance data

X	Accuracy @ $I_{PN}, T_A = 25^\circ\text{C}$	± 0.2	%
	Accuracy with R_{IM} @ $I_{PN}, T_A = 25^\circ\text{C}$	± 0.7	%
ε_L	Linearity	< 0.1	%
TCV_{OUT}	Thermal drift of V_{OUT} @ $I_p = 0$	-10 $^\circ\text{C}$.. +85 $^\circ\text{C}$	Typ 50 Max 100 ppm/K
$TC\varepsilon_G$	Thermal drift of the gain	-10 $^\circ\text{C}$.. +85 $^\circ\text{C}$	50 ³⁾ ppm/K
V_{OM}	Residual voltage @ $I_p = 0$, after an overload of $3 \times I_{PN}$		± 0.5 mV
	$5 \times I_{PN}$		± 2.0 mV
	$10 \times I_{PN}$		± 2.0 mV
t_{ra}	Reaction time @ 10 % of I_{PN}	< 50	ns
t_r	Response time @ 90 % of I_{PN}	< 400	ns
di/dt	di/dt accurately followed	> 60	A/ μs
f	Frequency bandwidth (0 .. -0.5 dB)	DC .. 100	kHz
	(-0.5 .. 1 dB)	DC .. 200	kHz

General data

T_A	Ambient operating temperature	-10 .. +85	$^\circ\text{C}$
T_S	Ambient storage temperature	-25 .. +100	$^\circ\text{C}$
	Insulating material group	III a	
m	Mass	10	g
	Standards ⁴⁾	EN 50178	
		EN 60950	

Notes : ¹⁾ Absolute value @ $T_A = 25^\circ\text{C}$, $2.475 < V_{OUT} < 2.525$

²⁾ Please see the operation principle on the other side

³⁾ Only due to TCR_{IM}

⁴⁾ Specification according to IEC 1000-4-3 are not guaranteed between 180 and 220 MHz.

Features

- Closed loop (compensated) multi-range current transducer using the Hall effect
- Unipolar voltage supply
- Insulated plastic case recognized according to UL 94-V0
- Compact design for PCB mounting
- Incorporated measuring resistance
- Extended measuring range.

Advantages

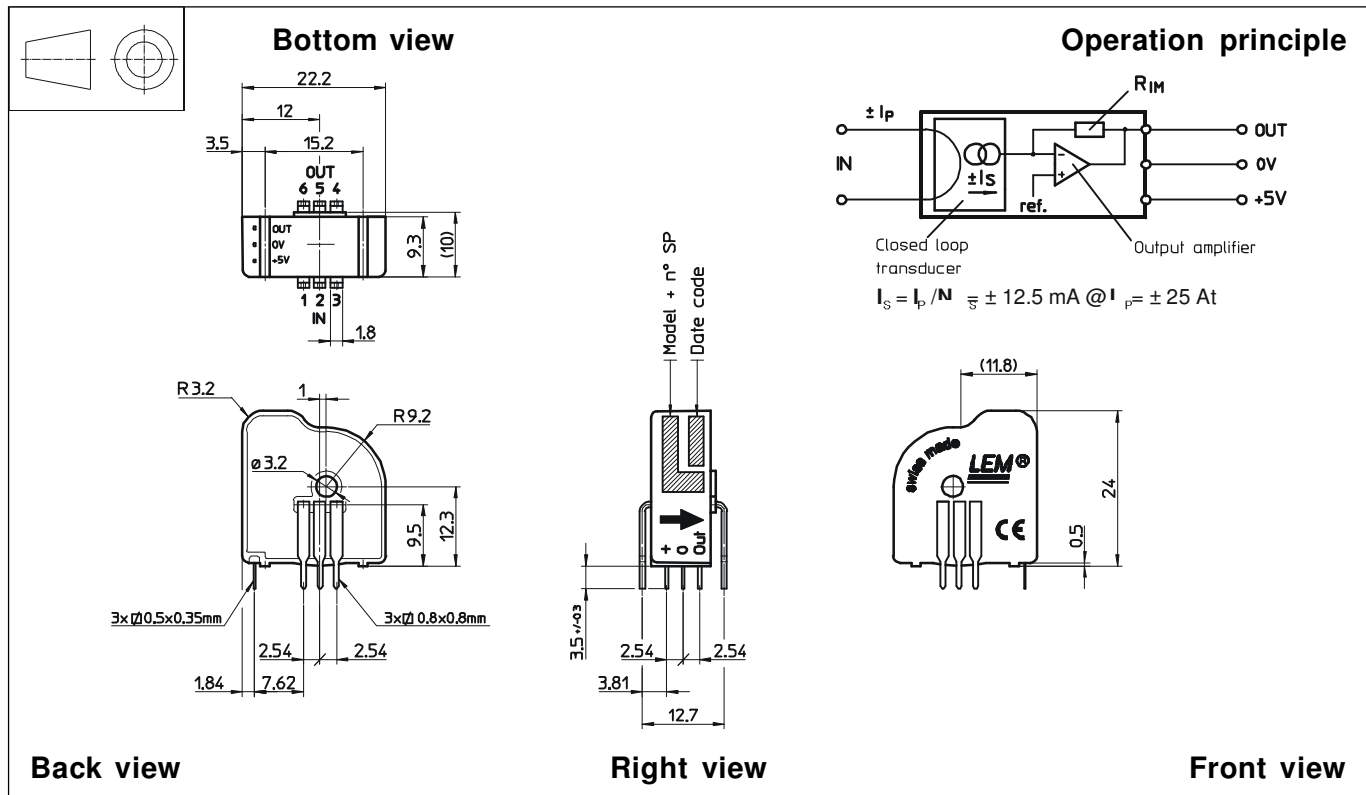
- Excellent accuracy
- Very good linearity
- Very low temperature drift
- Optimized response time
- Wide frequency bandwidth
- No insertion losses
- High immunity to external interference
- Current overload capability.

Applications

- AC variable speed drives and servo motor drives
- Static converters for DC motor drives
- Battery supplied applications
- Uninterruptible Power Supplies (UPS)
- Switched Mode Power Supplies (SMPS)
- Power supplies for welding applications.

Copyright protected.

Dimensions LTS 25-NP (in mm. 1 mm = 0.0394 inch)



Number of primary turns	Primary nominal r.m.s. current I_{PN} [A]	Nominal output voltage V_{OUT} [V]	Primary resistance R_P [mΩ]	Primary insertion inductance L_P [μH]	Recommended connections
1	± 25	2.5 ± 0.625	0.18	0.013	
2	± 12	2.5 ± 0.600	0.81	0.05	
3	± 8	2.5 ± 0.600	1.62	0.12	

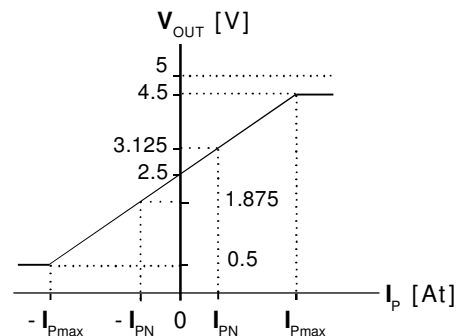
Mechanical characteristics

- General tolerance ± 0.2 mm
- Fastening & connection of primary 6 pins 0.8 x 0.8 mm
Recommended PCB hole 1.3 mm
- Fastening & connection of secondary 3 pins 0.5 x 0.35 mm
Recommended PCB hole 0.8 mm
- Additional primary through-hole ∅ 3.2 mm

Remark

- V_{OUT} is positive when I_p flows from terminals 1, 2, 3 to terminals 6, 5, 4

Output Voltage - Primary Current



Description

30:1 GEAR RATIO, 30 TEETH WORM GEAR

**Product Details**

Part Number A 1B 6-N32030
Unit Inch
Diametral Pitch 32
No. Of Teeth 30
Gear Ratio 30.00 To 1
Quality Class/mat'l Commercial / Bronze
Bore & Hub Config. 0.1875/NO S.S.
Face Width 0.188"
Pitch Dia. (PD) 0.938"
Mating Worm 32DP/1
 LEAD/0.438PD
Pressure Angle 14.5°
Lead Angle 4.08°

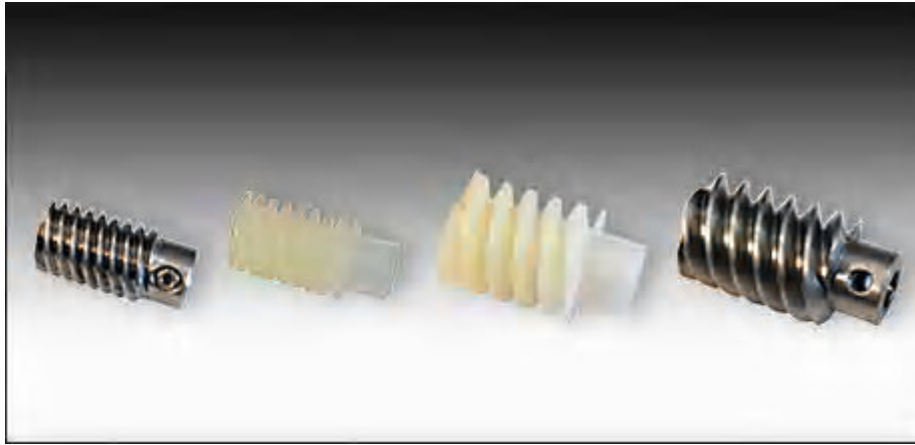
Price Information

Quantity	Price
1 to 24	\$20.25
25 to 99	\$14.13
100 to 249	\$11.33

[Higher quantities](#)**Availability** In Stock**Sell Unit** Each**Quantity** [ADD TO CART](#)[ADD TO RFQ](#)**CAD Models / Catalog Pages****Specs from printed catalog** [PDF](#)**AutoCAD Drawing** [Front View](#)[Right View](#)**PTC PartsLink** [3D CAD Models](#)Phone: (800) 819-8900X491 Fax: (516) 326-8827 Email: eservice@sdp-si.com

Description

32DP / 1 Lead / 0.438P.D, 4.08° Right Hand Worm

**Product Details**

Part Number A 1Q 5-N32
Unit Inch
Pitch 32
Material / Quality Carbon Steel/Commercial
Condition / Finish Hardened & Polished
Worm Spec. 4.08° R.H./1 Lead/0.438" P.D.
Bore / Set Screw 0.21875 / #47 Hole
Pressure Angle 14.5°
Face Width (FW) 0.688
Overall Width 0.875"
Outside Dia. (O.D.) 0.500"
Hub Dia. 0.320"

Price Information

Availability [Out of Stock](#)
Sell Unit Each

CAD Models / Catalog Pages

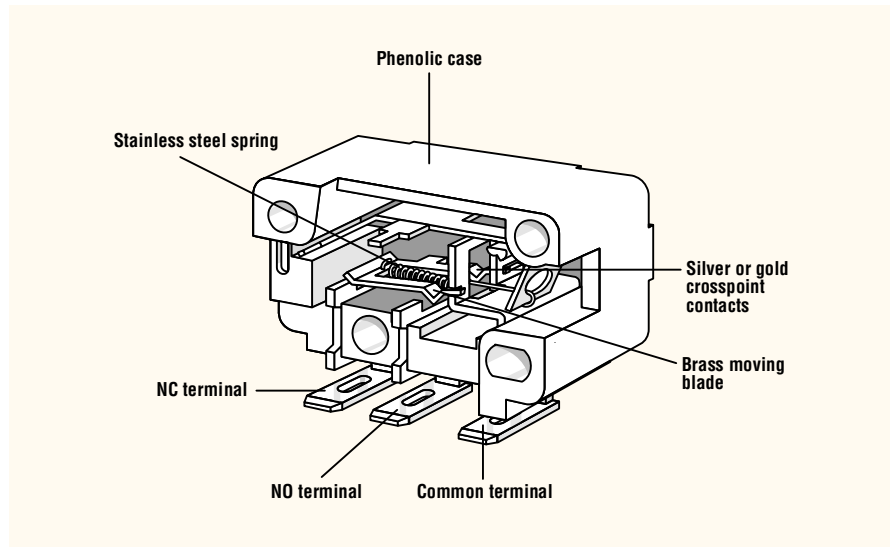
Specs from printed catalog [PDF](#)
AutoCAD Drawing [Section View](#)
[Left View](#)
[3D CAD Models](#)
PTC PartsLink

Phone: (800) 819-8900X491 Fax: (516) 326-8827 Email: eservice@sdp-si.com

MINIATURE LOW TORQUE E Series

Features

- Long life coil spring mechanism
- Low torque rotary actuation
- Clockwise or counter clockwise actuation
- 6 terminal types
- Double rivet sturdy case construction
- 3 contact arrangements



Electrical Ratings

Switch Series	EN61058 Rating	UL1054 Rating	Electrical Life at Rated Load	
			According to VDE (Min. Operations)	According to UL (Min. Operations)
E51	N/A	6A, 250VAC	N/A	6,000
E53	N/A	0.1A, 125VAC	N/A	6,000

Specifications

Electrical

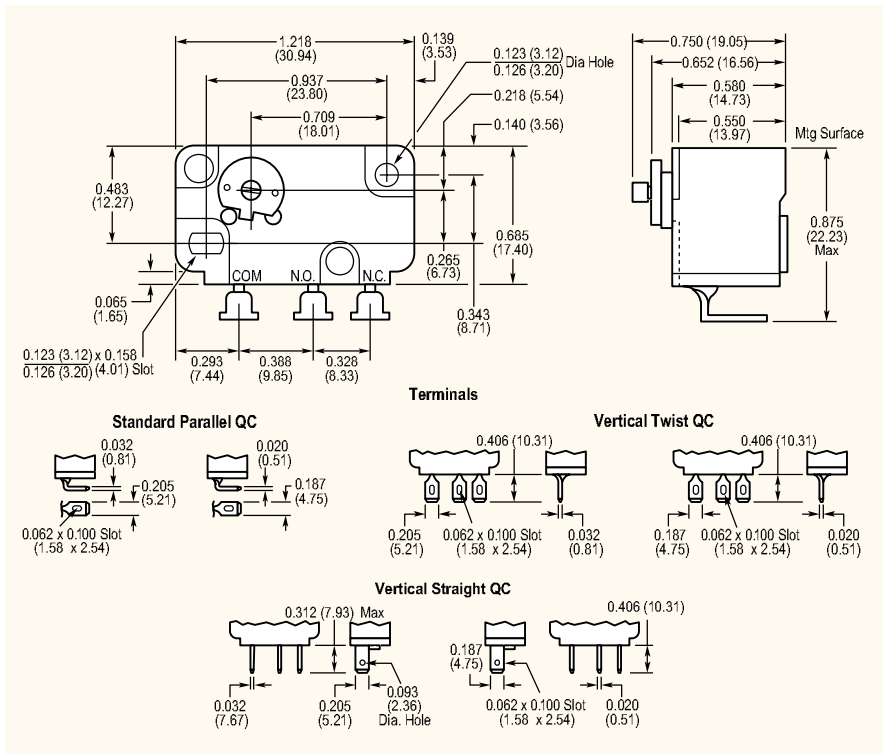
Temperature Rating:	-40° to +85°C
Flammability Rating:	UL94HB

Materials

Case:	General Purpose Phenolic
Terminal:	Silver-Plated Brass
Moving Blade:	Brass
Contacts:	Silver Alloy (E51), Gold Crosspoint (E53)
Spring:	Stainless Steel

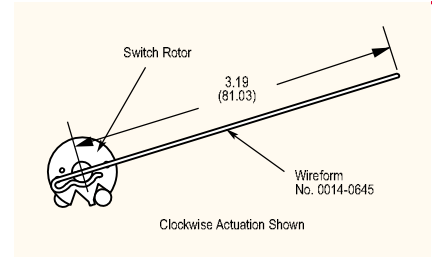


Dimensions inches (mm)



Actuators

Wireform actuators are supplied unassembled for each switch. Wireforms may be readily assembled to switch rotor as shown.



Circuitry

This series is available in single pole double throw and single pole single throw either normally open or normally closed. In general, normally open may be specified by adding 01 to suffix numbers, and normally closed by adding 02.

For example, E51-00B is double throw, E51-01B is normally open and E51-02B is normally closed.

Mounting

Recommended mounting screw size: #4-40 Round head. Recommended torque on screw: 4 inch lbs. max.

Operating Characteristics

Standard Force	4.0" gms. (max.)
Overtravel	15° min. (10.5 gram – cm)
Movement Differential	3° min.

Note: Special models and tooling capability available for custom wire form actuators.

Note: Additional operating forces available upon request. Consult factory.

Ordering Information

Select the current rating you need. Combine the corresponding Series/Prefix number with the appropriate suffix number for the switch type, circuitry and terminals you require.

Actuator Specifications

Switch Type	Actuator Type	Direction of Actuator	Terminals inches (mm)
	-00B	Clockwise	Standard Parallel 0.205 (5.21)
	-00R	Clockwise	Standard Parallel 0.187 (4.75)
	-00E	Counter Clockwise	Standard Parallel 0.205 (5.21)
	-00T	Counter Clockwise	Standard Parallel 0.187 (4.75)
	-50B	Clockwise	Vertical Twist 0.205 (5.21)
	-50R	Clockwise	Vertical Twist 0.187 (4.75)
	-50E	Counter Clockwise	Vertical Twist 0.205 (5.21)
	-50T	Counter Clockwise	Vertical Twist 0.187 (4.75)
	-60B	Clockwise	Vertical Straight 0.205 (5.21)
	-60R	Clockwise	Vertical Straight 0.187 (4.75)
	-60E	Counter Clockwise	Vertical Straight 0.205 (5.21)
	-60T	Counter Clockwise	Vertical Straight 0.187 (4.75)

SCA100T Series

Inclinometer



FEATURES

- 2-axis inclination measurement (X and Y)
- Available ranges $\pm 0.5\text{ g}$ ($\pm 30^\circ$), $\pm 1.0\text{ g}$ ($\pm 90^\circ$)
- Over damped frequency response by Sensing Element (-3 dB @ 8...28 Hz)
- 0.003° resolution (10 Hz BW, analog output)
- Advanced internal and external connection failure detection
- Digitally activated electrostatic sensing element self test
- Continuous memory parity check
- Single +5 V supply; ratiometric voltage output
- Serial Peripheral Interface (SPI) compatible
- Internal temperature sensor, accessible via SPI
- Lead-free reflow solderable lead-free component

BENEFITS

- Excellent reliability and stability over time and temperature
- Instrumentation grade performance
- High resolution and low noise
- Wide temperature range
- Outstanding overload and shock durability

APPLICATIONS

- 2-axis platform levelling
- Inclination based position measurement
- Tilt measurement with cross-axis compensation
- 360° vertical orientation measurement

ELECTRICAL CHARACTERISTICS

Parameter	Condition	Min	Typ.	Max	Units
Supply voltage Vdd ⁽¹⁾		4.75	5.0	5.25	V
Current consumption	Vdd = 5 V; No load		4	5	mA
Analogue output load	Vout to Vdd or Vss	10			kOhm
				20	nF
Digital output load	@ 500 kHz clock			1	nF
SPI clock frequency				500	kHz
AD conversion time			150		µs
Data transfer time	@500 kHz clock		38		µs

PERFORMANCE CHARACTERISTICS

Parameter	Condition	SCA100T-D01 (±30°)	SCA100T-D02 (±90°)	Units
Measuring range ⁽²⁾	Nominal	±30	±90	°
		±0.5	±1	g
Measuring direction ⁽³⁾	Mounting plane horizontal	Dual axis inclination	Dual axis inclination	
	Mounting plane vertical	Orthogonal rotation	Orthogonal rotation	
Zero point ⁽⁴⁾	Mounting position	Vdd/2	Vdd/2	V
Sensitivity	@ room temperature	4 ^(5a)	2 ^(5b)	V/g
Offset calibration accuracy ^(6a,13)	@ room temperature	±2	±4	mg
Offset temperature dependency ^(6a,13)	0...70°	±5	±5	mg
	-25...85 °C	±10	±10	mg
	-40...125 °C	±15	±15	mg
Sensitivity calibration accuracy ^(7a,13)	@ room temperature	±0.5	±0.5	%
Sensitivity temperature error ^(7b,13)	-40...85 °C	-1...1	-1...1	%
	85...125 °C	-2.5...1	-2.5...1	%
Typical non-linearity ⁽⁸⁾	Over measuring range	±2	±10	mg
Cross-axis sensitivity ⁽¹¹⁾	@ room temperature	4	4	%
Frequency response -3 dB (LP) ⁽⁹⁾	@ room temperature	8...28	8...28	Hz
Ratiometric error ⁽¹⁰⁾	Vdd = 4.75...5.25 V	±2	±2	%
Output noise density ⁽¹²⁾	From DC...100 Hz	15	15	µg/√Hz
Digital output resolution	FS	11	11	Bits
Long term stability ⁽¹⁴⁾	@ steady temp	0.25	T.B.D	mg

VDD = 5.00 V, APPLIES TO BOTH CHANNELS UNLESS OTHERWISE SPECIFIED

Note 1 For maximum accuracy the supply voltage should be $5 \pm 0.05\text{ V}$. 100 nF supply filtering capacitor is recommended.

Note 2 The measuring range is limited by sensitivity, offset and supply voltage rails of the device.

Note 3 Measuring directions in parallel to mounting plane, arrows showing positive acceleration direction

Note 4 Offset specified as $V_{\text{offset}} = V_{\text{out}}(0\text{ g})$ [V]. See note 12.

Note 5a Sensitivity specified as $V_{\text{sens}} = (V_{\text{out}}(+0.5\text{ g}) - V_{\text{out}}(-0.5\text{ g})) / 1$ [V/g]. See note 12.

Note 5b Sensitivity specified as $V_{\text{sens}} = (V_{\text{out}}(+1\text{ g}) - V_{\text{out}}(-1\text{ g})) / 2$ [V/g]. See note 12.

Note 6a Offset calibration error specified as $\text{Offset_Calib_error} = (V_{\text{out}}(0\text{ g}) - V_{\text{dd}}/2) / V_{\text{sens}}$ [g].

Note 6b Offset temperature error specified as $\text{Offset Error @ temp.} = (V_{\text{out}} @ \text{temp.} - V_{\text{out}} @ \text{room temp.}) / V_{\text{sens}}$ [g].

Note 7a Sensitivity calibration error specified as $\text{Sensitivity_calib_error} = (V_{\text{sens}} - V_{\text{sens_nom}}) / V_{\text{sens_nom}} \times 100\%$ [%] $V_{\text{sens_nom}}$ = nominal sensitivity.

Note 7b Sensitivity temperature error specified as $\text{Sensitivity error @ temp.} = [(V_{\text{sens}} @ \text{temp.} - V_{\text{sens}} @ \text{room temp.}) / V_{\text{sens}} @ \text{room temp.}] \times 100\%$ [%].

Note 8 From straight line through sensitivity calibration point.

Note 9 The output has true DC (0 Hz) response.

Note 10 The ratiometric error is specified as: $RE = 100\% \times \left(1 - \frac{V_{\text{out}}(@Vx) \times \frac{5.00V}{Vx}}{V_{\text{out}}(@5V)} \right)$

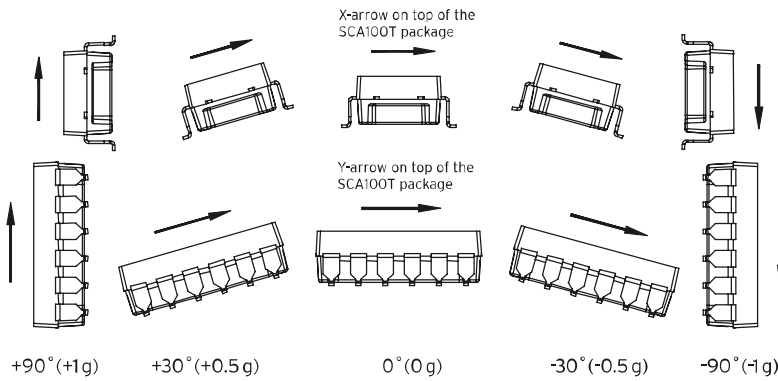
Note 11 The cross-axis sensitivity determines how much inclination / acceleration, perpendicular to the measuring axis, couples to the output. The total cross-axis sensitivity is the geometric sum of the sensitivities of the two axis which are perpendicular to the measuring axis.

Note 12 In addition, supply voltage noise couples to the output due to the ratiometric nature of the accelerometer.

Note 13 Factory calibration value.

Note 14 Power continuously connected.

MEASURING DIRECTIONS

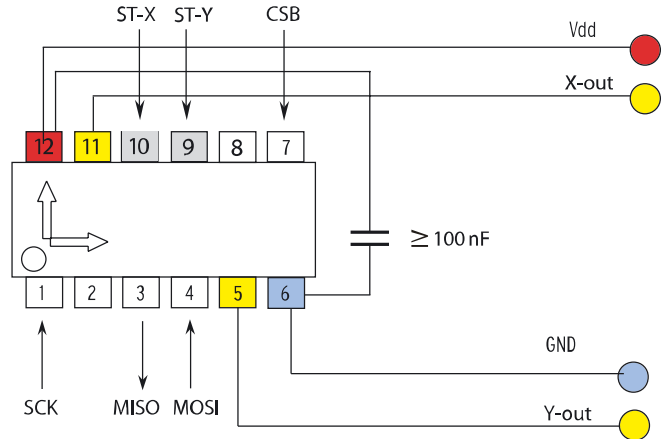


ABSOLUTE MAXIMUM RATINGS

Parameter	Value	Unit
Acceleration (powered or non-powered)	20 000	g
Supply voltage	-0.3 V to +5.5 V	V
Voltage at input/output pins	-0.3 V to (V _{dd} +0.3 V)	V
Temperature range	-55...125	°C

ELECTRICAL CONNECTION RECOMMENDED CIRCUIT

Pin#	Pin Name	I/O	Connection
1	SCK	Input	Serial clock
2	Ext_C_1	Input	X axis external capacitor input (Ch 1)
3	MISO	Output	Master in slave out; data output
4	MOSI	Input	Master out slave in; data input
5	Out_2	Output	Y axis Output (Ch 2)
6	GND	Power	round (GND)
7	CSB	Input	Chip select (active low)
8	Ext_C_2	Input	Y axis external capacitor input (Ch 2)
9	ST_2	Input	Self test input for Y axis (Ch 2)
10	ST_1 / Test_in	Input	Self test input for X axis (Ch 1)
11	Out_1	Output	X axis output (Ch 1)
12	VDD	Power	Positive supply voltage (VDD)

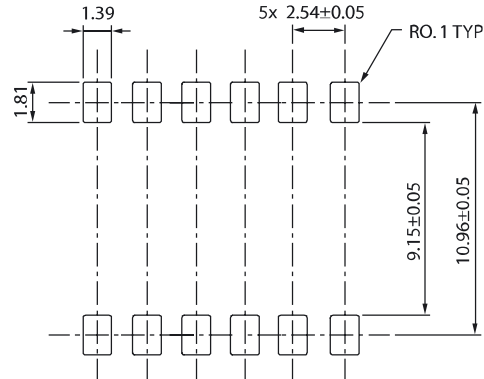
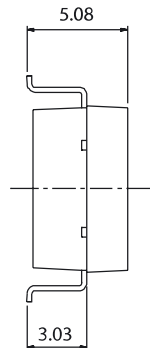
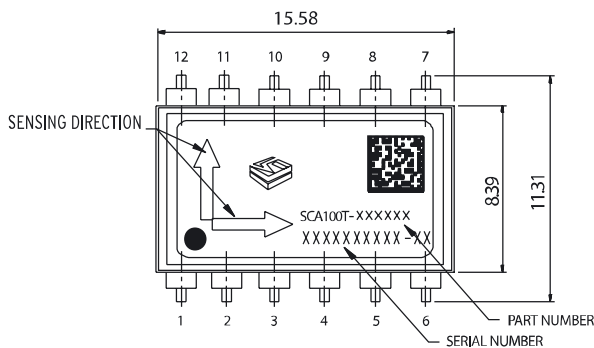


If the SPI interface is not used SCK (pin1), MISO (pin3), MOSI (pin4) and CSB (pin7) must be left floating.

Self test can be activated applying logic "1" (positive supply voltage level) to ST pin (pin 9 and 10). If ST feature is not used pins 9 and 10 must be left floating or connected to GND.

DIMENSIONS PCB PAD LAYOUTS

The part weights under 1.2 g. The size is appr. (w x h x l) 9 x 5 x 16 mm. Pin pitch is standard 100 mils.



Acceleration in the direction of the arrow will increase the output voltage.

Description:

The **E4P** miniature encoder is designed to provide digital quadrature encoder feedback for high volume applications with limited space constraints. The **E4P** version utilizes an innovative push-on hub disk assembly which accepts shaft diameters of 1.5mm to .250".

The **E4P** encoder is the leader for high quantity OEM applications, but the **E4** is the ideal choice when a set-screw hub disk assembly encoder is required (see the **E4** data sheet).

The **E4P** miniature encoder base provides mounting holes for two 3-48 x 1/4" or two 2.5mm x 6mm screws on a .586" bolt circle. When mounting holes are not available, a pre-applied transfer adhesive (with peel-off backing) is available for "stick-on" mounting.

The internal components consist of a precision machined aluminum hub and an encoder circuit board module.

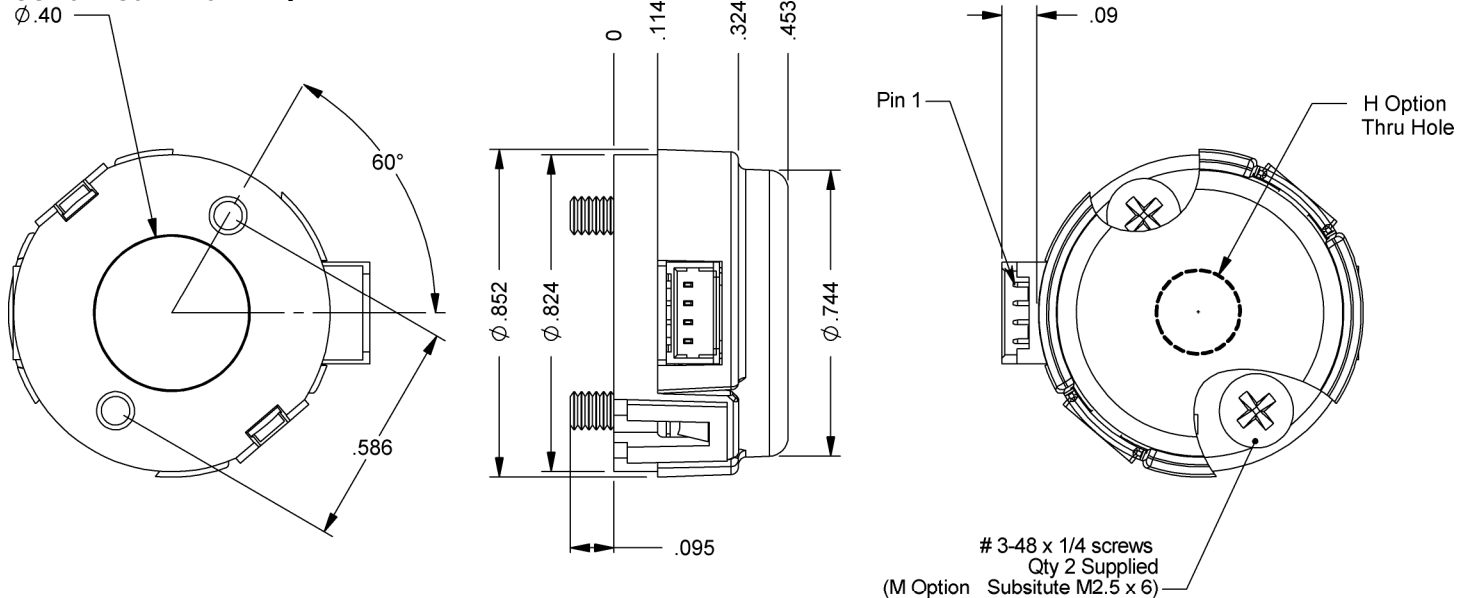
The encoder cover is easily snapped onto the base and is embossed with the connector pin-out.

The **E4P** series encoder can be connected by using a (high retention 4-conductor snap-in polarized 1.25mm pitch) connector. Mating cables and connectors (see the **Cables / Connectors** data sheet) are not included and are available separately.

Features:

- Low cost
- Miniature size
- Push-on hub - spring loaded collet design
- Minimum shaft length of .375"
- Fits shaft diameters of .059" to .250" (1.5mm to 1/4")
- High retention snap-in polarized connector
- Accepts $\pm .020"$ ($\pm .5\text{mm}$) axial shaft play
- Off-axis mounting tolerance of .010"
- Tracks from 0 to 60,000 cycles/sec
- 120 to 300 cycles per revolution (CPR)
- 480 to 1200 pulses per revolution (PPR)
- 2 channel quadrature TTL squarewave outputs
- -10° to +85°C operating temperature
- Single +5V supply
- Low power strobe option available
- Adhesive option available
- US Digital warrants its products against defects in materials and workmanship for two years. See complete warranty for details.

Mechanical Drawing:



Options:

H-option (Hole In Cover):

The H-option adds a hole to the cover for the shaft to pass through.

L-option (Low Power Strobe):

To reduce the average power requirements, the L-option version of the E4P power can be strobed on just long enough to sample outputs A and B. This option is the same as our standard E4P, except the internal power bypass capacitor is not installed. The outputs settling time is typically 200 to 400 nano seconds after power up. The minimum sample frequency must be less than the maximum RPM X the CPR / 10.

M-option (Metric Mounting Screws):

Provides alternate metric 2.5mm x 6mm screws. When M-option is NOT specified the default is 3-48 x 1/4" screws.

T-option (Transfer Adhesive):

When mounting holes are not available, a pre-applied transfer adhesive (with peel-off backing) is available for "stick-on" mounting. Use the centering tool to position the base. T-option specifies transfer adhesive.

Mechanical Specifications:

Parameter	Dimension	Units
Moment of Inertia	3.0 x 10 ⁻⁶	oz-in-s ²
Mounting Screw Size	#3-48 x 1/4"	
M-option Screw Size	2.5mm x 6mm	
Screw Bolt Circle Diameter	.586 ±.002	in.
Required Shaft Length*	.375 to .395	in.
Axial Length Hub / Disk Assembly	.270	in.

* Includes axial play.

Electrical Specifications:

For complete details see the AEDR data sheet.

Phase Relationship:

A leads B for clockwise shaft rotation, and B leads A for counterclockwise rotation viewed from the cover/label side of the encoder (see the AEDR data sheet).

Absolute Maximum Ratings:

Parameter	Min.	Max.	Units
Vibration (5 to 2kHz)	-	20	g
Shaft Axial Play	-	±.020	in.
Off-Axis Mounting Tolerance	-	.010	in.
Acceleration	-	250,000	rad/sec ²
Storage Temperature	-40°	85°	°C
Relative Humidity	-	90	%

Torque Specifications:

Parameter	Torque
Base to Mounting Surface	2-3 in.-lbs.

Compatible Cables & Connectors:

4-pin Micro:

CON-MIC4	Connector
CA-3285-1FT	Connector on one end with 4 12" wires
CA-3286-6FT	Connector on one end of a 6' round twisted pair cable

Attention:

- > Specify cable length when ordering.
- > Custom cable lengths are available. See the **Cables / Connectors** data sheet for more information.
- > The connector built into the encoder is Molex# 53048-0410.
- > The mating connector is made up of housing (Molex# 51021-0400) and 4 individual crimp-on pins (Molex# 50079-8100).
- > Special crimp tool (Molex# 50079) is needed to install connector pins.

Pin-out:

Pin	Description
1	+5VDC power
2	A channel
3	Ground
4	B channel

Accessories:

Spacer Tool:

Description: This reusable tool is used to properly space the hub / disk assembly from the encoder base.

Material: Aluminum.

SPACER-E4P Price: \$0.53

Please note: At least one **SPACER-E4P** is included with each order.



Centering Tool:

Description: This reusable tool provides a simple method for accurately centering the **E4** base onto the shaft.

Material: Aluminum.

Please note: A centering tool is highly recommended when using the T-option transfer adhesive.



Installation Tool:

Description: This optional installation tool is an alternative to the **SPACER-E4P**. The design of the tool allows for easy grip assembly in high volume applications. This tool *will NOT work* with T-option (transfer adhesive) applied encoders. This tool is *NOT* RoHS compliant.

Material: Aluminum.

HTOOL-E4P Price: \$5.25



MCTOOLP - —

Price
\$5.25

CPR:	Shaft Diameter:	
	Code	Size
100		
108	059	1.5mm
120	079	2mm
125	091	2.3mm
128	098	2.5mm
200	118	3mm
250	125	1/8"
256	156	5/32"
300	157	4mm
	187	3/16"
	197	5mm
	237	6mm
	250	1/4"

Ordering Information:

Price:

\$19.95 / 1
 \$17.33 / 10
 \$15.44 / 50
 \$14.07 / 100
 \$12.92 / 500
 \$11.97 / 1K
 \$11.18 / 5K
 \$10.00 / 10K

Cost Modifiers:

- Add 15% for T-option.
- Add \$3 for **PKG1**-option.
- Add \$4 for **PKG2**-option.
- Add \$7 for **PKG3**-option.

E4P - — — —

CPR:
100
108
120
125
128
200
250
256
300

Shaft Diameter:	
Code	Size
059	1.5mm
079	2mm
091	2.3mm
098	2.5mm
118	3mm
125	1/8"
156	5/32"
157	4mm
187	3/16"
197	5mm
237	6mm
250	1/4"

Options: (specify in order shown)
L = Low power strobe.
H = Adds hole in cover to allow the shaft to pass through.
T = Adds transfer adhesive.*
M = Provides alternate metric 2.5mm x 6mm screws.**

Packaging Options:
Blank (default) = Base, screws and PCBs are packaged separately in bulk. Extra assembly is required. One spacer tool per 100 encoders.
PKG1 = Each encoder packaged individually. One spacer tool per 100 encoders packaged in bulk.
PKG2 = One spacer tool individually packaged together with each encoder.
PKG3 = One spacer tool, and one centering tool individually packaged together with each encoder.

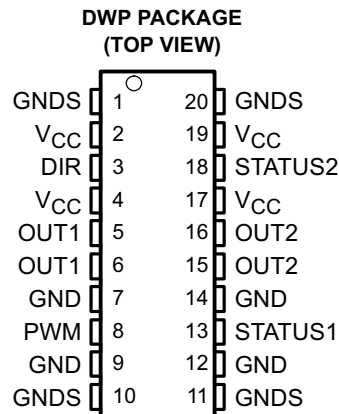
Important: When a centering tool is needed it may be most cost effective to use the default packaging option and to order a centering tool separately. This is especially true when ordering a single encoder.

Notes:

- * A centering tool is highly recommended when using this option.
- ** When **M**-option is NOT specified the default is 3-48 x 1/4" screws.

Technical Data, Rev. 03.20.07, March 2007
 All information subject to change without notice.

- **Dedicated PWM Input Port**
- **Optimized for Reversible Operation of Motors**
- **Two Input Control Lines for Reduced Microcontroller Overhead**
- **Internal Current Shutdown of 5 A**
- **40 V Load Dump Rating**
- **Integrated Fault Protection and Diagnostics**
- **CMOS Compatible Schmitt Trigger Inputs for High Noise Immunity**



description

The TPIC0107B is a PWM control intelligent H-bridge designed specifically for dc motor applications. The device provides forward, reverse, and brake modes of operation. A logic supply voltage of 5 V is internally derived from V_{CC}.

The TPIC0107B has an extremely low r_{DS(on)}, 280 mΩ typical, to minimize system power dissipation. The direction control (DIR) and PWM control (PWM) inputs greatly simplify the microcontroller overhead requirement. The PWM input can be driven from a dedicated PWM port while the DIR input is driven as a simple low speed toggle.

The TPIC0107B provides protection against over-voltage, over-current, over-temperature, and cross conduction faults. Fault diagnostics can be obtained by monitoring the STATUS1 and STATUS2 terminals and the two input control lines. STATUS1 is an open-drain output suitable for wired-or connection. STATUS2 is a push-pull output that provides a latched status output. Under-voltage protection ensures that the outputs, OUT1 and OUT2, will be disabled when V_{CC} is less than the under-voltage detection voltage V_(UVCC).

The TPIC0107B is designed using TI's LinBiCMOS™ process. LinBiCMOS allows the integration of low power CMOS structures, precision bipolar cells, and low impedance DMOS transistors.

The TPIC0107B is offered in a 20-pin thermally enhanced small-outline package (DWP) and is characterized for operation over the operating case temperature of –40°C to 125°C.

FUNCTION TABLE

DIR	PWM	OUT1	OUT2	MODE
0	0	HS	HS	Brake, both HSDs turned on hard
0	1	HS	LS	Motor turns counter clockwise
1	0	HS	HS	Brake, both HSDs turned on hard
1	1	LS	HS	Motor turns clockwise



Please be aware that an important notice concerning availability, standard warranty, and use in critical applications of Texas Instruments semiconductor products and disclaimers thereto appears at the end of this data sheet.

LinBiCMOS is a trademark of Texas Instruments Incorporated.

PRODUCTION DATA information is current as of publication date. Products conform to specifications per the terms of Texas Instruments standard warranty. Production processing does not necessarily include testing of all parameters.



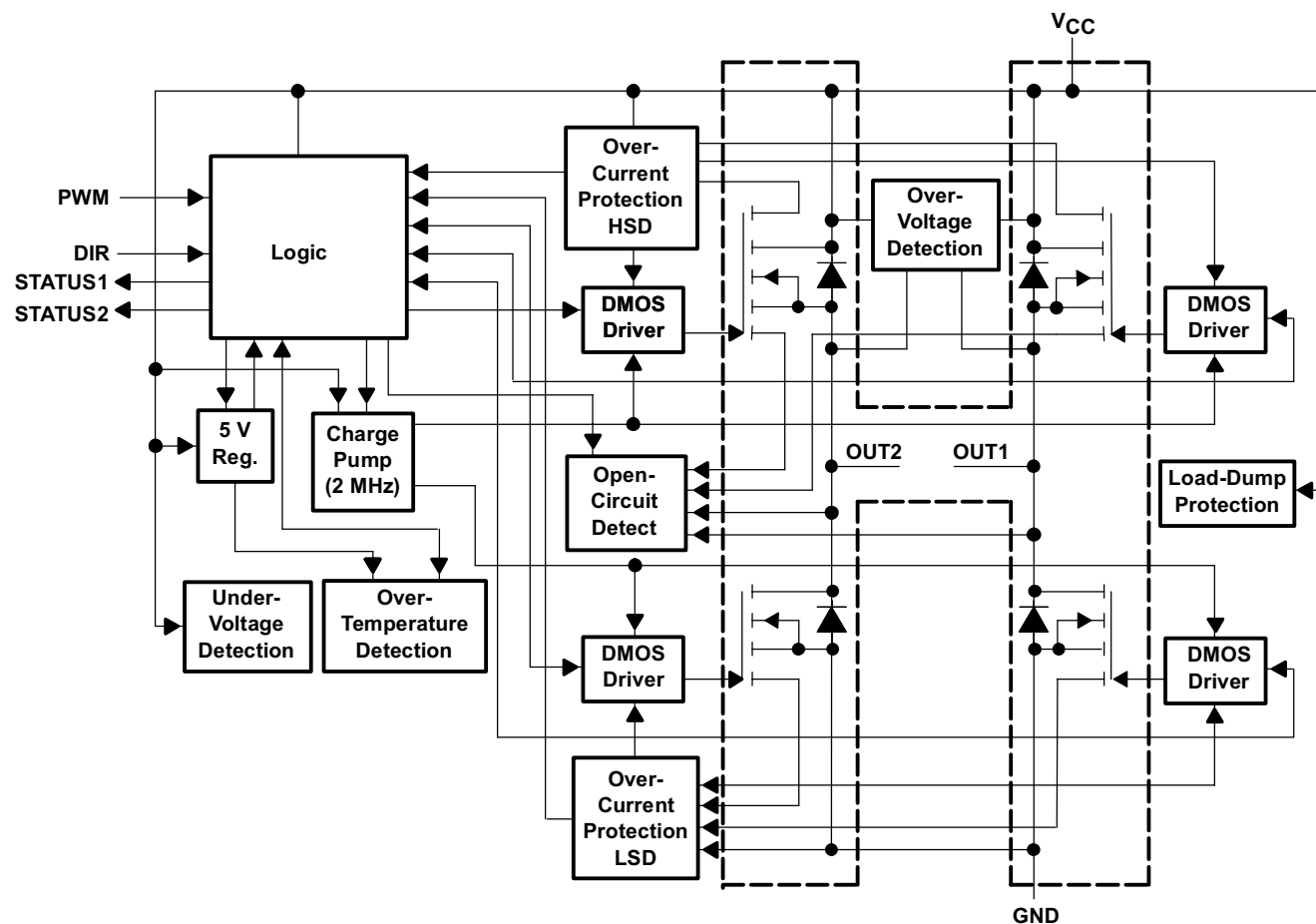
POST OFFICE BOX 655303 • DALLAS, TEXAS 75265

Copyright © 2002, Texas Instruments Incorporated

TPIC0107B PWM CONTROL INTELLIGENT H-BRIDGE

SLIS067A – NOVEMBER 1998 – REVISED APRIL 2002

block diagram



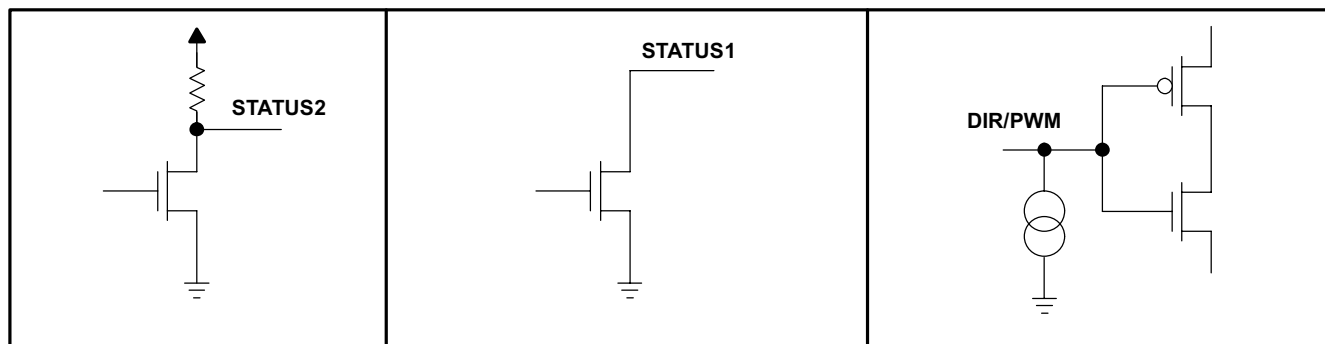
Terminal Functions

TERMINAL NAME	NO.	I/O	DESCRIPTION
DIR	3	I	Direction control input
GND	7, 9, 12, 14	I	Power ground
GNDS	1, 10, 11, 20	I	Substrate ground
OUT1	5, 6	O	Half-H output. DMOS output
OUT2	15, 16	O	Half-H output. DMOS output
PWM	8	I	PWM control input
STATUS1	13	O	Status output
STATUS2	18	O	Latched status output
VCC	2, 4, 17, 19	I	Supply voltage

NOTE: It is mandatory that all four ground terminals plus at least one substrate terminal are connected to the system ground. Use all VCC and OUT terminals.



schematics of inputs and outputs



absolute maximum ratings over operating case temperature range (unless otherwise noted)†

Power supply voltage range, V_{CC}	-0.3 V to 33 V
Logic input voltage range, V_{IN}	-0.3 V to 7 V
Load dump (for 400 ms, $T_C = 25^\circ\text{C}$)	40 V
Status output voltage range, $V_{O(\text{status})}$	-0.3 V to 7 V
Continuous power dissipation, $T_C = 25^\circ\text{C}$	1.29 W
Storage temperature range, T_{stg}	-55°C to 150°C
Maximum junction temperature, T_J	150°C

† Stresses beyond those listed under “absolute maximum ratings” may cause permanent damage to the device. These are stress ratings only, and functional operation of the device at these or any other conditions beyond those indicated under “recommended operating conditions” is not implied. Exposure to absolute-maximum-rated conditions for extended periods may affect device reliability.

DISSIPATION RATING TABLE

$T_A \leq 25^\circ\text{C}$	DERATING FACTOR	$T_A = 70^\circ\text{C}$	$T_A = 125^\circ\text{C}$
POWER RATING	ABOVE $T_A = 25^\circ\text{C}$	POWER RATING	POWER RATING
1.29 W	0.0104 W/°C	0.82 W	0.25 W

recommended operating conditions

	MIN	MAX	UNIT
Supply voltage, V_{CC}	6	18	V
Operating case temperature, T_C	-40	125	°C
Switching frequency, f_{PWM}		2	kHz

TPIC0107B

PWM CONTROL INTELLIGENT H-BRIDGE

SLIS067A – NOVEMBER 1998 – REVISED APRIL 2002

electrical characteristics over recommended operating case temperature range and $V_{CC} = 5\text{ V}$ to 6 V (unless otherwise noted)

PARAMETER		TEST CONDITIONS	MIN	TYP	MAX	UNIT
$r_{DS(on)}$	Static drain-source on-resistance (per transistor) $I_{(BR)} = 1\text{ A}$	LSD $T_J = 25^\circ\text{C}$			550	$\text{m}\Omega$
		$T_J = 150^\circ\text{C}$			850	
	HSD	$T_J = 25^\circ\text{C}$			600	$\text{m}\Omega$
		$T_J = 150^\circ\text{C}$			870	
$I_{(QCD)}$	Open circuit detection current		10	40	100	mA
$V_{(UVCC(OFF))}$	Under voltage detection on V_{CC} , switch off voltage	See Note 1			5	V
$V_{(UVCC(ON))}$	Under voltage detection on V_{CC} , switch on voltage	See Note 1			5.2	V
$V_{(STL)}$	STATUS low output voltage	$I_O = 100\ \mu\text{A}$, See Note 1			0.8	V
$V_{(ST2H)}$	STATUS2 high output voltage	$I_O = 20\ \mu\text{A}$, See Note 1	3		5.4	V
$I_{(ST(OFF))}$	STATUS output leakage current	$V_{(ST)} = 5\text{ V}$, See Note 1			5	μA
V_{IL}	Low level logic input voltage		-0.3		0.5	V
V_{IH}	High level logic input voltage		3.6		7	V
ΔV_I	Hysteresis of input voltage		0.3			V
I_{IH}	High level logic input current	$V_{IH} = 3.5\text{ V}$	2	10	50	μA

NOTE 1: The device functions according to the function table for V_{CC} between $V_{(UVCC)}$ and 5 V (no parameters specified). STATUS outputs are not defined for V_{CC} less than $V_{(UVCC)}$.



electrical characteristics over recommended operating case temperature and supply voltage ranges (unless otherwise noted) (see Note 2)

PARAMETER		TEST CONDITIONS	MIN	TYP	MAX	UNIT	
$r_{DS(on)}$	Static drain-source on-resistance (per transistor) $I_{BR} = 1$ A	$T_J = 25^\circ\text{C}$	$V_{CC} = 6$ V to 9 V		380	$m\Omega$	
			$V_{CC} = 9$ V to 18 V	280	340		
		$T_J = 150^\circ\text{C}$	$V_{CC} = 6$ V to 9 V		620		
			$V_{CC} = 9$ V to 18 V	400	560		
	HSD	$T_J = 25^\circ\text{C}$	$V_{CC} = 6$ V to 9 V		430		$m\Omega$
			$V_{CC} = 9$ V to 18 V	280	340		
		$T_J = 150^\circ\text{C}$	$V_{CC} = 6$ V to 9 V		640		
			$V_{CC} = 9$ V to 18 V	400	560		
$I_{(QCD)}$	Open circuit detection current		10	40	100	mA	
T_{SDS}	Static thermal shutdown temperature	See Notes 3 and 4	140			$^\circ\text{C}$	
T_{SDD}	Dynamic thermal shutdown temperature	See Notes 3 and 5	160			$^\circ\text{C}$	
I_{CS}	Current shutdown limit	$V_{CC} = 6$ V to 9 V	4.8		7.5	A	
		$V_{CC} = 9$ V to 18 V	5		7.5		
$I_{(CON)}$	Continuous bridge current	$T_J = 125^\circ\text{C}$, Operating lifetime 10,000 hours, (see Figure 1)			3	A	
$V_{(OVCC)}$	Over voltage detection on V_{CC}		27		36	V	
$V_{(STL)}$	STATUS low output voltage	$I_O = 100$ μA			0.8	V	
$V_{(ST2H)}$	STATUS2 high output voltage	$I_O = 20$ μA	3.9		5.4	V	
$I_{(ST(OFF))}$	STATUS output leakage current	$V_{(ST)} = 5$ V			5	μA	
V_{IL}	Low level logic input voltage		-0.3		0.8	V	
V_{IH}	High level logic input voltage		3.6		7	V	
ΔV_I	Hysteresis of input voltage		0.3			V	
I_{IH}	High level logic input current	$V_{IH} = 3.5$ V	2	10	50	μA	

- NOTES: 2. The device functions according to the function table for V_{CC} between 18 V and $V_{(OVCC)}$, but only up to a maximum supply voltage of 33 V (no parameters specified). Exposure beyond 18 V for extended periods may affect device reliability.
3. Exposure beyond absolute-maximum-rated condition of junction temperature may affect device reliability.
4. No temperature gradient between DMOS transistor and temperature sensor.
5. With temperature gradient between DMOS transistor and temperature sensor in a typical application (DMOS transistor as heat source).

switching characteristics over recommended operating case temperature and supply voltage ranges (unless otherwise noted)

PARAMETER		TEST CONDITIONS	MIN	TYP	MAX	UNIT
$t_{out(on)}$	High-side driver turn-on time	$V_{DS(on)} < 1$ V at 1 A, $V_{CC} = 13.2$ V			100	μs
	Low-side driver turn-on time				100	
SR	Slew rate, low-to-high sinusoidal ($\delta V/\delta t$)	$V_{CC} = 13.2$ V, $I_O = 1$ A resistive load	1		6	V/ μs
	Slew rate, high-to-low sinusoidal ($\delta V/\delta t$)		1		6	
$t_d(QCD)$	Under current spike duration to trigger open circuit detection	$V_{CC} = 5$ V to 18 V	1		10	ms
$t_d(CS)$	Delay time for over current shutdown		5	10	25	μs

thermal resistance

PARAMETER		MIN	MAX	UNIT
$R_{\theta JA}$	Junction-to-ambient thermal resistance		97	$^\circ\text{C}/\text{W}$
$R_{\theta JC}$	Junction-to-case thermal resistance		5	$^\circ\text{C}/\text{W}$



TPIC0107B PWM CONTROL INTELLIGENT H-BRIDGE

SLIS067A – NOVEMBER 1998 – REVISED APRIL 2002

PARAMETER MEASUREMENT INFORMATION

Maximum continuous bridge current versus time based on 50 FITs at 100,000 hours operating life (90% confidence model)

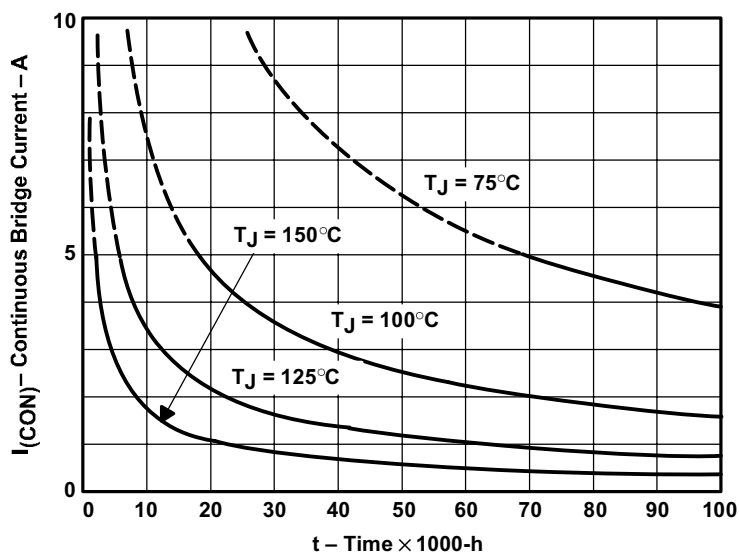


Figure 1. Electromigration Reliability Data

Example:

Average continuous bridge current, I_{CON}	Average junction temperature, T_J	Operating lifetime of device based on electromigration
2 A	125°C	>20,000 h
3 A	125°C	>10,000 h

PARAMETER MEASUREMENT INFORMATION

operating wave forms

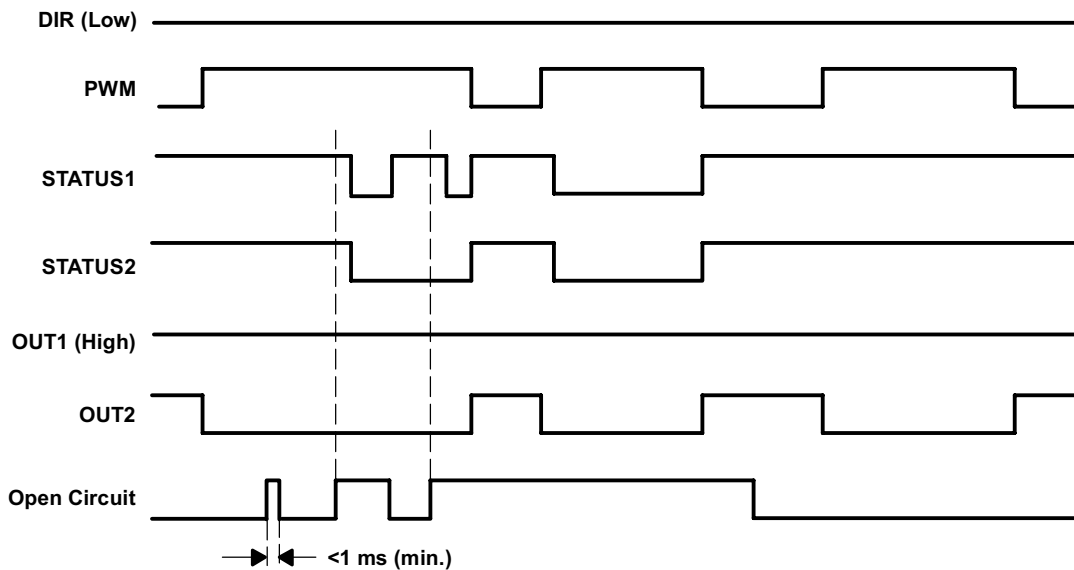


Figure 2. Open Circuit

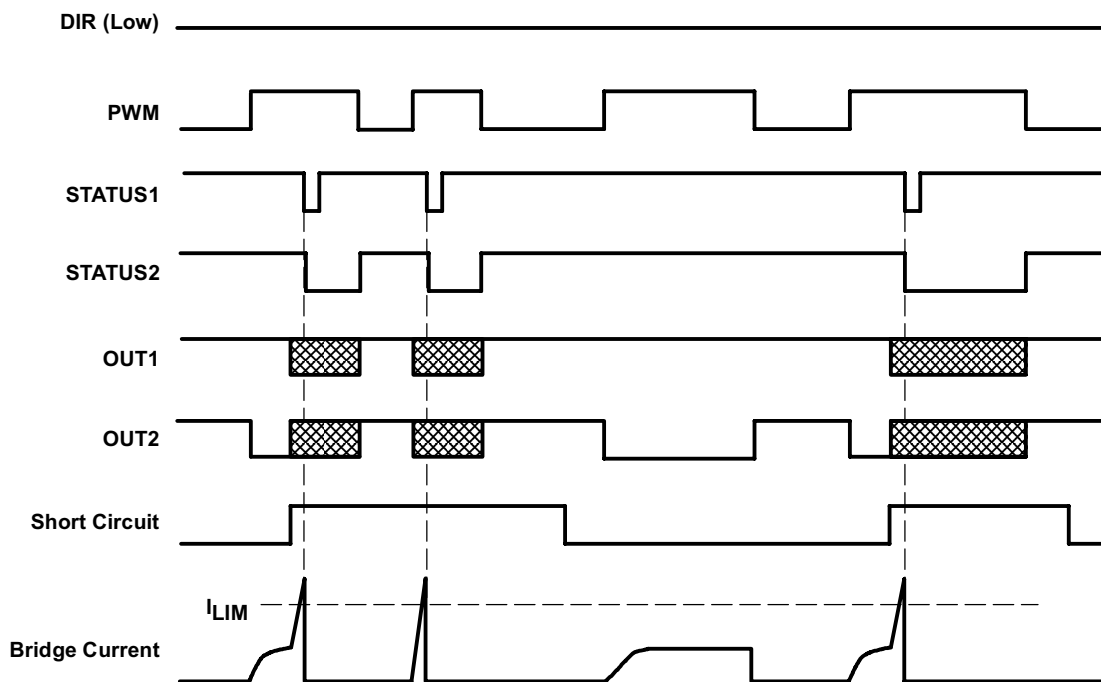


Figure 3. Short Circuit (e.g., OUT2 to V_{CC})

TPIC0107B PWM CONTROL INTELLIGENT H-BRIDGE

SLIS067A – NOVEMBER 1998 – REVISED APRIL 2002

PARAMETER MEASUREMENT INFORMATION

operating wave forms (continued)

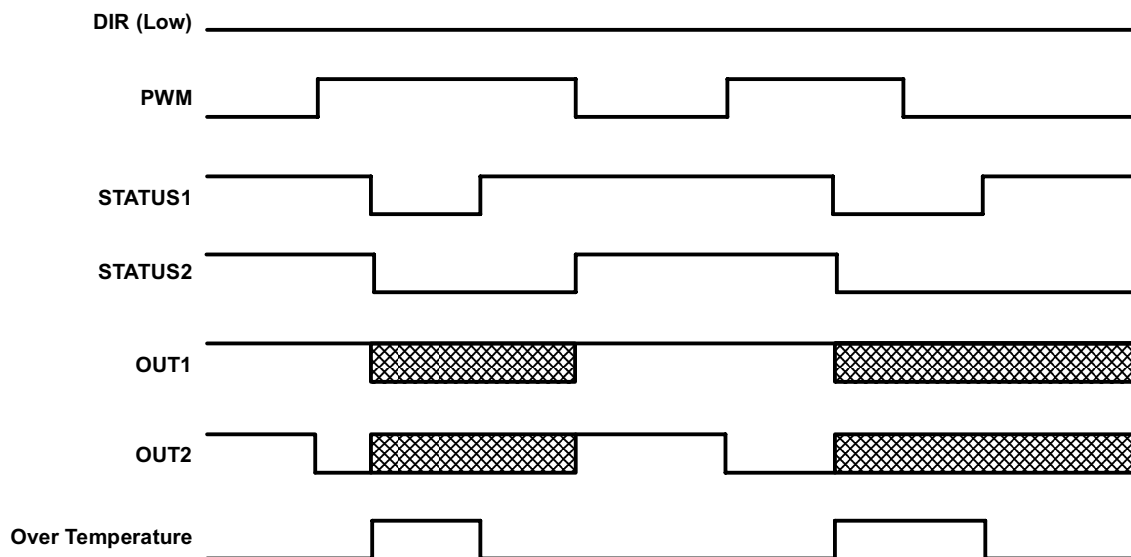


Figure 4. Over Temperature

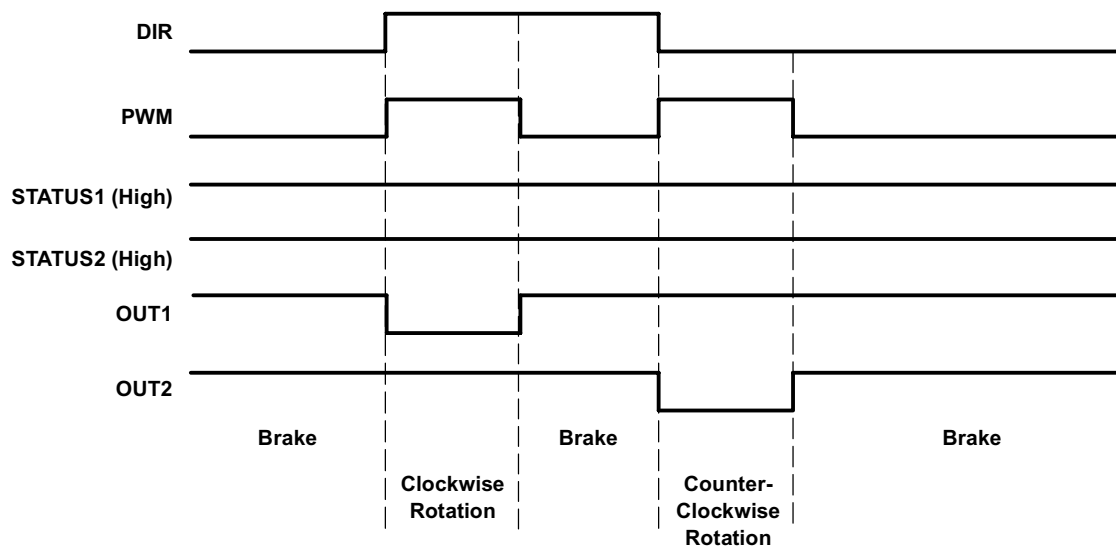


Figure 5. No Fault

PRINCIPLES OF OPERATION

protective functions and diagnostics†

over current/short circuit‡

The TPIC0107B detects shorts to V_{CC} , ground, or across the load being driven, by comparing the V_{DS} voltage drop across the DMOS outputs against the threshold voltage. The DMOS outputs of the TPIC0107B will be disabled and the fault flags will be generated 10 μ s after an over-current or short-circuit fault is detected. This 10 μ s delay is long enough to serve as a de-glitch filter for high current transients, yet short enough to prevent damage to the DMOS outputs. The DMOS outputs remain latched off until either DIR or PWM input is toggled.

In cases where the outputs have a continuous short-to-ground with a current rise time faster than 0.5 A/ μ s, the over-current shutdown threshold will decrease to 3 A to reduce power dissipation. This reduction to 3 A is achieved since the DMOS outputs will not be fully enhanced when the over-current threshold is reached if the current rise time exceeds 0.5 A/ μ s. Over-current and/or short-circuit protection is provided up to $V_{CC} = 16.5$ V and a junction temperature of 90°C.

over temperature

The TPIC0107B disables all DMOS outputs and the fault flags will be set when $T_J \geq 140^\circ\text{C}$ (min.). The DMOS outputs remain latched off until either DIR or PWM input is toggled.

under voltage

The TPIC0107B disables all DMOS outputs when $V_{CC} \leq V_{(UVCC)}$. The outputs will be re-enabled when $V_{CC} \geq V_{(UVCC)}$. No fault flags are set when under-voltage lockout occurs.

over voltage

In order to protect the DMOS outputs from damage caused by excessive supply voltage, the TPIC0107B disables all outputs when $V_{CC} \geq V_{(OVCC)}$. Once $V_{CC} \leq V_{(OVCC)}$, either DIR or PWM input must be toggled to re-enable the DMOS outputs.

cross conduction

Monitoring circuitry for each transistor detects whether the particular transistor is active to prevent the HSD or LSD of the corresponding half H-bridge from conducting.

open circuit

During operation, the bridge current is controlled continuously. If the bridge current is >10 mA (min.) for a period >1 ms (min.), the fault flags are set. However, the output transistors will not be disabled.

† All limits mentioned are typical values unless otherwise noted.

‡ If a short circuit occurs (i.e., the over-current detection circuitry is activated) at a supply voltage higher than 16.5 V and a junction temperature higher than 90°C, damage to the device may occur.

TPIC0107B

PWM CONTROL INTELLIGENT H-BRIDGE

SLIS067A – NOVEMBER 1998 – REVISED APRIL 2002

PRINCIPLES OF OPERATION

DIAGNOSTICS TABLE (see Note 6)

FLAG	DIR	PWM	OUT1	OUT2	STATUS1†	STATUS2
Normal operation	0	0	HS	HS	1	1
	0	1	HS	LS	1	1
	1	0	HS	HS	1	1
	1	1	LS	HS	1	1
Open circuit between OUT1 and OUT2	0	0	HS	HS	1	1
	0	1	HS	LS	0	0
	1	0	HS	HS	1	1
	1	1	LS	HS	0	0
Short circuit from OUT1 to OUT2 (see Notes 7 and 8)	0	1	X	X	0	0
	1	1	X	X	0	0
Short circuit from OUT1 to GND (see Notes 7 and 8)	0	0	X	X	0	0
	1	0	X	X	0	0
	0	1	X	X	0	0
Short circuit from OUT2 to GND (see Notes 7 and 8)	0	0	X	X	0	0
	1	0	X	X	0	0
	1	1	X	X	0	0
Short circuit from OUT1 to V _{CC} (see Notes 7 and 8)	1	1	X	X	0	0
Short circuit from OUT2 to V _{CC} (see Notes 7 and 8)	0	1	X	X	0	0
Over temperature	0	0	Z	Z	0	0
	0	1	Z	Z	0	0
	1	0	Z	Z	0	0
	1	1	Z	Z	0	0

† When wired with a pull-up resistor

SYMBOL	VALUE
0	Logic low
1	Logic high
HS	High-side MOSFET conducting
LS	Low-side MOSFET conducting
Z	No output transistors conducting
X	Voltage level undefined

- NOTES: 6. All input combinations not stated result in STATUS output = 1.
 7. STATUS1 active for a minimum of 3 μs.
 8. STATUS2 active until an input is toggled.



TYPICAL CHARACTERISTICS

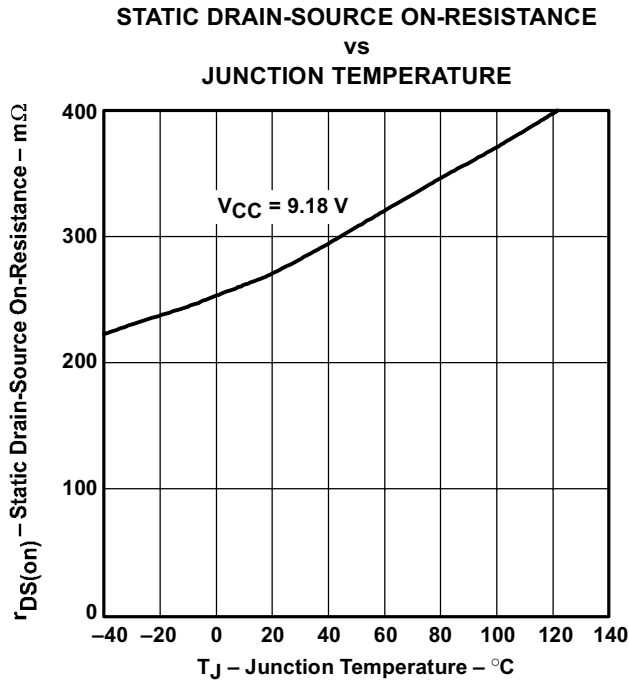


Figure 6

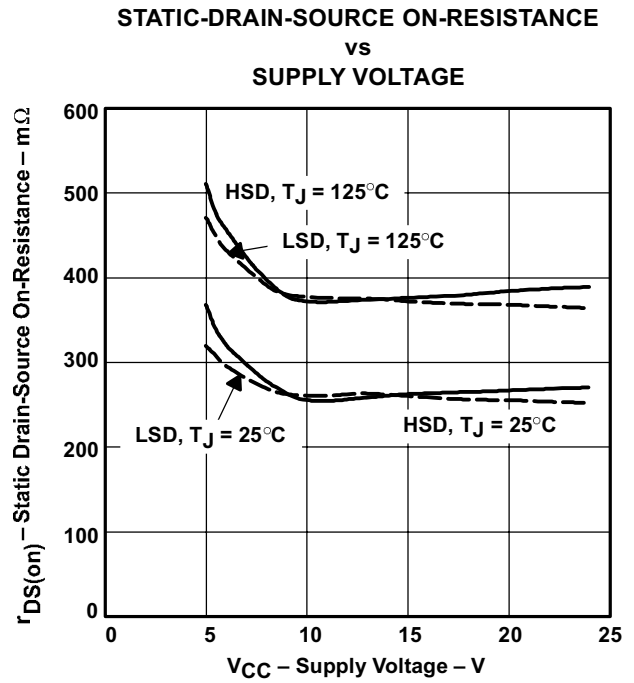


Figure 7

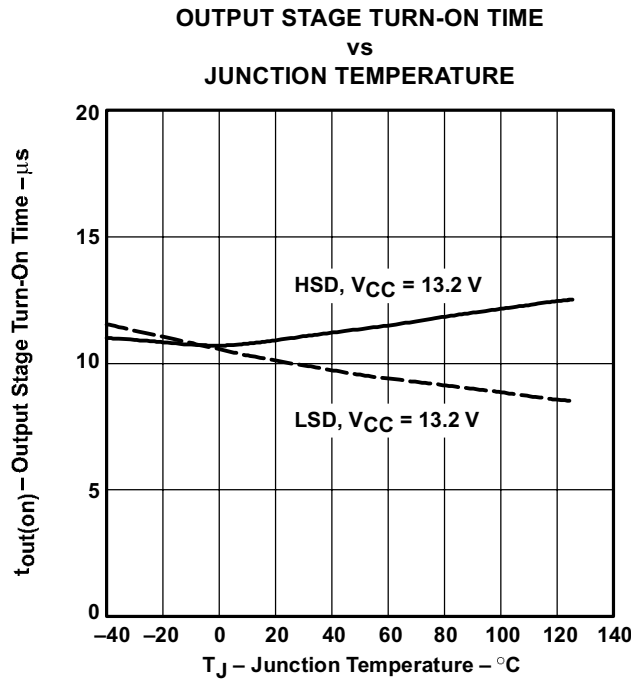
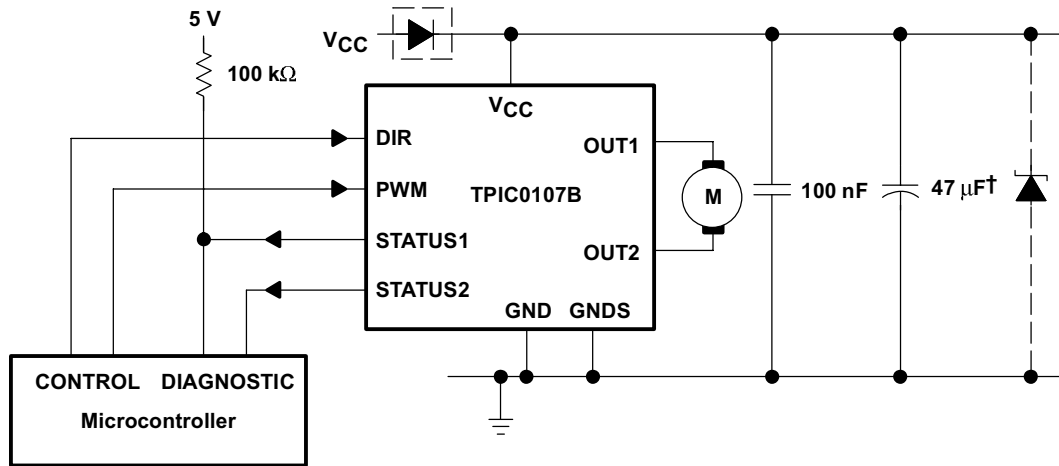


Figure 8

TPIC0107B PWM CONTROL INTELLIGENT H-BRIDGE

SLIS067A – NOVEMBER 1998 – REVISED APRIL 2002

APPLICATION INFORMATION



† Necessary for isolating supply voltage or interruption (e.g., 47 μF).

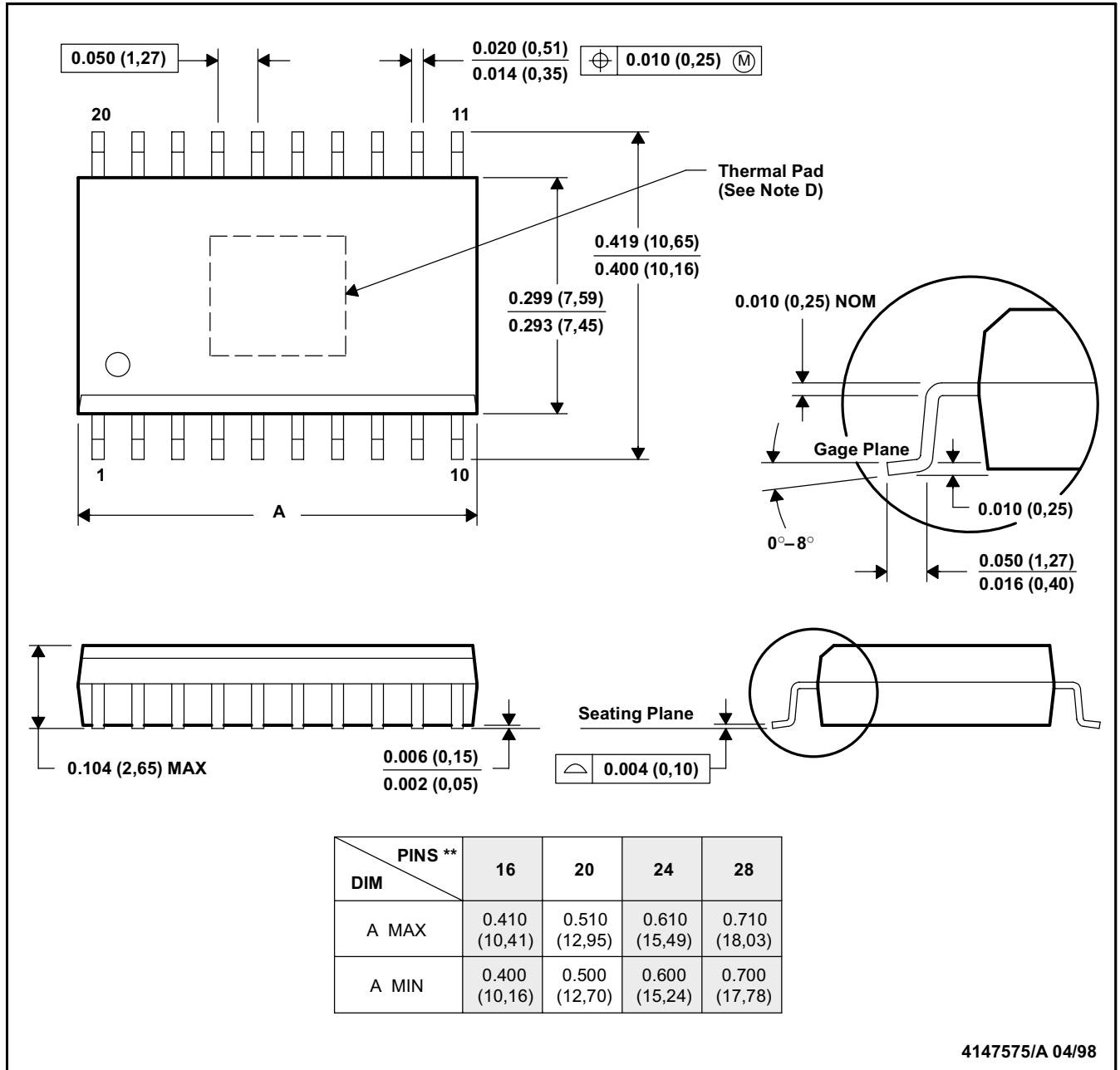
NOTE: If a STATUS output is not connected to the appropriate microcontroller input, it shall remain unconnected.

MECHANICAL DATA

DWP (R-PDSO-G**)

PowerPAD™ PLASTIC SMALL-OUTLINE PACKAGE

20 PINS SHOWN



4147575/A 04/98

- NOTES: A. All linear dimensions are in inches (millimeters).
 B. This drawing is subject to change without notice.
 C. Body dimensions do not include mold flash or protrusion not to exceed 0.006 (0,15).
 D. The package thermal performance may be enhanced by bonding the thermal pad to an external thermal plane. This pad is electrically and thermally connected to the backside of the die and possibly selected leads.

PowerPAD is a trademark of Texas Instruments Incorporated.



IMPORTANT NOTICE

Texas Instruments Incorporated and its subsidiaries (TI) reserve the right to make corrections, modifications, enhancements, improvements, and other changes to its products and services at any time and to discontinue any product or service without notice. Customers should obtain the latest relevant information before placing orders and should verify that such information is current and complete. All products are sold subject to TI's terms and conditions of sale supplied at the time of order acknowledgment.

TI warrants performance of its hardware products to the specifications applicable at the time of sale in accordance with TI's standard warranty. Testing and other quality control techniques are used to the extent TI deems necessary to support this warranty. Except where mandated by government requirements, testing of all parameters of each product is not necessarily performed.

TI assumes no liability for applications assistance or customer product design. Customers are responsible for their products and applications using TI components. To minimize the risks associated with customer products and applications, customers should provide adequate design and operating safeguards.

TI does not warrant or represent that any license, either express or implied, is granted under any TI patent right, copyright, mask work right, or other TI intellectual property right relating to any combination, machine, or process in which TI products or services are used. Information published by TI regarding third-party products or services does not constitute a license from TI to use such products or services or a warranty or endorsement thereof. Use of such information may require a license from a third party under the patents or other intellectual property of the third party, or a license from TI under the patents or other intellectual property of TI.

Reproduction of information in TI data books or data sheets is permissible only if reproduction is without alteration and is accompanied by all associated warranties, conditions, limitations, and notices. Reproduction of this information with alteration is an unfair and deceptive business practice. TI is not responsible or liable for such altered documentation.

Resale of TI products or services with statements different from or beyond the parameters stated by TI for that product or service voids all express and any implied warranties for the associated TI product or service and is an unfair and deceptive business practice. TI is not responsible or liable for any such statements.

Mailing Address:

Texas Instruments
Post Office Box 655303
Dallas, Texas 75265